Supersymmetric Models: Phenomenological and Dark Matter Analyses

Daniel Elbio López-Fogliani

Supervised by **Dr. Carlos Muñoz López**
Prof. Departamento de Física Teórica

Departamento de Física Teórica
& Instituto de Física Teórica
Universidad Autónoma de Madrid
Marzo 2007

A mi madre y la memoria de mi viejo

Agradecimientos

Quiero agradecerle en primer lugar a Carlos Muñoz la dirección de este trabajo y su valioso apoyo. Como así también las numerosas conversaciones y discusiones que hemos mantenido.

En segundo término a Silvia. A Natxo Alonso, Gaston Giribet, Juan Pedro Resco, Daniel Cremades y Juan Medina por su amistad y por las extensas y fructiferas conversaciones sobre física y otras yerbas. A Ana Teixeira y David Cerdeño, sobre todo por su paciencia con mi inglés y mis escasos conocimientos informáticos al principio de nuestra colaboración. A Jose Ramón Espinosa y Emidio Gabrielli. A Nico quien sufrió conmigo el kim-chi como fuente de alimento, además de las maravillas Coreanas. A Kiwoon Choi y demás personas del KAIST en Corea por su amabilidad durante mi estancia allí.

Por último a todos los alcohólicos con los que compartí grandes jornadas, David Temes, Hoyitos, el Gitano, el Astur, la srta. Curiel, Alicia, Jose, Irene, Sergios, Ernestos, Ramos, Olga. A Miguel Angel, Dieguito y Fermín con quienes compartí piso. A todos aquellos con los que compartí este tiempo, Juan, Edu, Guille, Mónica, Micke, Matteo, Mary, el moro Fouad, Enriquín, Jorge, Jaime, Enrique, Salgado, Saharas, Bea, Roberto, Javis, Tomás, y todos los demás a los cuales no nombro porque me cansé de escribir.

Contents

Chapter 1

Introducción

La supersimetría (SUSY) juega un papel muy importante en la física teórica. Mediante una transformación SUSY campos bosónicos rotan a fermiónicos y viceversa. Se dice que están en un mismo supermultiplete los campos que rotan entre sí a través de esta transformación. Es de notar que los campos de un mismo supermultiplete pueden describirse por un único ente matemático: el supercampo. De esta forma dos conceptos aparentemente distintos, bosones y fermiones, se ven unificados en un único concepto. Una consecuencia de SUSY es que el número de grados de libertad bosónicos y fermiónicos de la teoría es necesariamente igual.

Desde un punto de vista matemático el álgebra de supersimetría es la raíz cuadrada del álgebra de Poincaré. Su extensión local, conocida como teoría de Supergravedad (SUGRA), incluye el campo gravitatorio de la misma forma que la extensión local de una simetría ante un grupo de Lie global incluye los campos gauge. Por lo tanto, en los supermultipletes de SUGRA entre los campos bosónicos está incluida la métrica espacio-temporal. Debemos mencionar que a diferencia de las teorías SUSY, las teorías de SUGRA no son renormalizables.

Como es bien sabido tal simetría no se observa en la naturaleza y por tanto, si existe, debe estar rota. Una idea de cómo llevar a cabo una ruptura espontánea de SUSY consiste en postular un sector oculto de partículas. El sector oculto no tiene acoplos gauge con el sector visible y por tanto la ruptura de SUSY se transmite a través de efectos gravitatorios. El resultado a baja escala es una teoría SUSY global más los llamados términos "soft", que rompen SUSY explicitamente sin introducir peligrosas divergencias cuadráticas. Es con este tipo de teorías con las que trabajaremos en esta tesis, ya que nos interesa la descripción de la física por debajo de la energía de Planck.

Por encima de esta escala tienen lugar los efectos de gravedad cuántica y la propia noción de espacio-tiempo se ve alterada. Probablemente, en la teoría completa de todas las interacciones la noción de espacio-tiempo no sea un concepto fundamental sino una propiedad emergente y los conceptos fundamentales sean mucho más abstractos que la noción de espacio-tiempo y dimensión. En todo caso, esta hipotética teoría completa no ha sido formulada aún.

Hoy en día la teoría de supercuerdas es la candidata más prometedora para unificar todas la interacciones de la naturaleza. En general el límite de bajas energías queda descrito por una teoría de SUGRA. Por tanto, una teoría SUSY puede ser un límite de la teoría de cuerdas. En relación a esto debemos recordar que la descripción perturbativa de cuerdas sobre un espacio-tiempo plano exige que éste tenga 10 dimensiones. El número de dimensiones puede ser modificado por la presencia de un campo de Liouville o una fuente de curvatura. Por otro lado, la variedad puede ser una variedad compuesta por una parte no compacta 4-dimensional, para estar de acuerdo con el número de dimensiones que observamos, y por una parte compacta. La parte compacta puede ser una variedad compacta seis dimensional, o la variedad de un grupo compacto que no necesariamente tenga una interpretación geométrica (por ejemplo un modelo de Gepner). En muchas de las construcciones a baja escala la parte compacta desacopla a la escala de Planck dejando una teoría de SUGRA en cuatro dimensiones.

Por debajo de la escala de Planck la ambiciosa pregunta aún sin respuesta, *¿cuál es la teoría completa de todas las interacciones?*, da lugar a la pregunta *¿cual es la teoría cuántica de campos que rige la física por debajo de dicha escala?* En este sentido las teorias SUSY son candidatas muy interesantes y poseen la característica de poder ser verificadas (refutadas) con experimentos realizables a corto plazo, ya que en sus versiones más puras o naturales (excluimos por ejemplo split-SUSY) la escala de ruptura de supersimetría es del orden del TeV. Recordemos que esta es la escala necesaria para romper la simetria electrodébil (EW) de forma adecuada.

En cuanto a la teoría de cuerdas, su formulación actual es claramente incompleta, ya que dada la extraordinaria cantidad de posibilidades que brinda a baja escala carece de predictibilidad. Una formulación más completa exigiría por ejemplo un aún desconocido mecanismo de selección de vacíos que discrimine entre los muchos que posee.

Resumiendo, a escalas de energía donde los efectos cuánticos de la gravedad son despreciables, las teorías SUSY son excelentes candidatas a describir la física. Además están desprovistas del problema de naturalidad que poseen las versiones no SUSY. El modelo estándar (SM) posee el conocido problema de las jerarquías; la dependen-

cia cuadrática con la escala de nueva física ("cutoff") del cuadrado del parámetro de masa del Higgs, hace que dicha escala sea la natural para la masa del Higgs. Por ejemplo, en una teoría conteniendo gravedad, la masa del Higgs debido a las correcciones cuadráticas se haría del orden de la masa de Planck aun cuando inicialmente fuese pequeña, estropeándose de esta forma la ruptura EW. Afortunadamente, en las teorías SUSY la existencia de nuevos diagramas asociados a las compañeras SUSY de las partículas del SM, dan como resultado la cancelación de tal dependencia. En este sentido SUSY es la candidata natural para extender el SM. Es bien cierto que este mecanismo no resuelve todos los problemas y que todavía sobrevive el llamado segundo problema de las jerarquías, es decir ¿por qué las parámetros soft de ruptura de SUSY son del orden del TeV y no mayores? Esto se traduce en la necesidad de tener un mecanismo de ruptura de SUSY tal que los términos soft resultantes sean del orden del TeV. Mucho trabajo ha sido dedicado a esta tarea y en la literatura se pueden encontrar distintos modelos, como por ejemplo la condensación de gauginos.

Además de las cualidades ya descritas, las teorías SUSY nos pueden proveer de candidatos para resolver un gran enigma de la física contemporánea: la materia oscura. Éste es uno de los temas que motivan este trabajo y una de las cuestiones aún sin respuesta más fascinantes de la física. Observaciones en galaxias y cúmulos de galaxias han revelado desde hace casi un siglo, por simples argumentos gravitatorios, que debe haber más materia que la visible. Las teorías SUSY, cuando se impone una simetría discreta conocida como R-parity, proveen de forma natural una partícula como candidata para constituir tal materia oscura. Distinguiendo en un supermultiplete dado entre partículas supersimétricas y aquellas que podemos llamar del SM, la existencia de esta simetría implica que el número de partículas supersimétricas en un vértice debe ser par. Esto da como resultado que la partícula supersimétrica más ligera (LSP) no puede decaer y podría servir por tanto como materia oscura. En este sentido, uno de los problemas abiertos más importantes en este campo tiene una posible respuesta en las teorías SUSY.

Resulta entonces crucial analizar en detalle la viabilidad de la LSP para constituir la materia oscura del universo. Para la mínima extensión del SM conocida como Minimal Supersymmetric Standard Model (MSSM) este análisis se ha llevado a cabo extensamente en la literatura. Sin embargo, para su extensión más directa obtenida agregando un supercampo singlete, S, y conocida como Next-to-Minimal Supersymmetric Standard model (NMSSM), hay muy pocos trabajos realizados y son claramente incompletos. Es importante mencionar que esta extensión soluciona el problema de

naturalidad del MSSM conocido como "μ-problem" haciendo al NMSSM muy atractivo. Este problema de naturalidad se debe a la existencia en el superpotencial del MSSM de un término de masa $\mu H_1 H_2$ necesario para producir una ruptura EW correcta. Los únicos valores naturales para μ son cero o la masa de Planck, el primero introduce un bosón de Goldstone experimentalmente excluido y el segundo reintroduce el problema de las jerarquías. El NMSSM resuelve este problema a través del acoplo SH_1H_2, cuando el escalar S adquiere un valor esperado en el vacío (VEV).

En este trabajo de tesis vamos a explorar las posibilidades de la partícula SUSY llamada neutralino, la cual es frecuentemente la LSP, como candidata a materia oscura en el NMSSM. Calcularemos la densidad reliquia de neutralinos y la compararemos con los valores obtenidos mediante observaciones astrofísicas, así como por el obtenido recientemente por el experimento WMAP. Analizaremos también la posible detección directa de los neutralinos mediante la interacción de estos con los núcleos del material en un detector. Tendremos en cuenta en el análisis el rango ya explorado por los experimentos actuales y el esperado en los experimentos que próximamente se llevarán a cabo. Impondremos todas las cotas experimentales que vienen de física de aceleradores de partículas incluyendo procesos de física de sabores como $b \to s\gamma$ y el momento magnético anómalo del muón. Con respecto a este último, si bien hay todavía cierta controversia con respecto a los resultados teóricos, podría ser una señal de física más allá del SM.

Mencionábamos anteriormente el problema μ de las teorías SUSY, pues bien en este trabajo de tesis queremos analizar también una solución alternativa a las ya existentes, que a su vez nos lleva a proponer un nuevo modelo SUSY. Dicho modelo no sólo está a salvo del problema μ, sino que además contiene de manera natural la física de neutrinos tan relevante actualmente. Recordemos que el hecho de que los neutrinos sean masivos es la primera confirmación clara de física más allá del SM, en el régimen donde es válida una descripción mediante una teoría cuántica de campos.

La idea consiste en utilizar el supercampo del neutrino *right-handed* para solucionar el problema μ acoplándolo con los Higgses, $\nu^c H_1 H_2$. Cuando el sneutrino adquiere un VEV, el término μ se genera dinámicamente. Además, si imponemos que el superpotencial solo contenga parámetros adimensionales, la única escala del potencial escalar es la escala EW producida por los parámetros soft. La cualidad de poseer solo parámetros adimensionales en el superpotencial se puede motivar por ejemplo desde el punto de vista de la teoría de cuerdas, donde a baja energía los términos de masa están prohibidos. Podríamos decir que esta propuesta pretende intentar responder a la pregunta

crucial: ¿cuál es la teoría de campos que describe la física por debajo de la escala de Planck? Es una propuesta que está por un lado inspirada por los resultados experimentales y por otro intenta satisfacer todos las exigencias teóricas que la convierten en un modelo natural, simple, y factible de ser el límite de una hipotética teoría completa. El modelo ha sido publicado con el nombre μ from ν Supersymmetric Standard Model ($\mu\nu$SSM).

En el $\mu\nu$SSM R-parity no se conserva y por tanto el neutralino deja de ser un buen candidato para materia oscura. Habría que usar otros candidatos interesantes tales como el gravitino o el axión. Sin embargo, también presentaremos un límite en el que haciendo algunos parámetros iguales a cero introducimos conservación de R-parity y de nuevo el neutralino vuelve a ser candidato a materia oscura.

1.1 Contenidos de la tesis

Este trabajo de tesis esta dividido en cinco Capítulos.

En el siguiente introducimos los conceptos relevantes para este trabajo. Primero damos una breve introducción a SUSY, y después resumimos la situación actual con respecto a la naturaleza de la materia oscura del universo y su posible detección.

El tercero está dedicada a la presentación de algunos de los resultados originales de esta tesis [1, 2]. En concreto, después de introducir el NMSSM en la primera Sección y estudiado la sección eficaz neutralino-protón en la segunda, en la tercera Sección se presenta el análisis fenomenológico que hemos llevado a cabo del modelo. Primero estudiamos el espacio de parámetros e imponemos las cotas que vienen de física de aceleradores. Después identificamos las zonas donde la sección eficaz de detección de materia oscura neutralino-protón está en el rango asequible a los experimentos. En la cuarta Sección incluimos el cálculo de la densidad reliquia comparándola con los resultados experimentales de WMAP y aquellos que se obtienen de observaciones astrofísicas. Calculamos también el momento magnético anómalo del muón y cotas de física de sabores como el BR($b \to s\gamma$), siempre comparándolos con los resultados experimentales. Finalmente, completamos el análisis de la sección eficaz comenzado en la Sección anterior, imponiendo sobre la misma todas las cotas experimentales antes mencionadas.

El cuarto Capítulo está dedicado a presentar nuestra propuesta de un nuevo modelo SUSY, el $\mu\nu SSM$ [3]. En ella se utilizan los sneutrinos right-handed para dar solución

al problema μ del SM. La inclusión de sneutrinos right-handed es natural cuando quiere agregarse en el modelo la descripción de la física de neutrinos. Después de hacer una breve reseña sobre la misma en la primera Sección, en la siguiente describimos el modelo. Así mismo también estudiamos un caso particular en el que R-parity se sigue conservando [4]. La última Sección la dedicamos a describir futuros proyectos relacionados con esta propuesta.

Finalmente, el quinto y último Capítulo esta dedicado a las conclusiones finales de la tesis.

Chapter 2

General Overview

In this Chapter we introduce the two relevant topics for our discussion: SUSY and Dark Matter. In Section 2.1 we give a brief introduction to SUSY, and in particular how to build a SUSY model. In Section 2.2 we discuss dark matter from a theoretical and experimental point of view.

2.1 Supersymmetry

In this Section we will summarize how to build SUSY models in four dimensions. For that we will introduce the different SUSY supermultiplets and, working in components, we will arrive to the SUSY Lagrangian. The reader can find a lot of reviews in the literature about SUSY, see for example [5] and references therein.

2.1.1 Supersymmetric models

It is possible to build two kinds of supermultiplets: the gauge supermultiplet and the chiral supermultiplet. The propagating degrees of freedom in a gauge supermultiplet are a massless gauge boson field A^a_μ and a two-component Weyl fermion gaugino λ^a. The index a here runs over the adjoint representation of the gauge group ($a = 1 \dots 8$ for $SU(3)_C$ colour gluons and gluinos; $a = 1, 2, 3$ for $SU(2)_L$ weak isospin; $a = 1$ for $U(1)_Y$ weak hypercharge). Since the SUSY algebra must close off shell, auxiliary fields D^a must also be present in the supermultiplets.

For the chiral supermultiplet the propagating degrees of freedom are ϕ_i complex

scalars and ψ_i Weyl spinors. The index i runs over all flavour and family degrees of freedom. ϕ_i and ψ_i contain the same degrees of freedom on shell, but as in the case of the gauge supermultiplet, in the chiral supermultiplet there must also be an auxiliary field, F_i, which does not propagate.

The free Lagrangian for a gauge supermultiplet is then

$$\mathcal{L}_{\text{gauge}} = -\frac{1}{4}F^a_{\mu\nu}F^{\mu\nu a} - i\lambda^{\dagger a}\overline{\sigma}^\mu D_\mu \lambda^a + \frac{1}{2}D^a D^a, \tag{2.1.1}$$

where

$$F^a_{\mu\nu} = \partial_\mu A^a_\nu - \partial_\nu A^a_\mu - g f^{abc} A^b_\mu A^c_\nu \tag{2.1.2}$$

is the usual Yang-Mills field strength, and

$$D_\mu \lambda^a = \partial_\mu \lambda^a - g f^{abc} A^b_\mu \lambda^c \tag{2.1.3}$$

is the covariant derivative of the gaugino field.

The free chiral Lagrangian is

$$\mathcal{L}_{\text{chiral}} = -D^\mu \phi^{*i} D_\mu \phi_i - i\psi^{\dagger i}\overline{\sigma}^\mu D_\mu \psi_i + F^{*i}F_i, \tag{2.1.4}$$

where the covariant derivatives are:

$$D_\mu \phi_i = \partial_\mu \phi_i + igA^a_\mu (T^a \phi)_i, \tag{2.1.5}$$

$$D_\mu \phi^{*i} = \partial_\mu \phi^{*i} - igA^a_\mu (\phi^* T^a)^i, \tag{2.1.6}$$

$$D_\mu \psi_i = \partial_\mu \psi_i + igA^a_\mu (T^a \psi)_i, \tag{2.1.7}$$

and we sum over repeated indices i (not to be confused with the suppressed spinor indices), with the convention that fields ϕ_i and ψ_i always carry lowered indices, while their conjugates always carry raised indices.

The most general set of renormalizable interactions for these fields can be written in the simple form

$$\mathcal{L}_{\text{int}} = -\frac{1}{2}W^{ij}\psi_i\psi_j + W^i F_i + \text{c.c.}, \tag{2.1.8}$$

where W^{ij} and W^i are some functions of the bosonic fields with dimensions of (mass) and (mass)^2 respectively, and "c.c." henceforth stands for complex conjugate. In other words, W^{ij} is *analytic* (or *holomorphic*) in the complex fields ϕ_k.

We can write

$$W^{ij} = M^{ij} + y^{ijk}\phi_k, \tag{2.1.9}$$

where M^{ij} is a symmetric mass matrix for the fermion fields, and y^{ijk} is a Yukawa coupling of a scalar ϕ_k and two fermions $\psi_i\psi_j$ which must be totally symmetric under interchange of i, j, k. It is convenient to write

$$W^{ij} = \frac{\delta^2}{\delta\phi_i\delta\phi_j}W, \tag{2.1.10}$$

where we have introduced a very useful object

$$W = \frac{1}{2}M^{ij}\phi_i\phi_j + \frac{1}{6}y^{ijk}\phi_i\phi_j\phi_k, \tag{2.1.11}$$

which is called the *superpotential*, and

$$W^i = \frac{\delta W}{\delta\phi_i} = M^{ij}\phi_j + \frac{1}{2}y^{ijk}\phi_j\phi_k\,. \tag{2.1.12}$$

The auxiliary fields F_i and F^{*i} can be eliminated using their classical equations of motion. The part of $\mathcal{L}_{\rm chiral} + \mathcal{L}_{\rm int}$ that contains the auxiliary fields is $F_iF^{*i} + W^iF_i + W_i^*F^{*i}$, leading to the equations of motion

$$F_i = -W_i^*; \qquad\qquad F^{*i} = -W^i\,. \tag{2.1.13}$$

Thus the auxiliary fields are expressible algebraically (without any derivatives) in terms of the scalar fields. After making the replacement eq. (2.1.13) in $\mathcal{L}_{\rm chiral}+\mathcal{L}_{\rm int}$, we obtain the Lagrangian

$$\mathcal{L} = -D^\mu\phi^{*i}D_\mu\phi_i - i\psi^{\dagger i}\overline{\sigma}^\mu D_\mu\psi_i - \frac{1}{2}\left(W^{ij}\psi_i\psi_j + W^{*ij}\psi^{\dagger i}\psi^{\dagger j}\right) - W^iW_i^*. \tag{2.1.14}$$

(Since F_i and F^{*i} appear only quadratically in the action, the result of instead doing a functional integral over them at the quantum level has precisely the same effect.) Now that the non-propagating fields F_i, F^{*i} have been eliminated, it is clear from eq. (2.1.14) that the scalar potential for the theory is just given in terms of the superpotential by:

$$\begin{aligned} V(\phi,\phi^*) = W^iW_i^* = F_iF^{*i} = M^*_{ik}M^{kj}\phi^{*i}\phi_j \\ +\frac{1}{2}M^{in}y^*_{jkn}\phi_i\phi^{*j}\phi^{*k} + \frac{1}{2}M^*_{in}y^{jkn}\phi^{*i}\phi_j\phi_k + \frac{1}{4}y^{ijn}y^*_{kln}\phi_i\phi_j\phi^{*k}\phi^{*l}\,. \end{aligned} \tag{2.1.15}$$

The full Lagrangian for a renormalizable SUSY theory is

$$\begin{aligned} \mathcal{L} \;=\; & \mathcal{L}_{\rm gauge} + \mathcal{L}_{\rm chiral} \\ & -\sqrt{2}g\left[(\phi^*T^a\psi)\lambda^a + \lambda^{\dagger a}(\psi^\dagger T^a\phi)\right] \\ & +g(\phi^*T^a\phi)D^a. \end{aligned} \tag{2.1.16}$$

Replacing the auxiliary fields in eq. (2.1.16), using the equation of motion for D^a,

$$D^a = -g(\phi^* T^a \phi), \tag{2.1.17}$$

one finds that the complete scalar potential is (recall $\mathcal{L} \supset -V$):

$$V(\phi_l, \phi_l^*) = F^{*i} F_i + \frac{1}{2}\sum_a D^a D^a = W_i^* W^i + \frac{1}{2}\sum_G \sum_a \sum_{l,m} g_G^2 (\phi^{*l} T^a \phi_l)(\phi^{*m} T^a \phi_m). \tag{2.1.18}$$

We consider several chiral multiplets level by l, m. The two types of terms in this expression are called "F-term" and "D-term" contributions, respectively. In the second term in eq. (2.1.18), we have now written an explicit sum $\sum_G$ to cover the case that the gauge group has several distinct factors with different gauge couplings g_G. [For instance, in the MSSM the three factors $SU(3)_C$, $SU(2)_L$ and $U(1)_Y$ have different gauge couplings g_3, g and g'.] Since $V(\phi, \phi^*)$ is a sum of squares, it is always greater than or equal to zero for every field configuration. It is a very interesting and unique feature of SUSY theories that the scalar potential is completely determined by the *other* interactions in the theory. The F-terms are fixed by Yukawa couplings and fermion mass terms, and the D-terms are fixed by the gauge interactions.

With the above description we can build any SUSY model in four dimension. Let us remark that one expect that about 10^{16} GeV a grand unified theory (GUT) containing the SM should exist. In this sense the SUSY models that we will construct are valid up to that scale, and the usual renormalization group equations (RGEs) can be used.

2.1.2 The MSSM

We briefly describe here the minimal SUSY extension of the SM, the MSSM. For details see for example [5].

The superpotential for the MSSM is given by

$$W = \epsilon_{ij}\left(Y_u\, H_2^j\, Q^i\, u + Y_d\, H_1^i\, Q^j\, d + Y_e\, H_1^i\, L^j\, e\right) - \epsilon_{ij}\mu\, H_1^i H_2^j, \tag{2.1.19}$$

where i, j are SU(2) index, and $\epsilon_{12} = 1$. The objects H_1, H_2, Q, L, u, d, e appearing in eq. (2.1.19) are chiral superfields corresponding to the chiral supermultiplets in Table 2.1 (for completeness we also show in table 2.2 the gauge supermultiplets). The dimensionless Yukawa coupling parameters Y_u, Y_d, Y_e are 3×3 matrices in family space. Here we have suppressed the gauge $SU(3)_C$ colour and family indices.

Table 2.1: Chiral supermultiplets in the MSSM. In our convention $Q_{\rm EM} = T_3 + Y$.

Names		spin 0	spin 1/2	$SU(3)_C$, $SU(2)_L$, $U(1)_Y$
squarks, quarks	Q^T	$(\tilde{u}_L\ ,\ \tilde{d}_L)$	$(u_L\ ,\ d_L)$	$(\mathbf{3},\ \mathbf{2}\ ,\ \frac{1}{6})$
($\times$3 families)	u	$\tilde{u}_R^*$	$u_R^\dagger$	$(\overline{\mathbf{3}},\ \mathbf{1},\ -\frac{2}{3})$
	d	$\tilde{d}_R^*$	$d_R^\dagger$	$(\overline{\mathbf{3}},\ \mathbf{1},\ \frac{1}{3})$
sleptons, leptons	L^T	$(\tilde{\nu}\ \ \tilde{e}_L)$	$(\nu\ \ e_L)$	$(\mathbf{1},\ \mathbf{2}\ ,\ -\frac{1}{2})$
($\times$3 families)	e	$\tilde{e}_R^*$	$e_R^\dagger$	$(\mathbf{1},\ \mathbf{1},\ 1)$
Higgs, Higgsinos	H_2^T	$(H_2^+\ \ H_2^0)$	$(\tilde{H}_2^+\ \ \tilde{H}_2^0)$	$(\mathbf{1},\ \mathbf{2}\ ,\ +\frac{1}{2})$
	H_1^T	$(H_1^0\ \ H_1^-)$	$(\tilde{H}_1^0\ \ \tilde{H}_1^-)$	$(\mathbf{1},\ \mathbf{2}\ ,\ -\frac{1}{2})$

Table 2.2: Gauge supermultiplets in the MSSM.

Names	spin 1/2	spin 1	$SU(3)_C$, $SU(2)_L$, $U(1)_Y$
gluinos, gluons	$\tilde{g}$	g	$(\mathbf{8},\ \mathbf{1}\ ,\ 0)$
winos, W bosons	$\tilde{W}^\pm\ \ \tilde{W}^0$	$W^\pm\ \ W^0$	$(\mathbf{1},\ \mathbf{3}\ ,\ 0)$
Bino, B boson	$\tilde{B}^0$	B^0	$(\mathbf{1},\ \mathbf{1}\ ,\ 0)$

On the other hand, as discussed in the introduction, soft terms appear in the Lagrangian after local SUSY is broken. The most general soft breaking terms are:

$$\begin{aligned} -\mathcal{L}_{\rm soft} &= m_{\tilde{Q}}^2\,|\tilde{Q}|^2 + m_{\tilde{U}}^2\,|\tilde{u}|^2 + m_{\tilde{D}}^2\,|\tilde{d}|^2 + m_{\tilde{L}}^2\,|\tilde{L}|^2 + m_{\tilde{E}}^2\,|\tilde{e}|^2 \\ &+ m_{H_1}^2\,|H_1|^2 + m_{H_2}^2\,|H_2|^2 + \\ &+ \epsilon_{ij}\left(A_u\,Y_u\,H_2^j\,\tilde{Q}^i\,\tilde{u} + A_d\,Y_d\,H_1^i\,\tilde{Q}^j\,\tilde{d} + A_e\,Y_e\,H_1^i\,\tilde{L}^j\,\tilde{e} + \text{H.c.}\right) \\ &+ \left(-\epsilon_{ij} B\mu H_1^i H_2^j + \text{H.c.}\right) \\ &+ \frac{1}{2}\left(M_3\,\lambda_3\,\lambda_3 + M_2\,\lambda_2\,\lambda_2 + M_1\,\lambda_1\,\lambda_1 + \text{H.c.}\right). \end{aligned} \tag{2.1.20}$$

In addition to terms from $L_{\rm soft}$, the three-level Higgs potential receives the usual D and

F term contributions. Bringing together all the terms, one obtains:

$$\begin{aligned} V &= (|\mu|^2 + m_{H_2}^2)(|H_2^0|^2 + |H_2^+|^2) + (|\mu|^2 + m_{H_1}^2)(|H_1^0|^2 + |H_1^-|^2) \\ &\quad + B\mu\,(H_2^+ H_1^- - H_2^0 H_1^0) + \text{c.c.} \\ &\quad + \frac{1}{8}(g^2 + g'^2)(|H_2^0|^2 + |H_2^+|^2 - |H_1^0|^2 - |H_1^-|^2)^2 \\ &\quad + \frac{1}{2} g^2 |H_2^+ H_1^{0*} + H_2^0 H_1^{-*}|^2, \end{aligned} \tag{2.1.21}$$

and therefore the neutral Higgs potential relevant for the EW breaking is:

$$\begin{aligned} V &= (|\mu|^2 + m_{H_2}^2)|H_2^0|^2 + (|\mu|^2 + m_{H_1}^2)|H_1^0|^2 \\ &\quad - B\mu\, H_2^0 H_1^0 + \text{c.c.} \\ &\quad + \frac{1}{8}(g^2 + g'^2)(|H_2^0|^2 - |H_1^0|^2)^2. \end{aligned} \tag{2.1.22}$$

Concerning the SUSY spectrum, the Higgsinos and electroweak gauginos mix with each other because of the effects of EW breaking. The neutral Higgsinos ($\tilde{H}_2^0$ and $\tilde{H}_1^0$) and the neutral gauginos ($\tilde{B}$, $\tilde{W}^0$) combine to form four neutral mass eigenstates called *neutralinos*. The charged Higgsinos ($\tilde{H}_2^+$ and $\tilde{H}_1^-$) and winos ($\tilde{W}^+$ and $\tilde{W}^-$) mix to form two mass eigenstates with charge ± 1 called *charginos*. We will denote the neutralino and chargino mass eigenstates by $\tilde{\chi}_i^0$ $(i = 1, 2, 3, 4)$ and $\tilde{\chi}_i^\pm$ $(i = 1, 2)$. By convention, these are labelled in ascending order, so that $m_{\tilde{\chi}_1^0} < m_{\tilde{\chi}_2^0} < m_{\tilde{\chi}_3^0} < m_{\tilde{\chi}_4^0}$ and $m_{\tilde{\chi}_1^\pm} < m_{\tilde{\chi}_2^\pm}$. The lightest neutralino, $\tilde{\chi}_1^0$, is often the LSP, a therefore a good cold dark matter candidate. Here we will describe first the mass spectrum and mixing of the neutralinos and charginos in the MSSM.

In the gauge-eigenstate basis $\psi^0 = (\tilde{B}, \tilde{W}^0, \tilde{H}_1^0, \tilde{H}_2^0)$, the neutralino mass terms in the Lagrangian are

$$\mathcal{L} \supset -\frac{1}{2}(\psi^0)^T \mathbf{M}_{\tilde{N}} \psi^0 + \text{c.c.} \tag{2.1.23}$$

where

$$\mathbf{M}_{\tilde{\chi}^0} = \begin{pmatrix} M_1 & 0 & -\cos\beta\,\sin\theta_W\, m_Z & \sin\beta\,\sin\theta_W\, m_Z \\ 0 & M_2 & \cos\beta\,\cos\theta_W\, m_Z & -\sin\beta\,\cos\theta_W\, m_Z \\ -\cos\beta\,\sin\theta_W\, m_Z & \cos\beta\,\cos\theta_W\, m_Z & 0 & -\mu \\ \sin\beta\,\sin\theta_W\, m_Z & -\sin\beta\,\cos\theta_W\, m_Z & -\mu & 0 \end{pmatrix}. \tag{2.1.24}$$

The resulting masses for the charginos are

$$m_{\tilde{\chi}_{1,2}^\pm} = \frac{1}{2}[M^2 + \mu^2 + 2M_W^2 \mp \sqrt{(M^2 + \mu^2 + 2M_W^2)^2 - 4|\mu M_2 - M_W^2 \sin 2\beta|^2}\,]\,. \tag{2.1.25}$$

On the other hand, concerning the squarks and sleptons, the mass eigenstates are obtained by diagonalization of 6×6 mass matrix for up squarks, down squarks and charged sleptons. However most of the mixing terms are very small and it is a good approximation to consider only 2×2 mass matrix mixing left and right handed parts of a giving generation. The mixing will be really important only for the third generation, and then the relevant matrices are:

$$m^2_{\tilde{t}} = \begin{pmatrix} (m^2_{\tilde{Q}} + m^2_{\tilde{t}} + \frac{1}{6}(4M^2_W - M^2_Z)\cos 2\beta & m_t(A_t - \mu \cot \beta) \\ m_t(A_t - \mu \cot \beta) & m^2_{\tilde{Q}} + m^2_{\tilde{t}} - \frac{2}{3}(M^2_W - M^2_Z)\cos 2\beta) \end{pmatrix},$$

$$m^2_{\tilde{b}} = \begin{pmatrix} (m^2_{\tilde{Q}} + m^2_{\tilde{t}} + \frac{1}{6}(4M^2_W - M^2_Z)\cos 2\beta & m_t(A_t - \mu \cot \beta) \\ m_t(A_t - \mu \cot \beta) & m^2_{\tilde{Q}} + m^2_{\tilde{t}} - \frac{2}{3}(M^2_W - M^2_Z)\cos 2\beta) \end{pmatrix},$$

$$m^2_{\tilde{\tau}} = \begin{pmatrix} (m^2_{\tilde{L}} + m^2_{\tau} - \frac{1}{2}(2M^2_W - M^2_Z)\cos 2\beta & m_\tau(A_\tau - \mu \tan \beta) \\ m_\tau(A_\tau - \mu \tan \beta) & m^2_{\tilde{\tau}_R} + m^2_{\tilde{\tau}} + (M^2_W - M^2_Z)\cos 2\beta) \end{pmatrix}.$$

2.2 Dark Matter

The presence of dark matter [6] in galaxies is the most plausible explanation for their anomalous rotation curves. In this sense, the dark matter provides a potentially important relation between particle physics and cosmology, since only elementary particles are reliable candidates for the dark matter in the Universe. In particular we will see that baryonic objects, such as e.g. gas, brown dwarfs, etc., can be components of the dark matter, but more candidates are needed. The reason being that they cannot be present in the right amount to explain the observed matter density of the Universe, $\Omega h^2 \sim 0.1$.

Fortunately, particle physics, and mainly extensions of the SM offer candidates for dark matter. Indeed, detecting non-baryonic dark matter in the Universe might be a signal for new physics beyond the SM. We will see that very interesting and plausible candidates for dark matter are Weakly Interacting Massive Particles (WIMPs), since long-lived or stable WIMPs can be left over from the Big Bang in sufficient number to account for a significant fraction of relic matter density. As suggested in 1985 by Goodman and Witten [7], and also by Wasserman [8], this raises the hope of detecting relic WIMPs directly.

It is important to observe that SUSY, whose original motivation has nothing to do with the dark matter problem, might solve it. In SUSY models, the so-called R-parity is often imposed in order to avoid fast proton decay or lepton number violation. This yields important phenomenological implications. SUSY particles are produced or destroyed only in pairs and therefore the lightest supersymmetric particle (LSP) is absolutely stable, implying that it might constitute a possible candidate for dark matter.

In SUSY models the fermionic partner of the B^0 mixes with the fermionic partner of the W^0, the two neutral Higgs bosons, and the singlets in the theory. Therefore one has particles called neutralinos, $\tilde{\chi}_i^0$, with $i = 1, ..., 4$ in the MSSM and $i = 1, ..., 5$ in the NMSSM. The lightest neutralino in the model, $\tilde{\chi}_1^0$, will be the dark matter candidate [9].

The fact that the LSP turns out to be an electrically neutral particle (also with no strong interactions) is welcome since otherwise it would bind to nuclei and would be excluded as a candidate for dark matter from unsuccessful searches for exotic heavy isotopes.

In the next Subsection we will concentrate on the dark matter problem, and its solutions. For a recent review, see [10].

2.2.1 The dark matter problem

If the mass distribution of a galaxy can be approximated as spherical or ellipsoidal, Newton's law implies that $v^2(r)/r = GM(r)/r^2$, where $v(r)$ is the average orbital velocity of an object orbiting around the galaxy, G is the Newton's constant and $M(r)$ is the total mass inside the orbit. Therefore

$$v(r) = \sqrt{\frac{G\ M(r)}{r}} \tag{2.2.26}$$

can be used as an estimate. Thus if the mass of the galaxy is concentrated in its visible part, one would expect $v(r) = \sqrt{GM_{vis}(r)/r} \propto 1/\sqrt{r}$ for distances far beyond the visible radius.

Instead, astronomers, by means of the Doppler effect, observe that the velocity rises towards a constant value $v_c \approx 100$ to 200 km s^{-1}. An example of this can be seen in Fig. 2.1 (from Ref. [11]), where the rotation curve of M33, one of the about 45 galaxies which form our small cluster, the Local Group, is shown. For comparison, the expected velocity from luminous disk is also shown. This phenomenon has already been observed for about a thousand spiral galaxies [12, 13, 14], and in particular also for our galaxy, the Milky Way. Although this observation is more problematic in galaxies other than spirals, such as ellipticals, dwarf irregulars, dwarf spheroidals, lenticulars, etc., they also produce similar results [14, 15, 16].

The most common explanation for these flat rotation curves is to assume that disk galaxies are immersed in extended dark matter halos. Thus for large distances $M(r)/r$ is generically constant because the mass interior to r increases linearly with r, $M_{tot}(r) = G^{-1}v_c^2 r$. In fact, a self-gravitating ball of ideal gas at an uniform temperature of $kT = \frac{1}{2}m_{\rm DM}v_c^2$, where $m_{\rm DM}$ is the mass of one dark matter particle, would have this mass profile [17].

Therefore the above analysis of rotation curves implies that 90% of the mass in galaxies is dark.

Whereas current observations of luminous matter in galaxies determine $\Omega_{\rm lum} \lesssim 0.01$, analyses of rotation curves imply in fact $\Omega \approx 0.1$. Let us recall that $\Omega = \rho/\rho_c$ is the present-day mass density averaged over the Universe, ρ, in units of the critical density,

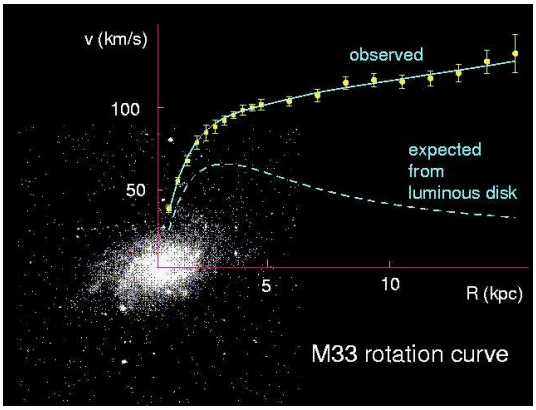

Figure 2.1: Observed rotation curve of the nearby dwarf spiral galaxy M33, superimposed on its optical image.

$\rho_c = 10^{-5} h^2$ GeV cm^{-3}, with $h \sim 0.7$. In fact, the previous value, $\Omega \approx 0.1$, is really a lower bound, since almost all rotation curves remain flat out to the largest values of r where one can still find objects orbiting galaxies. We do not really know how much further the dark matter halos of these galaxies extend (see e.g. Fig. 2.1). Thus we can conclude that galactic rotation curves imply $\Omega \gtrsim 0.1$.

All these analyses, including those for cluster of galaxies and large scale flows [18], favour a value $\Omega \approx 0.2 - 0.3$. Thus the following astrophysical bounds are commonly used in the literature:

$$0.1 \lesssim \Omega_{\rm DM} h^2 \lesssim 0.3 \ . \tag{2.2.27}$$

In particular, the (cold) dark matter range

$$0.095 \lesssim \Omega_{\rm DM} h^2 \lesssim 0.112 \ , \tag{2.2.28}$$

can be deduced from the recent data obtained by the WMAP satellite [19].

To conclude this Subsection, we refer that a small number of authors suggests that dark matter is not really necessary to explain the galaxies rotation curves [16]. Basically their approach consists of modifying Newton's law at galactic scales. However, these attempts are not only rather *ad hoc* in general (the authors impose specific values for the free parameters of the theory in order to reproduce *some* of the rotation curves that have been observed) but also insufficient to account for the necessity of dark matter in scales larger than galactic ones [20] (values of the parameters necessary to reproduce galactic rotation curves cannot reproduce the observations at larger scales).

Recently, the authors of Ref. [21], using the Sloan Digital Sky Survey, have shown the first observational evidence that the halo density declines as $1/r^3$, as predicted by cold dark matter cosmological models. Alternative theories of gravity are in contradiction with this result. Needles to say, the recent observations concerning the bullet cluster [22] go also in this direction.

2.2.2 Dark matter candidates

The scenario of Big-Bang nucleosynthesis, which explains the origin of the elements after the Big Bang, taking into account measured abundances of helium, deuterium and lithium, sets a limit to the number of baryons that can exist in the Universe, namely $\Omega_{\rm baryon}h^2 < 0.05$. This density is clearly small to account for the whole dark matter in the Universe (see bounds in eq. (2.2.27)).

The conclusion is that baryonic objects are likely components of the dark matter but more candidates are needed. This result is also confirmed by observations of MACHOs in our galactic halo through their gravitational lensing effect on the light emitted by stars. Their contribution to the dark matter density is small. Thus non-baryonic matter is required in the Universe.

Particle physics provides non-baryonic candidates for dark matter. In principle, the standard ones are 'axions', 'neutrinos' and 'neutralinos' with masses of the order of 10^{-5} eV, 30 eV and 100 GeV, respectively. In fact although neutrinos are the only candidates which are known to exist, there is now significant evidence against them as the bulk of the dark matter. On the one hand, their experimental masses seem to be too small, below 1 eV, as to be cosmologically significant since $\Omega_\nu \approx m_\nu/30$ eV [23]. On the other hand, neutrinos belong to the so-called 'hot' dark matter because they were moving with relativistic velocities at the time the galaxies started to form. But hot dark matter cannot reproduce correctly the observed structure in the Universe. A Universe dominated by neutrinos would form large structures first, and the small structures later by fragmentation of the larger objects. Such a Universe would produced a 'top-down' cosmology, in which the galaxies form last and quite recently. This time scale seems incompatible with our present ideas of galaxy evolution. This lead to fade away the initial enthusiasm for a neutrino-dominated Universe. Hence, many cosmologists now favour an alternative model, one in which the particles dominating the Universe are 'cold' (non-relativistic) rather than hot. This is the case of the axions and neutralinos. Both are well motivated by extensions of the SM, because they are crucial to solve

important theoretical problems of this model.

Axions are spin 0 particles with zero charge associated with the spontaneous breaking of the global $U(1)$ Peccei-Quinn symmetry, which was introduced to dynamically solve the strong CP problem [24]. Typically the axion has a very large lifetime, larger than the age of the Universe by many orders of magnitude. As a consequence, the axion is a candidate for dark matter [25]. Axions would have been produced copiously in the Big Bang, they were never in thermal equilibrium and are always nonrelativistic (i.e. they are cold dark matter). In addition the mass of the axion has to be about 10^{-5} eV if the axion is to be a significant component of the dark matter.

Concerning the WIMPs, they were in thermal equilibrium with the SM particles in the early Universe, and decoupled when they became non-relativistic, via the following process. When the temperature T of the Universe was larger than the mass of the WIMP, the number density of WIMPs and photons was roughly the same, $n \propto T^3$, and the WIMP was annihilating with its own antiparticle into lighter particles and *vice versa*. However, after the temperature dropped below the mass of the WIMP, m, its number density dropped exponentially, $n \propto e^{-m/T}$, because only a small fraction of the light particles mentioned above had sufficient kinetic energy to create WIMPs. As a consequence, the WIMP annihilation rate $\Gamma = \langle \sigma_{ann} v \rangle n$ dropped below the expansion rate of the Universe, $\Gamma \lesssim H$. At this point WIMPs came away, they could not annihilate, and their density has remain stable (freeze-out typically occurs at $T_F \approx m/20$). This can be obtained using the Boltzmann equation, which describes the time evolution of the number density $n(t)$ of WIMPs

$$\frac{dn}{dt} + 3Hn = -\langle \sigma_{ann} v \rangle \left[(n)^2 - (n^{eq})^2 \right] \ , \tag{2.2.29}$$

where H is the Hubble expansion rate, σ_{ann} is the total cross section for annihilation of a pair of WIMPs into standard model particles, v is the relative velocity between the two WIMPs, $\langle ... \rangle$ denotes thermal averaging, and n^{eq} is the number density of WIMPs in thermal equilibrium.

One can discuss qualitatively the solution using the freeze-out condition $\Gamma = \langle \sigma_{ann} v \rangle_F n = H$. Then, the current WIMP $\Omega h^2 = (\rho/\rho_c) h^2$, turns out to be

$$\Omega h^2 \simeq \frac{3 \times 10^{-27} \text{ cm}^3 \text{ s}^{-1}}{\langle \sigma_{ann} \ v \rangle} \ , \tag{2.2.30}$$

where the numerator is obtained using the value of the temperature of the cosmic background radiation, the Newton's constant, etc. As expected from the above discussion, the WIMP relic density decreases with increasing annihilation cross section

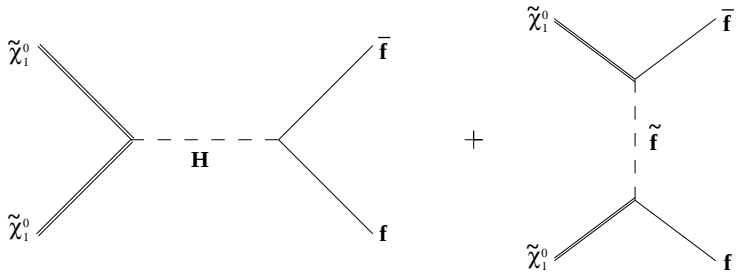

Figure 2.2: Feynman diagrams contributing to early-Universe neutralino ($\tilde{\chi}_1^0$) annihilation into fermions through neutral Higgses ($H \equiv H, h, A$) and squarks and sleptons ($\tilde{f}$).

Now we can easily understand why WIMPs are so good candidates for dark matter. If a new particle with weak interactions exists in Nature, its cross section will be $\sigma \simeq \alpha^2/m_{\rm weak}^2$, where $\alpha \simeq \mathcal{O}(10^{-2})$ is the weak coupling and $m_{\rm weak} \simeq \mathcal{O}(100$ GeV) is a mass of the order of the W gauge boson mass. Thus one obtains $\sigma \approx 10^{-9}$ GeV$^{-2} \approx 1$ pb (recall that in natural units 1 GeV$^{-2} = 0.389 \times 10^{-27}$ cm$^2 = 0.389 \times 10^9$ pb). Since at the freeze-out temperature the velocity is a significant fraction of the speed of light ($v^2 \approx c^2/20$), one obtains $< \sigma_{ann}\ v > \approx 10^{-26}$ cm^3 s^{-1}. Remarkably, this number is close to the value that we need in eq. (2.2.30) in order to obtain the observed density of the Universe. This is a possible hint that new physics at the weak scale provides us with a reliable solution to the dark matter problem, *and also a qualitative improvement with respect to the axion dark matter case*, where a small mass for the axion about 10^{-5} eV has to be postulated.

SUSY is a theory that introduces new physics precisely at the weak scale, and that, as discussed above, predicts a new particle, the neutralino, which could be stable. These are the reasons to consider the neutralino as a very serious candidate for the sought-after dark matter. Concerning the annihilation cross section contributing to the density of the Universe in eq. (2.2.30), there are numerous final states into which the neutralino can annihilate [26]. The most important of these are the two body final states which occur at the tree level. These are fermion-antifermion pairs $f\bar{f}$ (where f are the standard model quarks and leptons), as those shown in Fig. 2.2 [27]-[31]. Others are weak gauge bosons pairs W^+W^-, Z^0Z^0[29, 31, 32], and those containing Higgs bosons such as W^+H^-, W^-H^+, Z^0A, Z^0H, Z^0h, H^+H^- and all six combinations of A, h, H [29, 31, 32, 33]. Different subtleties of the analysis have been discussed in

Refs. [34, 35]. The annihilation cross section is of the form

$$\sigma_{ann} \simeq N_{ann} m^2_{\tilde{\chi}^0_1} |\mathcal{A}_{ann}|^2 \ , \tag{2.2.31}$$

where $\mathcal{A}_{ann}$ is the amplitude which depends on the dynamics of the collision and N_{ann} is the number of annihilation channels. Generically $\mathcal{A}_{ann} \sim 1/\mathcal{M}^2$, where $\mathcal{M}$ is the mass of the particles mediating the interaction. Thus $\sigma_{ann} \sim 1/m^2_{\tilde{\chi}^0_1}$, and therefore in order to satisfy the upper bound in eq. (2.2.27), moderate values of the LSP mass are necessary. There are several exceptions to this rule, let us mention here one of them which is particularly interesting.

In principle using the above discussed neutralino annihilation cross section is sufficient, since the effects of heavier particles are suppressed by the Boltzmann factor. However, the next to lightest supersymmetric particle (NLSP) may lie near in mass to the LSP so that both particles freeze out of equilibrium at approximately the same temperature. Thus the NLSP should be included in principle in the reaction network, since coannihilation channels NLSP-LSP (and also channels NLSP-NLSP) might be now relevant [34]. In fact, this is only when $(m_{\rm NLSP} - m_{\tilde{\chi}^0_1})/m_{\tilde{\chi}^0_1} \lesssim 0.2$, since the NLSP number density is suppressed by $e^{-(m_{\rm NLSP} - m_{\tilde{\chi}^0_1})/T_F}$ relative to the neutralino number density, where we recall that $T_F \approx m_{\tilde{\chi}^0_1}/20$. Actually, special regions of the parameter space of the MSSM fulfil this condition, and therefore including coannihilations is important.

Taking into account all the above comments concerning SUSY scenarios, it is possible to see that significant regions of the parameter space of the MSSM produce values of the cross section in the interesting range mentioned below Eq. (2.2.30) [10].

On the other hand, since neutralinos, or WIMPs in general, interact with ordinary matter with roughly weak strength, their presence in galactic scales, and in particular in our galaxy, raises the hope of detecting relic WIMPs directly in a detector by observing their scattering on target nuclei through nuclear recoils. This will be the subject of the next Subsection.

2.2.3 Dark matter detection

Given the discussion in the previous Subsection, one can say that WIMPs, and in particular neutralinos, are good particle candidates for dark matter. As a matter of fact, we saw that WIMPs and axions are particularly interesting. Since the former can be left over from the Big Bang in sufficient number to account for the relic matter density

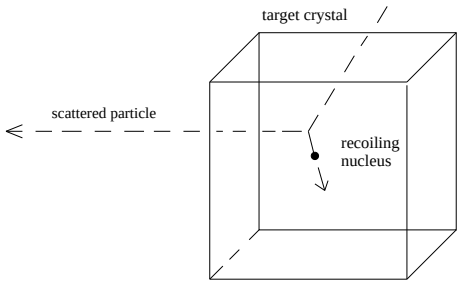

Figure 2.3: Elastic scattering of a dark matter particle with an atomic nucleus in a detector.

in a natural way, we will concentrate on them. Thus we will review in this Subsection current and projected experiments for detecting WIMPs directly by observing their scattering on the material in a detector.

As discussed above, if neutralinos, or WIMPs in general, are the bulk of the dark matter, they will form not only a background density in the Universe, but also will cluster gravitationally with ordinary stars in the galactic halos. In particular they will be present in our own galaxy, the Milky Way. This raises the hope of detecting relic WIMPs directly, by experiments on the Earth. In particular, through scattering with the material in a detector. In fact general studies of the possibility of dark matter detection began around 1982. Since the detection will be on the Earth we need to know the properties of our galaxy in order to be sure that such a detection is feasible.

As a matter of fact, rotation curves are much better known for external galaxies than for ours, due to the position of the Earth inside the galaxy. In any case, analyses have been carried out with the conclusion that indeed the Milky Way contains large amounts of dark matter [36]. Besides, some observational evidence seems to point at a roughly spherical distribution of dark matter in the galaxy. At the position of the Sun, around 8.5 kpc away from the galactic center, the mean density of elementary particles trapped in the gravitational potential well of the galaxy is expected to be $\rho_0 \approx 5 \times 10^{-25}$ gr cm^{-3} $\simeq 0.3$ GeV cm^{-3}. For WIMPs with masses about 100 GeV this means a number density $n_0 \approx 3 \times 10^{-3}$ cm^{-3}. In addition, their velocity will be similar to the one of the Sun since they move in the same gravitational potential well, $v_0 \approx 220$ km s^{-1}, implying a flux of dark matter particles $J_0 = n_0\ v_0 \approx 10^5$ cm^{-2} s^{-1} incident on the Earth. Although this number is apparently large, the fact that WIMPs interact weakly with matter makes their detection very difficult. Most of them will pass through matter without prevention. In any case, as suggested in 1985

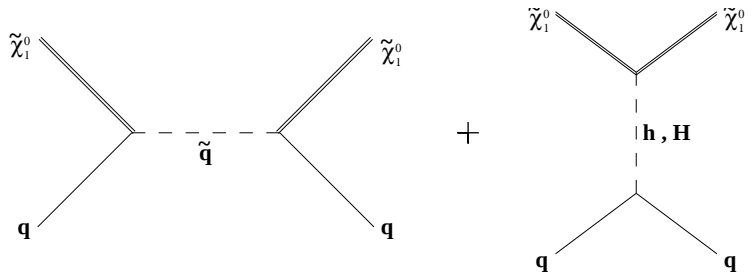

Figure 2.4: Feynman diagrams contributing to neutralino-nucleon cross section through squark ($\tilde{q}$) exchange and CP-even light (h) and heavy (H) neutral Higgs exchange.

[7, 8], direct experimental detection of WIMPs is in principle possible through elastic scattering.

The detection of WIMPs through elastic scattering with nuclei in a detector is shown schematically in Fig. 2.3. As we can see the nucleus recoils as a whole. A very rough estimate of the rate R in a detector is the following. A particle with a mass of order 100 GeV and electroweak interactions will have a cross section $\sigma \approx 1$ pb. Thus for a material with nuclei composed of about 100 nucleons, i.e. $M_N \sim 100$ GeV $= 177 \times 10^{-27}$ kg, one obtains $R \sim J_0\ \sigma/M_N \approx 10$ events kg^{-1} yr^{-1}. This means that every day a few WIMPs, the precise number depending on the number of kilograms of material, will hit an atomic nucleus in a detector.

Of course the above computation is just an estimate and one should take into account in the exact computation the interactions of WIMPs with quarks and gluons, the translation of these into interactions with nucleons, and finally the translation of the latter into interactions with nuclei. In the case of neutralinos as WIMPs, diagrams contributing to neutralino-quark cross section are shown in Fig. 2.4. The relevant (scalar) $\tilde{\chi}_1^0$-nucleus cross section is of the form

$$\sigma_{scat} \simeq M_r^2 |\mathcal{A}_{scat}|^2 \ , \tag{2.2.32}$$

where $M_r = M_N m_{\tilde{\chi}_1^0}/(M_N + m_{\tilde{\chi}_1^0})$ is the reduced mass with M_N the mass of the nucleus, and $\mathcal{A}_{scat}$ is the amplitude which depends on the dynamics of the collision. In particular, the quarks masses m_q, the hadronic matrix elements $f_{T_q}^{(p)}$, the proton mass m_p, and the masses of the particles mediating the interaction, such as $m_{\tilde{q}}$, m_H, m_h, enter in $\mathcal{A}_{scat}$. Significant regions of the parameter space of the MSSM produce values of the neutralino-nucleus cross section $\sigma_{scat} \simeq 1$ pb, and therefore giving rise to a reasonable number of events. As a matter of fact, in the experimental results that

one finds in the literature the authors prefer to give the WIMP-nucleon cross section. This is about eight orders of magnitude smaller than the WIMP-nucleus cross section, and therefore a typical value is $\approx 10^{-8}$ pb. In the next Sections, when talking about scattering cross section, we will always consider this one.

Let us finally remark that the diagrams for neutralino annihilation (see Fig. 2.2) are related to these by crossing symmetry. Thus, provided that the main annihilation channel is into fermions, the amplitudes of annihilation and scattering with nucleons are similar, and this leads for the amplitudes with the nucleus to the relation $|\mathcal{A}_{scat}|^2 \simeq c^2 A^2 |\mathcal{A}_{ann}|^2$, where A is the atomic weight and c^2 is a constant (we can deduce from that $c \simeq f_{T_s}^{(p)} m_p/m_s = \mathcal{O}(1)$ [10]). From eqs. (2.2.31) and (2.2.32) it is obvious that $\sigma_{scat}/\sigma_{ann} \simeq const.$ However, if the neutralinos are heavy they have other annihilation channels, such as Higgs bosons or vector boson pairs, and therefore the crossing argument does not apply.

Experiments

A large number of experiments for the direct detection of dark matter are running or in preparation around the world. For example, Germanium is a very pure material and has been used for many years for detecting dark matter in this way. In this type of experiments, in order to detect the nuclear recoil energy, they measure the ionization produced by collision with electrons. In fact, ^{76}Ge ionization detectors has been applied to WIMP searches since 1987 [37]. In 2000 the situation was the following. The best combination of data from these experiments, together with the last data from the Heidelberg-Moscow [38] and IGEX experiments [39] located at the Gran Sasso (Láquila, Italy) and Canfranc (Huesca, Spain) Underground Laboratories, respectively, were able to exclude a WIMP-nucleon cross section larger than about 10^{-5} pb for masses of WIMPs ~ 100 GeV, due to the negative search result. Although this was a very interesting bound, it was still well above the expected value $\sim 10^{-8}$ pb.

Let us remark that it is convenient to carry the experiments out in the deep underground. For a slow moving (~ 300 km s^{-1}) and heavy ($\sim 100 - 1000$ GeV) particle forming the dark matter halo, the kinetic energy is very small, around 100 keV, and in fact the largest recoil energy transfer to a nucleus in the detector will only be a few keV. Since cosmic rays with energies $\sim$ keV-MeV bombard the surface of the Earth, the experiments must have an extremely good background discrimination. In particular, neutrons coming from collisions between cosmic-ray muons and nuclei produce nuclear recoils similar to those expected from WIMPs at a rate $\sim 10^3$ events kg^{-1}

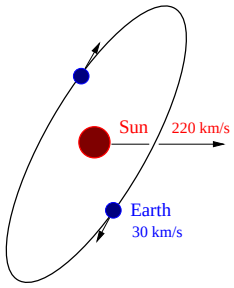

Figure 2.5: Earth's motion around the Sun.

day^{-1}. Thus detectors located in the deep underground, reduce the background by orders of magnitude in comparison with the sea level intensity.

In fact, this is still not enough since the detector has to be protected also against the natural radioactivity from the surroundings (e.g. the rocks) and the materials of the detector itself. This produces again neutrons but also X rays, gamma rays and beta rays giving rise to electron recoils. The latter may be a problem for detectors based only on ionization or scintillation light since nuclear recoils with energies of a few keV are much less efficient in ionizing or giving light than electrons of the same energy. Various protections aim to reduce these backgrounds. In particular, low radioactive materials, such as e.g. high-purity copper or aged lead, are used for the shielding. In addition, high-purity materials for the detector are also used.

Summarizing, with this type of experiments the WIMP nuclear recoil signal will appear as an excess of recoil events above the expected background rate. However, it would be very interesting to also look for some additional feature of the WIMP signal that positively identifies it as galactic in origin. In this sense a different method for discriminating a dark matter signal from background is the so-called annual modulation signature [40]. As it is shown schematically in Fig. 2.5, as the Sun orbits the galaxy with velocity $v_0 \approx 220$ km s^{-1}, the Earth orbits the Sun with velocity ≈ 30 km s^{-1} and with the orbital plane inclined at an angle of 60° to the galactic plane. Thus e.g. in June the Earth's rotation velocity adds to the Sun's velocity through the halo with a maximum around June 2, whereas in December the two velocities are in opposite directions. When this is taken into account the Earth velocity is given by

$$v_E = v_0 \left\{ 1.05 + 0.07 \cos \left[\frac{2\pi(t - t_m)}{1\text{year}} \right] \right\} , \tag{2.2.33}$$

where t_m= June 2± 1.3 days. This fluctuation produces a rate variation between the two extreme conditions. The variation is so small $\approx 7\%$ that the experiment can

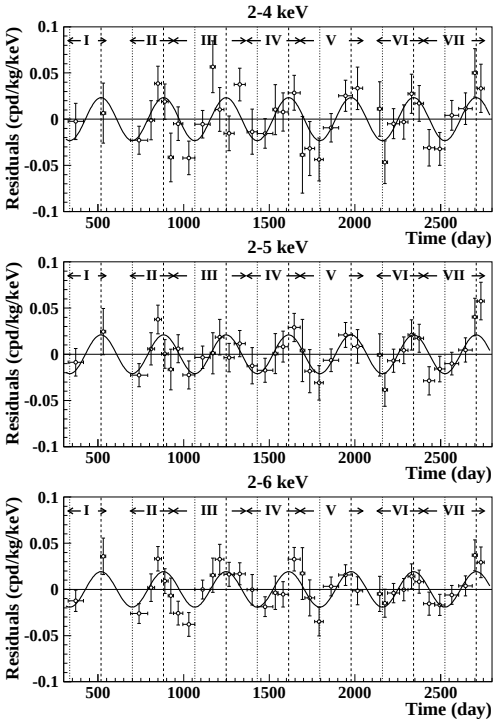

Figure 2.6: Model independent residual rate for events in the (2–4), (2–5) and (2–6) keV energy intervals as a function of the time elapsed since January 1st of the first year of data taking. The experimental points present the errors as vertical bars and the associated time bin width as horizontal bars. The superimposed curves represent the cosinusoidal functions behaviours expected for a WIMP signal with a period equal to 1 year and phase at 2nd June.

only work if large number of events are found, implying that large mass apparata are necessary.

The DArk MAtter (DAMA) experiment [41] investigated the annual modulation of this signature rather than discriminating signal events against background. It consisted of about 100 kg of material in a small room at the Gran Sasso National Laboratory located beside the Gran Sasso Tunnel on the highway connecting Teramo to Rome (see Fig. 2.8 for a similar experiment DAMA/LIBRA). The maximum thickness of the rock overburden is 1400 m. In the experiment they used nine 9.70 kg NaI crystal scintillators which measured the ionization produced by the nuclear recoil through the emission of photons. Remarkably, they found that their detectors flashed more times in June than in December. The data collected [41] over four yearly cycles, DAMA/NaI-1,2,3,4, until

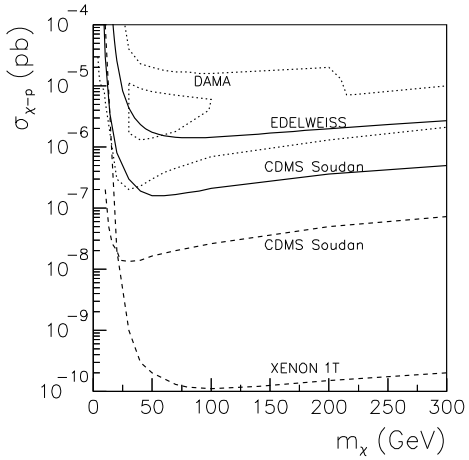

Figure 2.7: Areas allowed by different experiments for the direct detection of dark matter in the parameter space ($\sigma_{\text{WIMP-nucleon}}$, m_{WIMP}), where $\sigma_{\text{WIMP-nucleon}}$ is the WIMP-nucleon cross section and m_{WIMP} is the WIMP mass. The sensitivities of present amd projected experiments are depicted with solid and dashed lines, respectively. The large (small) area bounded by dotted lines is allowed by the DAMA experiment when astrophysical uncertaties are (are not) taken into account.

the second half of August 1999, strongly favoured the presence of a yearly modulation of the rate of the events. Moreover, in 2003, more data were reported [42] confirming this result. In particular the DAMA/NaI-5 data were collected from August 1999 to end of July 2000. Afterwards, the DAMA/NaI-6 data were collected from November 2000 to end of July 2001, while the DAMA/NaI-7 data were collected from August 2001 to July 2002. The analysis of the data of the seven annual cycles offers an immediate evidence of the presence of an annual modulation of the rate of the events in the lowest energy region as shown in Fig. 2.6 (from Ref. [42]), where the time behaviours of the (2–4), (2–5) and (2–6) keV residual rates are depicted. This signal is compatible [41, 42] with WIMP masses up to 100 GeV and WIMP-nucleon cross sections in the interval $10^{-6} - 10^{-5}$ pb, as shown with the small dotted region in Fig. 2.7, where the data [43] from DAMA/NaI-0 have also been taken into account.

It is worth remarking that this result has been obtained assuming the simple isothermal sphere halo model with dark-matter density $\rho_0 = 0.3$ GeV cm^{-3} and WIMP velocity $v_0 = 220$ km s^{-1} (to be precise one assumes a Maxwell-Boltzmann local velocity distribution $f(v) \propto e^{-v^2/v_0^2}$ producing a velocity dispersion $\bar{v} =< v^2 >^{1/2} = (3/2)^{1/2} v_0 \approx$

270 km s^{-1}). However, when uncertainties on the halo model are taking into account, the signal is consistent with a larger region of the parameter space. In particular, in Refs. [41, 42] and [44] modifications in the velocity distribution function for different galactic halo models were considered, using in addition the allowed ranges for v_0 and ρ_0 in each model. One obtains that the signal is compatible with larger values of the parameters, i.e. WIMP masses up to 270 GeV, and WIMP-nucleon cross sections in the interval $10^{-7} - 6 \times 10^{-5}$ pb. This result corresponds at a rate of about 1 event per kg per day. In fact, as discussed in Ref. [44] (see also Ref. [42]), when co-rotation of the galactic halo is also considered, the mass range extends further to $500 - 900$ GeV, for cross sections in the interval few$\times 10^{-6} - 2 \times 10^{-5}$ pb.

Although the DAMA group is confident about the data, since they claim to have ruled out systematic effects which could fake the signature [45, 46], as e.g. temperature changes, it is worth remarking that the above values for the cross section are generically above the expected weak-interaction value, and therefore they are not easy to obtain in SUSY models with neutralino dark matter. But in fact, the DAMA result is controversial, mainly because the negative search result obtained by other recent experiments. In particular, this is the case of the Cryogenic Dark Matter Search (CDMS) experiment [47] in the US. This is located in the Soudan mine in Minnesota (approximately 700 metres below ground), with Ge/Si targets. Two detection techniques are used for this discrimination, both the ionization and the temperature rise produced during a recoil are measured. The latter can be observed since the recoiling nucleus is stopped within $10^{-7} - 10^{-6}$ cm ($\sim 10^{-14}$ s) releasing a spherical wave of phonons traveling at $\sim 5 \times 10^5$ cm s^{-1}, and subsequently converted to a thermal distribution. These two techniques allow to discriminate electron recoils caused by interactions of background particles from WIMP-induced nuclear recoils. The ratio of deposited energies heat/ionization would be $\sim 2 - 3$ for the former and larger than 10 for the latter. These data exclude much of the region allowed by the DAMA annual modulation signal, as shown in Fig. 2.7 with a solid line.

In addition, the results from the EDELWEISS collaboration exclude also a large region of DAMA, as shown in Fig. 2.7. The EDELWEISS experiment [48] is located at the Modane Underground Laboratory in the Frejus Tunnel under the French-Italians Alps, under a 1780 m rock overburden. As CDMS, this experiment also uses a heat-and-ionization cryogenic Ge detector. Finally, the ZEPLIN experiment [49] at the Boubly salt mine (Yorkshire, UK) also excludes a region similar to that of EDELWEISS. In this case, the experiment consists of a series of liquid Xenon detectors operating some 1100

Figure 2.8: Left picture: during the LIBRA detectors installation in HP Nitrogen atmosphere. Right picture: view at end of the detectors installation. All the used materials have been deeply selected for radiopurity (see for example the cables with teflon envelop).

m underground, where the nuclear recoil produces both an ionization and a scintillation signal.

Owing to this controversy between DAMA and the other experiments, one cannot be sure whether or not the first direct evidence for the existence of dark matter has already been observed. Fortunately, the complete DAMA region will continue being tested by similar dark matter detectors. First of all, the DAMA collaboration dismounted the 100 kg NaI set-up and installed the new LIBRA set-up. This consisting of about 250 kg of NaI made of 25 detectors, 9.70 kg each one. Of course, this will make the experiment more sensitive to the annual modulation signal. Some pictures taken during the installation can be seen in Fig. 2.8 (from Ref. [46]). This was completed at the end of 2002. It is worth noticing here that another (independent) experiment similar to DAMA, ANAIS [50], is under construction in the Canfrac laboratory, and therefore it should be able to reproduce the DAMA results (if the DAMA collaboration is right).

On the other hand, in the future, the CDMS collaboration will be able to test a WIMP-nucleon cross section as low as $\sigma \gtrsim 10^{-8}$ pb as shown in Fig. 2.7. There, is also shown the line corresponding to upcoming detectors working with 1 tonne of Ge/Xe. Their limit can be as low as 10^{-10}pb [51].

Chapter 3

NMSSM Phenomenology and Dark Matter

As discussed in the previous Chapter, one of the most important enigmas in physics is the problem of the dark matter in the Universe. Particle physics, and in particular extensions of the standard model (SM) offer candidates for dark matter. Among the most interesting ones are the Weakly Interacting Massive Particles (WIMPs), since these can be left over from the Big Bang in sufficient number to account for a significant fraction of the observed matter density.

Assuming therefore that the dark matter is a WIMP, it is necessary to analyse the theoretical predictions for the WIMP-nucleon cross section, in order to compare it with the sensitivity of detectors. Obviously, the answer to this question depends on the particular WIMP considered. The leading candidate in this class of particles is the lightest neutralino, $\tilde{\chi}_1^0$, which appears in supersymmetric (SUSY) extensions of the SM [9]. The cross section for the elastic scattering of $\tilde{\chi}_1^0$ on nucleons has been examined exhaustively in the context of the Minimal Supersymmetric Standard Model (MSSM) [10]. In particular, there are regions of the parameter space of the MSSM where the neutralino-nucleon cross section is compatible with the sensitivity of present (and future) dark matter detectors [52].

However, it is well known that the MSSM faces a naturalness problem – the so-called μ problem [53] – arising from the presence of a mass term for the Higgs fields in the superpotential, $\mu H_1 H_2$. The only natural values for the μ parameter are either zero or the Planck scale. The first is experimentally excluded since it leads to an unacceptable axion once the electroweak (EW) symmetry is broken, while the latter

reintroduces the hierarchy problem. There exist explanations for an $\mathcal{O}(M_W)$ value for the μ term, although all in extended frameworks [53, 54].

The Next-to-Minimal Supersymmetric Standard Model (NMSSM) [55] provides an elegant solution to the μ problem of the MSSM via the introduction of a singlet superfield S. In the simplest form of the superpotential, which is scale invariant and contains the SH_1H_2 coupling, an effective μ term is generated when the scalar component of S acquires a vacuum expectation value (VEV) of order the SUSY breaking scale. This effective coupling is naturally of order the EW scale if the SUSY breaking scale is not too large compared with M_W. In fact, the NMSSM is the simplest SUSY extension of the SM in which the EW scale exclusively originates from the SUSY breaking scale. Another appealing feature of the NMSSM is related to the "little fine tuning problem" of the MSSM, or equivalently, the non-observation of a neutral CP-even Higgs boson at LEP II. As shown in [56], in the context of the NMSSM the latter problem becomes less severe. Although the symmetries of the NMSSM may give rise to the possibility of a cosmological domain wall problem [57], this can be avoided by the introduction of suitable non-normalisable operators [58] that do not generate dangerously large singlet tadpole diagrams [59]. These additional operators can be chosen small enough as not to alter the low energy phenomenology.

In addition to the MSSM fields, the NMSSM contains an extra CP-even and CP-odd neutral Higgs bosons, as well as one additional neutralino. These new fields mix with the corresponding MSSM ones, giving rise to a richer and more complex phenomenology [55, 60, 61, 62, 63]. A very light neutralino may be present [60]. The upper bound on the mass of the lightest Higgs state is larger than in the MSSM [61]. Moreover, a very light Higgs boson is not experimentally excluded [62, 63]. All these properties may modify the results concerning the neutralino-nucleon cross section with respect to those of the MSSM.

In fact, in comparison with the MSSM, there are only a few works in the literature studying the direct detection of the lightest neutralino in the NMSSM [64, 65], as well as its relic density [66]. Thus, given the experimental results concerning the detection of dark matter discussed in Section 2.2.3, and in view of the appealing theoretical and phenomenological properties of the NMSSM, it is important to carry out a detailed study of the neutralino as a dark matter candidate in this framework. This is the aim of this Chapter [1, 2].

The outline of the Chapter is as follows: In Section 3.1 we introduce the model, discussing in particular its Higgs potential, Higgs and neutralino mass matrices, and the

parameter space. In Section 3.2 we examine the relevant effective Lagrangian describing the elastic $\tilde{\chi}_1^0$-nucleon scattering and its associated cross section. Section 3.3 is devoted to the presentation of the results for the $\tilde{\chi}_1^0$-nucleon cross section in the NMSSM, taking into account relevant constraints on the parameter space from accelerator data. On the other hand, in addition to LEP II and Tevatron limits on the spectrum, one should also take into account SUSY contributions to low-energy observables. The most stringent bounds arise from kaon and B decays, as well as from the muon anomalous magnetic moment, $a_\mu^{\rm SUSY}$. Naturally, in order to be a viable dark matter candidate, the NMSSM lightest neutralino must also satisfy the present astrophysical bounds on the relic abundance. All this will be discussed in Section 3.4, where we will also see that regions fulfilling all experimental and astrophysical constraints, with a detection cross section within the reach of dark matter experiments, are possible. Finally, our conclusions are given in Subsection 3.4.4.

3.1 Overview of the NMSSM

In this Section, we review some important features of the NMSSM. In particular, we discuss the Higgs and neutralino sectors of the model, presenting the tree-level mass matrices and mixings which are relevant for our analysis. We also discuss theoretical and experimental constraints, and how these are reflected in the parameter space.

3.1.1 Higgs scalar potential

In addition to the MSSM Yukawa couplings for quarks and leptons, the NMSSM superpotential contains two additional terms involving the Higgs doublet superfields, H_1 and H_2, and the new superfield S, a singlet under the SM gauge group $SU(3)_c \times SU(2)_L \times U(1)_Y$,

$$W = \epsilon_{ij}\left(Y_u\, H_2^j\, Q^i\, u + Y_d\, H_1^i\, Q^j\, d + Y_e\, H_1^i\, L^j\, e\right) - \epsilon_{ij}\lambda\, S\, H_1^i H_2^j + \frac{1}{3}\kappa S^3\,, \qquad (3.1.1)$$

where we take $H_1^T = (H_1^0, H_1^-)$, $H_2^T = (H_2^+, H_2^0)$, i, j are $SU(2)$ indices, and $\epsilon_{12} = 1$. In this model, the usual MSSM bilinear μ term is absent from the superpotential, and only dimensionless trilinear couplings are present in W. However, when the scalar component of S acquires a VEV, an effective interaction $\mu H_1 H_2$ is generated, with $\mu \equiv \lambda\langle S\rangle$.

As mentioned above, the superpotential in Eq. (3.1.1) is scale invariant, and the EW scale will only appear through the soft SUSY breaking terms in $\mathcal{L}_{\rm soft}$, which in our conventions is given by

$$\begin{aligned}
-\mathcal{L}_{\rm soft} &= m_{\tilde{Q}}^2\,\tilde{Q}^*\,\tilde{Q} + m_{\tilde{U}}^2\,\tilde{u}^*\,\tilde{u} + m_{\tilde{D}}^2\,\tilde{d}^*\,\tilde{d} + m_{\tilde{L}}^2\,\tilde{L}^*\,\tilde{L} + m_{\tilde{E}}^2\,\tilde{e}^*\,\tilde{e} \\
&+ m_{H_1}^2\,H_1^*\,H_1 + m_{H_2}^2\,H_2^* H_2 + m_S^2\,S^* S \\
&+ \epsilon_{ij}\left(A_u\,Y_u\,H_2^j\,\tilde{Q}^i\,\tilde{u} + A_d\,Y_d\,H_1^i\,\tilde{Q}^j\,\tilde{d} + A_e\,Y_e\,H_1^i\,\tilde{L}^j\,\tilde{e} + \text{H.c.}\right) \\
&+ \left(-\epsilon_{ij}\lambda\,A_\lambda S H_1^i H_2^j + \frac{1}{3}\kappa\,A_\kappa\,S^3 + \text{H.c.}\right) \\
&- \frac{1}{2}\left(M_3\,\lambda_3\,\lambda_3 + M_2\,\lambda_2\,\lambda_2 + M_1\,\lambda_1\,\lambda_1 + \text{H.c.}\right). \qquad (3.1.2)
\end{aligned}$$

In our subsequent analysis we assume that the soft breaking parameters are free at the EW scale. In addition to terms from $\mathcal{L}_{\rm soft}$, the tree-level scalar Higgs potential receives the usual D and F term contributions:

$$\begin{aligned}
V_D &= \frac{g_1^2+g_2^2}{8}\left(|H_1|^2 - |H_2|^2\right)^2 + \frac{g_2^2}{2}|H_1^\dagger H_2|^2\,, \\
V_F &= |\lambda|^2\left(|H_1|^2|S|^2 + |H_2|^2|S|^2 + |\epsilon_{ij}H_1^i H_2^j|^2\right) + |\kappa|^2|S|^4 \\
&- \left(\epsilon_{ij}\lambda\kappa^* H_1^i H_2^j S^{*2} + \text{H.c.}\right). \qquad (3.1.3)
\end{aligned}$$

3.1.2 Minimization of the tree level scalar potential

Once the EW symmetry is spontaneously broken, the neutral Higgs scalars develop the following VEV's:

$$\langle H_1^0\rangle = v_1\,, \quad \langle H_2^0\rangle = v_2\,, \quad \langle S\rangle = s\,. \qquad (3.1.4)$$

One has to ensure the absence of non-vanishing VEV's for the charged Higgs fields, which would induce the appearance of charge breaking minima. By means of an $SU(2)_L \times U(1)_Y$ transformation, one can take, without loss of generality, $\langle H_2^+\rangle = 0$ while $\langle H_2^0\rangle = v_2 \in \mathbb{R}^+$. The condition to have $v_1^- = \langle H_1^-\rangle = 0$ as a global minimum is quite involved; still, imposing that $v_1^- = 0$ is a local minimum is equivalent to requiring that the physical charged Higgses have positive mass squared.

Bringing together all the terms in Eqs. (3.1.2) and (3.1.3), we then obtain for the tree-level neutral Higgs potential:

$$\begin{aligned}
\langle V_{\rm neutral}^{\rm Higgs}\rangle &= \frac{g_1^2+g_2^2}{8}\left(|v_1|^2 - |v_2|^2\right)^2 \\
&+ |\lambda|^2\left(|s|^2|v_1|^2 + |s|^2|v_2|^2 + |v_1|^2|v_2|^2\right) + |\kappa|^2|s|^4 \\
&+ m_{H_1}^2|v_1|^2 + m_{H_2}^2|v_2|^2 + m_S^2|s|^2
\end{aligned}$$

$$+ \quad \left(-\lambda\kappa^* v_1 v_2 s^{*2} - \lambda A_\lambda s v_1 v_2 + \frac{1}{3}\kappa A_\kappa s^3 + \text{H.c.} \right) . \qquad (3.1.5)$$

In the following, we assume that λ, κ, as well as the soft SUSY breaking terms are real. This implies the absence of explicit CP violation in the scalar sector. Although v_1 and s can be complex parameters, the global $\mathbb{Z}_3$ symmetry exhibited by the superpotential implies that CP-violating extrema of $V^{\text{Higgs}}_{\text{neutral}}$ are maxima rather than minima [67]. In principle, λ, κ, and the trilinear soft-breaking terms, A_λ and A_κ, in Eq. (3.1.5) can have both signs.

Ensuring that the tree-level potential has a minimum with respect to the phases of the VEV's directly excludes some combinations of signs for the parameters. After conducting this analysis, and given that the potential is invariant under the symmetries λ, κ, $s \to -\lambda$, $-\kappa$, $-s$ and λ, $v_1 \to -\lambda$, $-v_1$, we adopt, without loss of generality, the sign convention where both λ and v_1 are positive. We then have only positive values for λ and $\tan\beta$, while κ and $\mu\,(= \lambda s)$, as well as A_λ and A_κ, can have both signs.

In what follows, we summarise the conditions for κ, A_λ, A_κ and $\mu\,(= \lambda s)$ obtained from the minimization of the potential with respect to the phases of the VEV's. In particular, for $\kappa > 0$, one can analytically show that minima of $V^{\text{Higgs}}_{\text{neutral}}$ may be obtained for the following three combinations of signs, provided that in each case the corresponding conditions are fulfilled,

(i) $\text{sign}(s) = \text{sign}(A_\lambda) = -\text{sign}(A_\kappa)$,

which always leads to a minimum with respect to the phases.

(ii) $\text{sign}(s) = -\text{sign}(A_\lambda) = -\text{sign}(A_\kappa)$,

with $|A_\kappa| > 3\lambda v_1 v_2 |A_\lambda|/(-|sA_\lambda| + \kappa|s^2|)$, where the denominator has to be positive.

(iii) $\text{sign}(s) = \text{sign}(A_\lambda) = \text{sign}(A_\kappa)$,

with $|A_\kappa| < 3\lambda v_1 v_2 |A_\lambda|/(|sA_\lambda| + \kappa|s^2|)$.

Similarly, for $\kappa < 0$, minima can only be obtained for the combination

(iv) $\text{sign}(s) = \text{sign}(A_\lambda) = \text{sign}(A_\kappa)$,

with $|A_\kappa| > 3\lambda v_1 v_2 |A_\lambda|/(|sA_\lambda| - \kappa|s^2|)$, where the denominator has to be positive.

Numerically, one finds that these tree-level conditions generally hold even after the inclusion of higher order corrections.

One can derive three minimization conditions for the Higgs VEV's and use them to re-express the soft breaking Higgs masses in terms of λ, κ, A_λ, A_κ, v_1, v_2 and s:

$$\begin{aligned} m_{H_1}^2 &= -\lambda^2\left(s^2+v^2\sin^2\beta\right)-\frac{1}{2}M_Z^2\cos 2\beta+\lambda s\tan\beta\left(\kappa s+A_\lambda\right), \\ m_{H_2}^2 &= -\lambda^2\left(s^2+v^2\cos^2\beta\right)+\frac{1}{2}M_Z^2\cos 2\beta+\lambda s\cot\beta\left(\kappa s+A_\lambda\right), \\ m_S^2 &= -\lambda^2 v^2-2\kappa^2 s^2+\lambda\kappa v^2\sin 2\beta+\frac{\lambda A_\lambda v^2}{2s}\sin 2\beta-\kappa A_\kappa s, \end{aligned} \tag{3.1.6}$$

where $v^2=v_1^2+v_2^2=2M_W^2/g_2^2$ and $\tan\beta=v_2/v_1$.

3.1.3 Higgs boson mass matrices

Subsequent to EW symmetry breaking, and after rotating away the CP-odd would-be Goldstone boson, we are left with five neutral Higgs states and 2 charged Higgs states. Assuming

$$H_1^0\equiv v_1+\frac{H_{1R}+iH_{1I}}{\sqrt{2}}, \quad H_2^0\equiv v_2+\frac{H_{2R}+iH_{2I}}{\sqrt{2}}, \quad S\equiv s+\frac{S_R+iS_I}{\sqrt{2}}, \tag{3.1.7}$$

among the neutral Higgses we find three CP-even states - H_{1R}, H_{2R}, S_R and two CP-odd components, A^0, S_I, with A^0 related to the original fields as $H_{1(2)I}=\sin\beta(\cos\beta)A^0$. Using the minimization conditions above, the tree-level mass matrix for the neutral Higgs bosons can be easily obtained. Since we have made the assumption that there is no CP-violation on the Higgs sector, CP-even and CP-odd states do not mix, and the corresponding mass matrices can be written in the respective basis, $H^0=(H_{1R},H_{2R},S_R)$ and $P^0=(A^0,S_I)$. For the CP-even states, we have

$$\begin{aligned} \mathcal{M}_{S,11}^2 &= M_Z^2\cos^2\beta+\lambda s\tan\beta(A_\lambda+\kappa s), \\ \mathcal{M}_{S,22}^2 &= M_Z^2\sin^2\beta+\lambda s\cot\beta(A_\lambda+\kappa s), \\ \mathcal{M}_{S,33}^2 &= 4\kappa^2 s^2+\kappa A_\kappa s+\frac{\lambda}{s}A_\lambda v_1 v_2, \\ \mathcal{M}_{S,12}^2 &= \left(\lambda^2 v^2-\frac{M_Z^2}{2}\right)\sin 2\beta-\lambda s\left(A_\lambda+\kappa s\right), \\ \mathcal{M}_{S,13}^2 &= 2\lambda^2 v_1 s-\lambda v_2\left(A_\lambda+2\kappa s\right), \\ \mathcal{M}_{S,23}^2 &= 2\lambda^2 v_2 s-\lambda v_1\left(A_\lambda+2\kappa s\right). \end{aligned} \tag{3.1.8}$$

The CP-even Higgs interaction and physical eigenstates are related by the transformation

$$h_a^0 = S_{ab} H_b^0 \,, \tag{3.1.9}$$

where S is the unitary matrix that diagonalises the above symmetric mass matrix, $a, b = 1, 2, 3$, and the physical eigenstates are ordered as[1] $m_{h_1^0} \lesssim m_{h_2^0} \lesssim m_{h_3^0}$. In the pseudoscalar sector, after rewriting the CP-odd mass terms in the P^0 basis, the corresponding (symmetric) mass matrix reads

$$\begin{aligned} \mathcal{M}^2_{P,11} &= \frac{2\lambda s}{\sin 2\beta} \left(\kappa s + A_\lambda\right), \\ \mathcal{M}^2_{P,22} &= \lambda \left(2\kappa + \frac{A_\lambda}{2s}\right) v^2 \sin 2\beta - 3\kappa A_\kappa s, \\ \mathcal{M}^2_{P,12} &= \lambda v \left(A_\lambda - 2\kappa s\right) , \end{aligned} \tag{3.1.10}$$

and the relation between physical and interaction eigenstates is given by

$$a_i^0 = P_{ij} P_j^0 \,. \tag{3.1.11}$$

Regarding the charged Higgs mass, at the tree level it is given by

$$m^2_{H^\pm} = M_W^2 - \lambda^2 v^2 + \lambda(A_\lambda + \kappa s)\frac{2s}{\sin 2\beta} \,. \tag{3.1.12}$$

3.1.4 Neutralino mass matrix

When compared to the MSSM case, the structure of chargino and squark mass terms is essentially unaffected, provided that one uses $\mu = \lambda s$. However, in the neutralino sector, the situation is more involved, since the fermionic component of S mixes with the neutral Higgsinos, giving rise to a fifth neutralino state. In the weak interaction basis defined by $\Psi^{0T} \equiv \left(\tilde{B}^0 = -i\lambda', \tilde{W}_3^0 = -i\lambda_3, \tilde{H}_1^0, \tilde{H}_2^0, \tilde{S}\right)$, the neutralino mass terms in the Lagrangian are

$$\mathcal{L}^{\tilde{\chi}^0}_{\text{mass}} = -\frac{1}{2}(\Psi^0)^T \mathcal{M}_{\tilde{\chi}^0} \Psi^0 + \text{H.c.} \,, \tag{3.1.13}$$

[1] Throughout the work we always adopt the convention $m_i \lesssim m_j$ for $i < j$.

with $\mathcal{M}_{\tilde{\chi}^0}$ a 5×5 matrix,

$$\mathcal{M}_{\tilde{\chi}^0} = \begin{pmatrix} M_1 & 0 & -M_Z \sin\theta_W \cos\beta & M_Z \sin\theta_W \sin\beta & 0 \\ 0 & M_2 & M_Z \cos\theta_W \cos\beta & -M_Z \cos\theta_W \sin\beta & 0 \\ -M_Z \sin\theta_W \cos\beta & M_Z \cos\theta_W \cos\beta & 0 & -\lambda s & -\lambda v_2 \\ M_Z \sin\theta_W \sin\beta & -M_Z \cos\theta_W \sin\beta & -\lambda s & 0 & -\lambda v_1 \\ 0 & 0 & -\lambda v_2 & -\lambda v_1 & 2\kappa s \end{pmatrix} . \tag{3.1.14}$$

The above matrix can be diagonalised by means of a unitary matrix N,

$$N^* \mathcal{M}_{\tilde{\chi}^0} N^{-1} = \mathrm{diag}(m_{\tilde{\chi}_1^0}, m_{\tilde{\chi}_2^0}, m_{\tilde{\chi}_3^0}, m_{\tilde{\chi}_4^0}, m_{\tilde{\chi}_5^0}) \,, \tag{3.1.15}$$

where $m_{\tilde{\chi}_1^0}$ is the lightest neutralino mass. Under the above assumptions, the lightest neutralino can be expressed as the combination

$$\tilde{\chi}_1^0 = N_{11}\tilde{B}^0 + N_{12}\tilde{W}_3^0 + N_{13}\tilde{H}_1^0 + N_{14}\tilde{H}_2^0 + N_{15}\tilde{S} \,. \tag{3.1.16}$$

In the following, neutralinos with $N_{13}^2 + N_{14}^2 > 0.9$, or $N_{15}^2 > 0.9$, will be referred to as Higgsino- or singlino-like, respectively.

3.1.5 NMSSM parameter space

At the weak scale, the free parameters in the Higgs sector are (at tree level): λ, κ, $m_{H_1}^2$, $m_{H_2}^2$, m_S^2, A_λ and A_κ. Using the three minimization conditions of the Higgs potential (including the dominant one- and two-loop corrections), one can eliminate the soft Higgs masses in favour of $M_Z, \tan\beta$ and μ. We thus consider as independent parameters the following set of variables

$$\lambda,\ \kappa,\ \tan\beta,\ \mu,\ A_\lambda,\ A_\kappa \,. \tag{3.1.17}$$

In our study, the soft scalar masses as well as the soft gaugino soft masses M_i are free parameters at the EW scale. We scanned over the parameter space using the program NMHDECAY [62], and in what follows we overview the most relevant aspects of the analysis.

For each point in the parameter space, one requires the absence of Landau singularities for λ, κ, Y_t and Y_b below the GUT scale. For $m_t^{\rm pole} = 175$ GeV, this translates into $\lambda \lesssim 0.75$, $\kappa \lesssim 0.65$, and $1.7 \lesssim \tan\beta \lesssim 54$. In addition one verifies that the physical

minimum is a true one, in other words, that it is deeper than the local unphysical minima with $\langle H^0_{1,2}\rangle = 0$ and/or $\langle S\rangle = 0$.

One then computes the scalar, pseudo-scalar and charged Higgs masses and mixings, taking into account 1- and 2-loop radiative corrections. The dominant 1-loop corrections to the Higgs masses originate from top, stop, bottom and sbottom loops, and the corresponding corrections to $m^2_{h^0_1}$ are of $\mathcal{O}(Y^4_{t,b})$. Pure electroweak contributions of $\mathcal{O}(g^2)$ are also taken into account. Regarding 2-loop corrections to the effective potential, the dominant ones are associated with top-stop loops, and only the leading (double) logarithms are included. The chargino and neutralino masses and mixings are computed and the couplings of the scalar and pseudoscalar Higgs to charginos and neutralinos are calculated.

Finally, all available experimental constraints from LEP are checked:

1) In the neutralino sector, we check that the lightest neutralino does not contribute excessively to the invisible width of the Z boson ($\Gamma(Z \to \tilde{\chi}^0_1\tilde{\chi}^0_1) < 1.76$ MeV [68]) if $m_{\tilde{\chi}^0_1} < M_Z/2$, and that $\sigma(e^+e^- \to \tilde{\chi}^0_1\tilde{\chi}^0_i) < 10^{-2}$ pb if $m_{\tilde{\chi}^0_1} + m_{\tilde{\chi}^0_i} < 209$ GeV ($i > 1$) and $\sigma(e^+e^- \to \tilde{\chi}^0_i\tilde{\chi}^0_j) < 10^{-1}$ pb if $m_{\tilde{\chi}^0_i} + m_{\tilde{\chi}^0_j} < 209$ GeV ($i, j > 1$) [69].

2) In the chargino sector, we verify that the lightest chargino is not too light ($m_{\tilde{\chi}^+_1} > 103.5$ GeV [70]). This leads to a lower bound on $|\mu| \gtrsim 100$ GeV.

3) In the charged Higgs sector, we impose $m_{H^+} > 78.6$ GeV [71].

4) In the neutral Higgs sector, we check the constraints on the production rates (reduced couplings) $\times$ branching ratios versus the masses, for all the CP-even states h^0 and CP-odd states a^0, in all the channels studied at LEP [72]: $e^+e^- \to h^0Z$, independent of the h^0 decay mode (IHDM); $e^+e^- \to h^0Z$, dependent on the h^0 decay mode (DHDM), with the Higgs decaying via $h^0 \to b\bar{b}$, $h^0 \to \tau^+\tau^-$, $h^0 \to 2\,\text{jets}$ $h^0 \to \gamma\gamma$ and $h^0 \to$ invisible; associated production modes (APM), $e^+e^- \to h^0a^0$, with $h^0a^0 \to 4b$'s, $h^0a^0 \to 4\tau$'s and $h^0a^0 \to a^0a^0a^0 \to 6b$'s (see [62] for a detailed discussion).

3.2 Neutralino-nucleon cross section

The most general supersymmetric low-energy effective four-fermion Lagrangian that describes the elastic scattering of the lightest neutralino with the nucleon is given by [26, 73],

$$\begin{aligned}\mathcal{L}_{\text{eff}} = \quad & \bar{\tilde{\chi}}_1^0 \gamma^\mu \gamma_5 \tilde{\chi}_1^0 \bar{q}_i \gamma_\mu (\alpha_{1i} + \alpha_{2i}\gamma_5) q_i + \alpha_{3i} \bar{\tilde{\chi}}_1^0 \tilde{\chi}_1^0 \bar{q}_i q_i + \\ & + \alpha_{4i} \bar{\tilde{\chi}}_1^0 \gamma_5 \tilde{\chi}_1^0 \bar{q}_i \gamma_5 q_i + \alpha_{5i} \bar{\tilde{\chi}}_1^0 \tilde{\chi}_1^0 \bar{q}_i \gamma_5 q_i + \alpha_{6i} \bar{\tilde{\chi}}_1^0 \gamma_5 \tilde{\chi}_1^0 \bar{q}_i q_i \,, \end{aligned} \tag{3.2.18}$$

where $i = 1, 2$ denotes up- and down-type quarks, and the Lagrangian is summed over the three quark generations. In the absence of CP-violating phases, the terms proportional to α_5 and α_6 vanish. Moreover, those associated with α_1 and α_4 (as well as α_5 and α_6, should these be present) are velocity-dependent, and can be safely neglected for our present purposes. The cross section associated with the spin-dependent coefficient (α_2) is only non-zero if the target nucleus has a non-vanishing spin and, contrary to case of the scalar (spin-independent) term, adds incoherently. For the case of heavy targets, as those used in the experiments mentioned in Subsection 2.2.3, the scalar cross section associated with α_3 is in general substantially larger, and henceforth we shall focus our discussion on the latter.

We begin by decomposing α_{3i} into two terms, one arising from squark s-channel exchange and the other from the t-channel, neutral Higgs mediated interaction (Fig. 3.1

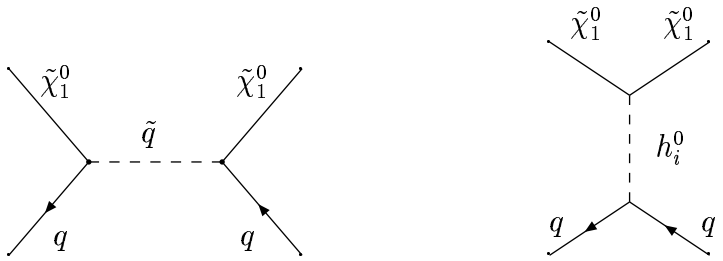

(a) (b)

Figure 3.1: Feynman diagrams contributing to the neutralino-nucleon scalar cross section: (a) squark exchange and (b) scalar Higgs exchange.

(a) and (b), respectively). One obtains[2]

$$\alpha_{3i}^{\tilde{q}} = -\sum_{X=1}^{2} \frac{1}{4(m_{Xi}^2 - m_{\tilde{\chi}_1^0}^2)} \mathrm{Re}\left[\left(C_R^{Xi}\right)\left(C_L^{Xi}\right)^*\right] , \alpha_{3i}^{h} = \sum_{a=1}^{3} \frac{1}{m_{h_a^0}^2} C_Y^i \mathrm{Re}\left[C_{HL}^a\right], \tag{3.2.19}$$

where $X = 1, 2$ denotes the squark mass eigenstates and $a = 1, 2, 3$ refers to the scalar Higgs mass eigenstates. The relevant NMSSM couplings for the neutralino-squark-quark ($C_{L,R}^{Xi}$), neutralino-neutralino-Higgs ($C_{HL,R}^{a}$) and Higgs-quark-quark (C_Y^i) interactions are given in Appendix A.

The term $\alpha_{3i}^{\tilde{q}}$ is formally identical to the MSSM case, differing only in the new neutralino mixings stemming from the presence of a fifth component. In particular, in regions of the NMSSM parameter space where the singlino component dominates the lightest neutralino state, there will be a significant reduction in the Bino- and Wino-squark-quark couplings, and hence in $\alpha_{3i}^{\tilde{q}}$.

Regarding the Higgs mediated interaction term (α_{3i}^{h}), the situation is slightly more involved since both vertices and the exchanged Higgs scalar significantly reflect the new features of the NMSSM. First, let us recall that in regions of the parameter space where the lightest Higgs boson has a sizable singlet component, the Higgs-quark-quark coupling might be substantially reduced. Regarding the Higgs-$\tilde{\chi}_1^0$-$\tilde{\chi}_1^0$ interaction, in addition to a new component in the lightest $\tilde{\chi}^0$ state, the most important alteration emerges from the presence of new terms, proportional to λ and κ (cf. Appendix A). Nevertheless, and as already mentioned, light Higgs bosons can be experimentally allowed in the context of the NMSSM. Should this occur, and if these states are not pure singlets (thus displaying a non-vanishing coupling to matter) the exchange of light Higgs scalars in the t-channel might provide a considerable enhancement to the neutralino-nucleon cross section.

It is worth mentioning that an enhancement of α_{3i}^{h} with respect to $\alpha_{3i}^{\tilde{q}}$ is not an effect unique to the NMSSM. In fact, it has been already noticed that in the MSSM, and once the mSUGRA inspired universality for the soft scalar and gaugino masses is abandoned, the cross section associated with the channels involving scalar Higgs exchange can be substantially enhanced. Similar to what will occur in the present model, the MSSM t-channel contributions become larger once the Higgsino components of $\tilde{\chi}_1^0$ are augmented and/or the Higgs masses are reduced (via non-universal soft masses

[2]When compared to the analogous expression of Ref. [65], we find some discrepancies in α_{3i}^{h}, namely a missing singlet-Higgsino-Higgsino term (proportional to λ), and the presence of an additional overall weak coupling constant, g.

at the GUT scale) [74].

The scalar interaction term contributes to the $\tilde{\chi}_1^0$-Nucleon cross section as

$$\sigma_{3N} = \frac{4m_r^2}{\pi} f_N^2 \,, \tag{3.2.20}$$

where m_r is the Nucleon-$\tilde{\chi}_1^0$ reduced mass, $m_r = m_N m_{\tilde{\chi}_1^0}/(m_N + m_{\tilde{\chi}_1^0})$, and

$$\frac{f_N}{m_N} = \sum\nolimits_{q=u,d,s} f_{Tq}^{(N)} \frac{\alpha_{3q}}{m_q} + \frac{2}{27} f_{TG}^{(N)} \sum\nolimits_{q=c,b,t} \frac{\alpha_{3q}}{m_q} \,. \tag{3.2.21}$$

In the above, m_q is the quark mass, and the parameters $f_{Tq}^{(N)}$ are defined as $\langle N|m_q \bar{q} q|N\rangle = m_N f_{Tq}^{(N)}$. $f_{TG}^{(N)}$ can be derived from $f_{Tq}^{(N)}$ as $f_{TG}^{(N)} = 1 - \sum_{q=u,d,s} f_{Tq}^{(N)}$. Following [75], we take the following values for the hadronic matrix elements:

$$\begin{aligned} f_{Tu}^{(p)} &= 0.020 \pm 0.004 \,, \qquad f_{Td}^{(p)} = 0.026 \pm 0.005 \,, \quad f_{Ts}^{(p)} = 0.118 \pm 0.062 \,, \\ f_{Tu}^{(n)} &= 0.014 \pm 0.003 \,, \qquad f_{Td}^{(n)} = 0.036 \pm 0.008 \,, \quad f_{Ts}^{(n)} = 0.118 \pm 0.062 \,. \end{aligned} \tag{3.2.22}$$

In the numerical analysis of the next Subsection we will use the central values of the above matrix elements. Notice that $f_{Ts}^{(n)} = f_{Ts}^{(p)}$ and both are much larger than f_{Tq} for u and d quarks, and therefore f_p and f_n are basically equal. Thus we will focus on the neutralino-proton cross section,

$$\sigma_{3p} \equiv \sigma_{\tilde{\chi}_1^0 - p} = \frac{4m_r^2}{\pi} f_p^2 \,, \tag{3.2.23}$$

with $m_r = m_p m_{\tilde{\chi}_1^0}/(m_p + m_{\tilde{\chi}_1^0}) \sim m_p$.

3.3 Parameter space and neutralino-nucleon cross section

In this Section the viability of the detection of the lightest NMSSM neutralino as a dark matter candidate will be studied. In particular, we will compute the theoretical predictions for the direct detection of neutralinos through their elastic scattering with nucleons inside a detector. In our computation we will take into account for the moment only the constraints on the parameter space from accelerator data described in Subsection 3.1.5. This will allow us to find the regions of the NMSSM where the cross section is in the range of detectors. With this information we will carry out more easily the whole analysis in Section 3.4, where bounds arising from kaon and B decays, as well as from $a_\mu^{\rm SUSY}$, and the relic abundance, are included.

As discussed in Subsection 2.2.3, many experiments for the direct detection of dark matter are running or in preparation. Thus, in our analysis, we will be particularly interested in the various NMSSM scenarios which might potentially lead to values of $\sigma_{\tilde{\chi}_1^0-p}$ in the sensitivity range of those detectors.

Although the free parameters in our model have already been presented in Subsection 3.1.5, it is worth recalling that the Higgs and neutralino sectors of the theory are specified by

$$\lambda\,, \quad \kappa\,, \quad \mu(=\lambda s)\,, \quad \tan\beta\,, \quad A_\lambda\,, \quad A_\kappa\,, \quad M_1\,, \quad M_2\,. \tag{3.3.24}$$

As aforementioned, we take these parameters to be free at the EW scale. Based on an argument of simplicity[3], the low-energy squark masses and trilinear couplings, which appear in the computation of the neutralino-nucleon cross section, are taken to be degenerate[4]. Unless otherwise stated, the common SUSY scale will be $M_{\rm SUSY} = 1$ TeV. Having free squark and slepton soft parameters at the EW scale allows us to ensure that in our analysis the lightest SUSY particle is indeed the χ_1^0. Also led by arguments of naturalness, we shall take a lower bound for λ, $\lambda_{\rm min} \sim \mu/s_{\rm max}$. Thus, taking the conservative range $s \lesssim 10$ TeV, this translates into $\lambda_{\rm min} \sim \mu({\rm GeV}) \times 10^{-4}$.

[3]Since in our analysis of the neutralino-nucleon cross section the detection channels mediated by Higgs scalars will be enhanced with respect to those mediated by squarks, the sensitivity of the results to variations of the squark parameters will be very small.

[4]Regarding the stop mass matrix we will work in the maximal-mixing regime, where the off-diagonal term takes the form $m_t\, X_t = m_t\, \sqrt{6}\, M_{\rm SUSY}$. Departures from this case would not affect significantly the theoretical predictions for the neutralino-nucleon cross section.

We begin our analysis by taking values for the soft gaugino masses that mimic at low scale the results from a hypothetical unified value at the GUT scale. Consequently, we will choose $M_2 = 1$ TeV and $M_1 = 500$ GeV. For the gluino mass, the value $M_3 = 3$ TeV will be taken. In Section 3.4 we will address variations of these values. In the following we take $|\mu| \geq 110$ GeV, since in most cases this allows to safely avoid the LEP bound on the lightest chargino mass. Throughout this Section, we shall consider several choices for the values of A_λ, A_κ, μ and $\tan\beta$, and for each case, we will study the associated phenomenology.

In order to simultaneously analyse the dark matter predictions and understand the effect of the experimental constraints on the parameter space of the NMSSM, it is very illustrative to begin our study in the plane generated by the Higgs couplings in the superpotential, λ and κ. In Subsection 3.1.2 we commented on the conditions to be applied to each of the sign combinations of the parameters, which arise from ensuring that the tree-level potential has a minimum with respect to the phases of the VEV's. In the following it will be clarifying to discuss each case separately. Let us first consider the cases associated with positive values of κ.

3.3.1 $\mu A_\kappa < 0$ and $\mu A_\lambda > 0$ ($\kappa > 0$)

As a first choice, we will consider the two cases where $\mu A_\kappa < 0$ and $\mu A_\lambda > 0$, namely those with μ, A_λ, $-A_\kappa > 0$ and μ, A_λ, $-A_\kappa < 0$.

In both cases, part of the parameter space can be excluded due to the occurrence of tachyons in the CP-even Higgs sector. Namely, it is easy to see from the expression of the CP-even Higgs matrix (3.1.8) that the off-diagonal terms $|\mathcal{M}^2_{S,13}|$ or $|\mathcal{M}^2_{S,23}|$ can become significantly bigger than $\mathcal{M}^2_{S,33}$, thus leading to the appearance of a negative eigenvalue. This will typically happen for moderate to large values of λ and small κ, for which $m_{h^0_1}$ is small. Large values of $|A_\kappa|$ and $\tan\beta$ lead to an increase of the tachyonic region, as we will later see. On the other hand, the eigenvalues of the CP-odd Higgs mass matrix are never negative. The CP-odd Higgs masses also decrease for large λ and small κ, but their minimum value is bounded by the appearance of tachyons in the CP-even sector.

The (λ, κ) parameter space is shown in Fig. 3.2 for an example with $\tan\beta = 3$, $A_\lambda = 200$ GeV, $A_\kappa = -50$ GeV and $\mu = 110$ GeV. The points which are excluded due to the occurrence of a Landau pole are indicated, as well as those not fulfilling the experimental constraints. According to the discussion above, the tachyons appearing in

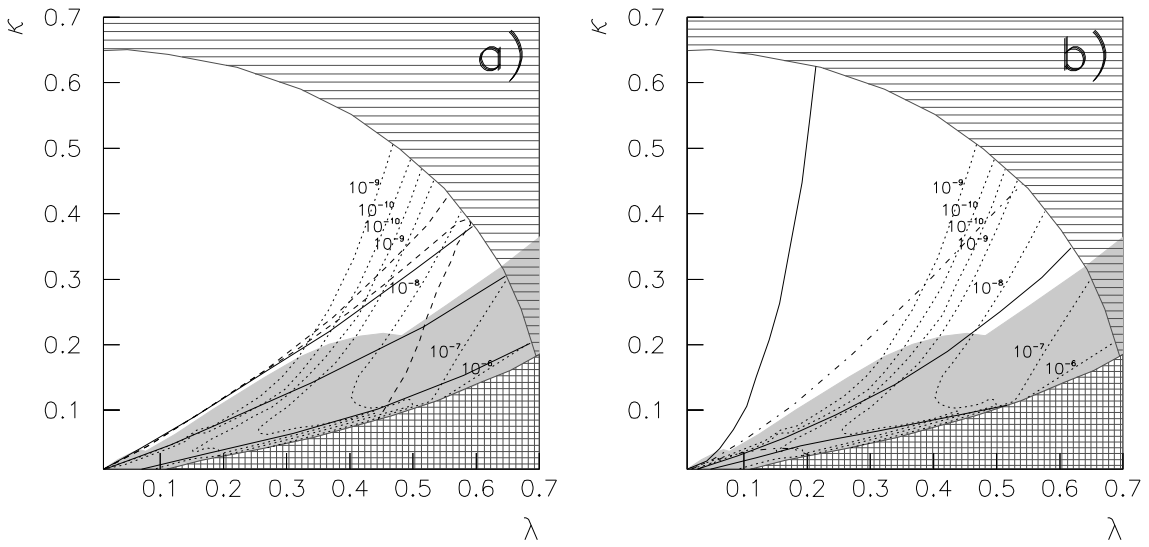

Figure 3.2: (λ, κ) parameter space for $\tan\beta = 3$, $A_\lambda = 200$ GeV, $A_\kappa = -50$ GeV and $\mu = 110$ GeV. In both cases, the ruled area represents points which are excluded due to the occurrence of a Landau pole. The grided area is excluded because of the appearance of tachyons. The grey area is associated to those points that do not satisfy the LEP constraints or where (at least) the LEP bound on direct neutralino production is violated. Dotted lines in the experimentally accepted region represent contours of scalar neutralino-proton cross section $\sigma_{\tilde{\chi}_1^0-p}$. In (a), from top to bottom, solid lines indicate different values of lightest Higgs scalar mass, $m_{h_1^0} = 114$, 75, 25 GeV, and dashed lines separate the regions where the lightest scalar Higgs has a singlet composition given by $S_{13}^2 = 0.1$, 0.9. In (b), from top to bottom, solid lines are associated with different values of the lightest neutralino mass, $m_{\chi_1^0} = 100$, 75, 50 GeV, while dot-dashed lines reflect the singlino composition of the lightest neutralino, $N_{15}^2 = 0.1$, 0.9 .

the lower right corner are due to the CP-even Higgs sector. It is worth remarking that in these cases, due to the smallness of the lightest CP-even Higgs mass, the experimental constraints (see Subsection 3.1.5) from $e^+e^- \to h^0 Z$, both IHDM and DHDM ($h^0 \to b\bar{b}$, $h^0 \to \tau^+\tau^-$, and $h^0 \to 2\,\text{jets}$), become very important and typically exclude the regions in the vicinity of those excluded by tachyons.

Dashed lines in Fig. 3.2a indicate the singlet composition of the lightest scalar Higgs. Singlet-like Higgses can be found for small values of κ, whereas doublet-like Higgses appear for large κ. This can be qualitatively understood from the expression of the corresponding mass matrix (3.1.14). In particular, the diagonal term $\mathcal{M}_{S,33}^2$ becomes

very small when κ decreases. Interestingly, when the singlet composition is significant, the reduced coupling can be smaller and thus Higgses with $m_{h_1^0} \lesssim 114$ GeV can escape detection and be in agreement with experimental data. This opens a new window in the allowed parameter space, characteristic of the NMSSM, which can have relevant consequences for dark matter detection as we will discuss below.

In Fig. 3.2b the same case is represented, but emphasizing the information on the neutralino properties. The singlino composition of the lightest neutralino is shown with dot-dashed lines, while solid lines correspond to different values of its mass. As one would expect from the structure of the neutralino mass matrix (3.1.14), for small κ, the lightest neutralino is essentially a singlino, with a small mass which can be approximated as $m_{\tilde{\chi}_1^0} \sim 2\mu\kappa/\lambda$. In the present case, singlino-like neutralinos appear for $\kappa \lesssim 0.04$ and $\lambda \lesssim 0.2$, whereas heavier, Higgsino-like, neutralinos (due to our choice of input values with $\mu < M_1$) populate the rest of the parameter space. Regions with small masses of the neutralino may be excluded due to the bound on direct neutralino production, which becomes quite severe for light Higgsino-like neutralinos.

In both figures, the different values of the neutralino-nucleon cross section are represented with dotted lines. As already commented in Section 3.2, the cross section increases in those regions with a light CP-even Higgs, as long as it is not a pure singlet. This behaviour is clearly illustrated in these figures, which feature very large values for $\sigma_{\tilde{\chi}_1^0-p}$ in the vicinity of the areas where the lightest Higgs becomes tachyonic. On the other hand far from these regions the cross section stabilizes at 10^{-8} pb $> \sigma_{\tilde{\chi}_1^0-p} > 10^{-9}$ pb.

In order to illustrate this point in more detail, we have represented in Fig. 3.3 the resulting $\sigma_{\tilde{\chi}_1^0-p}$ versus the lightest Higgs mass and the neutralino mass. Black dots fulfil all the experimental constraints, whereas grey dots are those experimentally excluded (we do not plot those regions ruled out due to theoretical arguments, such as the occurrence of a Landau pole). The sensitivities of present and projected dark matter experiments are also depicted as a function of $m_{\tilde{\chi}_1^0}$ for comparison. The small area bounded by dotted lines is allowed by the DAMA experiment in the simple case of an isothermal spherical halo model. The larger area also bounded by dotted lines represents the DAMA region when uncertainties to this simple model are taken into account. The (upper) areas bounded by solid lines are excluded by EDELWEISS and CDMS Soudan. Finally, the dashed lines represent the sensitivities of the projected, CDMS Soudan and Xe 1 tonne experiments.

Very large values for the cross section could in principle be obtained. However,

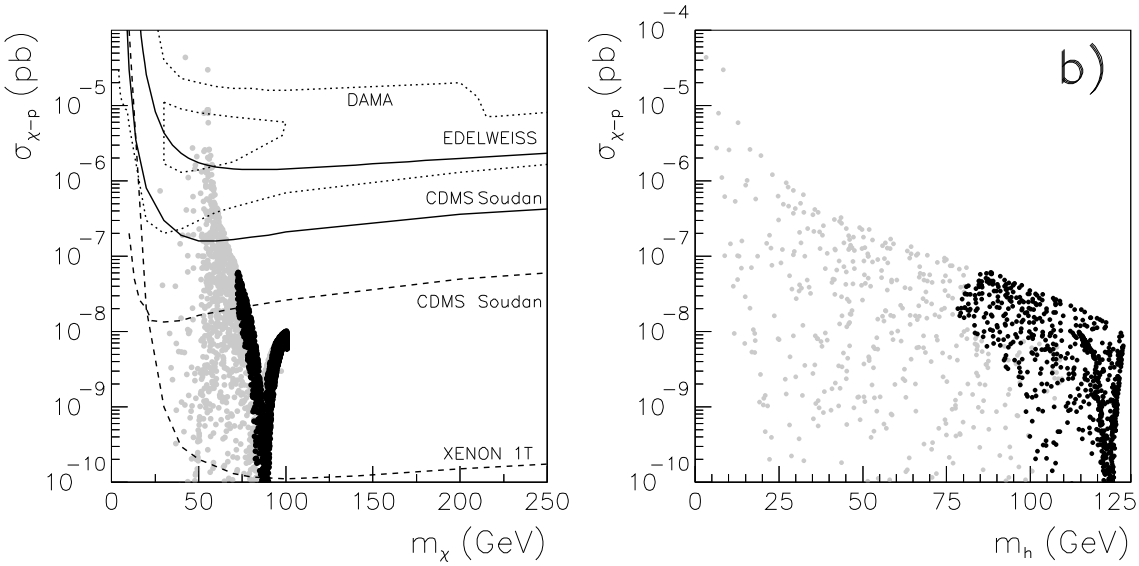

Figure 3.3: Scatter plot of the scalar neutralino-nucleon cross section, $\sigma_{\tilde{\chi}_1^0-p}$, as a function of (a) the neutralino mass, $m_{\tilde{\chi}_1^0}$, and (b) the lightest scalar Higgs mass, $m_{h_1^0}$, for $A_\lambda = 200$ GeV, $\mu = 110$ GeV, $A_\kappa = -50$ GeV, and $\tan\beta = 3$. Black dots correspond to points fulfilling all the experimental constraints, whereas grey dots represent those excluded. In (a) the sensitivities of present and projected experiments are also depicted with solid and dashed lines, respectively. The large (small) area bounded by dotted lines is allowed by the DAMA experiment when astrophysical uncertainties are (are not) taken into account.

these are associated to very light Higgses and are therefore subject to the strong constraints on $e^+e^- \to h^0 Z$ discussed above. Once every constraint is taken into account, points with $\sigma_{\tilde{\chi}_1^0-p} \lesssim 10^{-7}$ pb appear, which correspond to light scalar Higgses with $m_{h_1^0} \gtrsim 75$ GeV, surviving the experimental constraints due to their important singlet character, $S_{13}^2 \gtrsim 0.85$. This is a clear consequence of the NMSSM that we will exploit in subsequent examples, since it allows for a significant increase in the cross section. The neutralinos in these regions have $m_{\tilde{\chi}_1^0} \gtrsim 70$ GeV and have exhibit a have a mixed singlino-Higgsino composition ($N_{15}^2 \lesssim 0.3$ and $N_{13}^2 + N_{14}^2 \gtrsim 0.7$ in the region with larger cross section).

Notice that $\sigma_{\tilde{\chi}_1^0-p}$ displays an important suppression around $m_{\tilde{\chi}_1^0} \approx 90$ GeV. This is due to the cancellation of the contribution of the cross section coming from neutralino-neutralino-Higgs interaction due to the occurrence of terms with different signs. This type of accidental cancellations is analogous to those appearing in MSSM analyses for

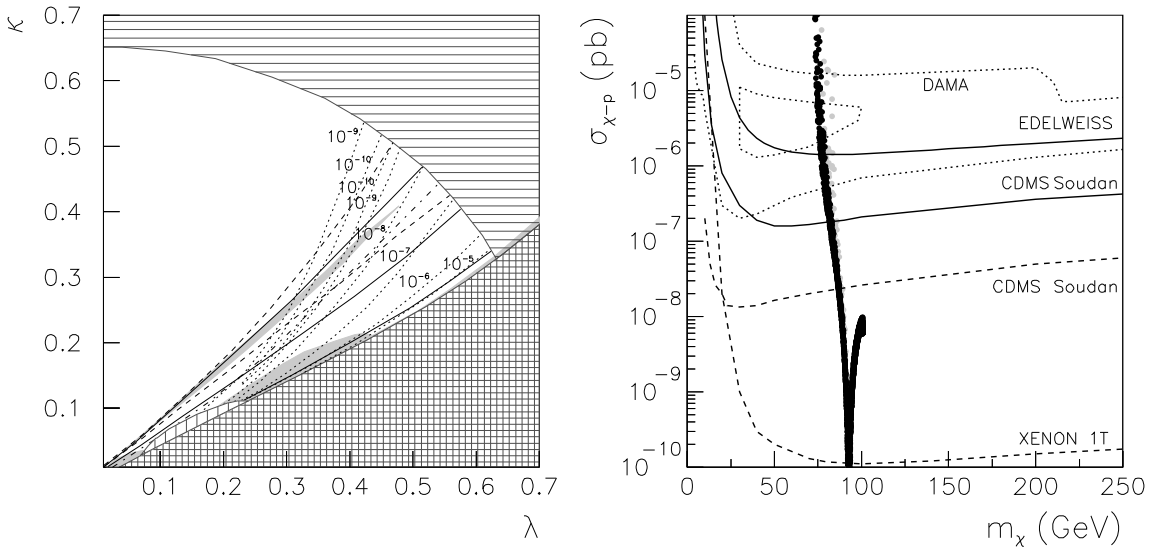

Figure 3.4: (λ, κ) parameter space with the corresponding constraints and neutralino-nucleon cross section as a function of the lightest neutralino mass for the case $A_\lambda = 200$ GeV $A_\kappa = -200$ GeV, $\mu = 110$ GeV and $\tan\beta = 3$. In the (λ, κ) plane the mass and composition of the lightest scalar Higgs, the composition of the lightest neutralino (only the line with $N_{15}^2 = 0.1$), and the predictions for $\sigma_{\tilde{\chi}_1^0 - p}$ are represented with the same line conventions as in Fig. 3.2, and the new ruled area (vertical lines) is excluded due to the occurrence of unphysical minima. The colour convention for the plot $\sigma_{\tilde{\chi}_1^0 - p}$ versus $m_{\tilde{\chi}_1^0}$ is as in Fig. 3.3.

$\mu < 0$ [75].

These results are also sensitive to variations in the rest of the input parameters (A_κ, $\tan\beta$, μ, and A_λ). For instance, increasing $|A_\kappa|$ (i.e., making it more negative) leads to a further decrease in $\mathcal{M}_{S,33}^2$ in the CP-even Higgs mass matrix, and therefore lighter Higgses can be obtained with a larger singlet composition. Although this translates into an enlargement of the regions where one has a tachyonic scalar Higgs, one may nevertheless find a larger $\sigma_{\tilde{\chi}_1^0 - p}$ in the allowed areas. Choosing $\tan\beta = 3$, $A_\lambda = 200$ GeV and $\mu = 110$ GeV, but with $A_\kappa = -200$ GeV, one can obtain $\sigma_{\tilde{\chi}_1^0 - p} \gtrsim 10^{-4}$ pb (points which in fact are already excluded by direct dark matter searches). The corresponding (λ, κ) parameter space, as well as $\sigma_{\tilde{\chi}_1^0 - p}$ versus the neutralino mass, are represented in Fig. 3.4. Remarkably, very light Higgses are allowed in this case ($m_{h_1^0} \gtrsim 20$ GeV) due to their significant singlet character ($0.9 \lesssim S_{13}^2 \lesssim 0.95$). Once again, the lightest neutralino ex-

hibits a large singlino-Higgsino composition ($N_{15}^2 \lesssim 0.3$ and $N_{13}^2 + N_{14}^2 \gtrsim 0.7$). For these reasons, one hardly finds experimentally excluded regions: only narrow stripes, mostly due to direct production of $\tilde{\chi}^0$ and $h^0 \to b\bar{b}$. Also, for small values of λ and κ, a very thin region excluded by the existence of false minima (see Subsection 3.1.5) appears. Conversely, decreasing $|A_\kappa|$ helps reducing tachyonic regions. In the particular case where $A_\kappa = 0$, no tachyons emerge from the CP-even sector[5]. The implications of this variation in the value of $\sigma_{\tilde{\chi}_1^0 - p}$ are minimal.

Changing $\tan\beta$ has an important impact in the analysis, mainly due to the effect on the Higgs sector. The tachyonic regions become larger as $\tan\beta$ increases (extending towards higher values of λ and κ). As a consequence, the neutralino is never a pure singlino and its mass increases due to the larger mixing with Higgsinos. For this reason the exclusion due to direct neutralino production becomes larger. In the end, not only the allowed region is reduced, but also the predictions for $\sigma_{\tilde{\chi}_1^0 - p}$ are smaller. Also, for very small values of $\tan\beta$ very light Higgsino-like neutralinos can be found in large regions of the parameter space. The experimental constraints are, nevertheless, more important and only small areas survive. Fig. 3.5 illustrates these properties.

[5]Only the region with $\lambda = 0$ would present a CP-odd Higgs with negative mass-squared. Obviously, we will not consider such a choice, since it would not solve the μ problem (it implies $\mu = 0$).

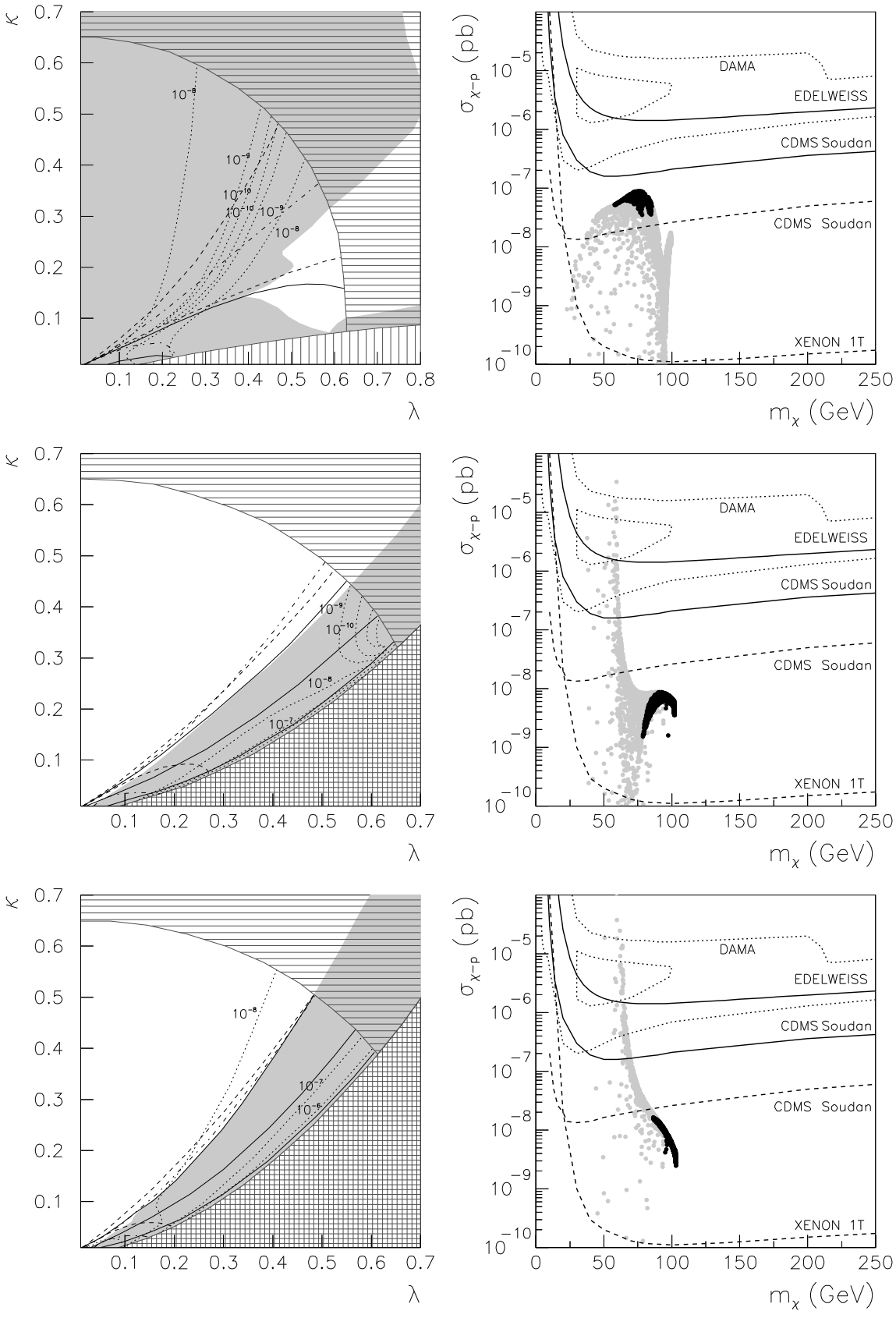

Figure 3.5: The same as in Fig. 3.4 but for the cases $A_\lambda = 200$, GeV $A_\kappa = -50$ GeV, $\mu = 110$ GeV, and $\tan\beta = 2$, 5, 10, from top to bottom. In the case with $\tan\beta = 2$, only the lines with $m_{h_1^0} = 75$, 25 GeV are represented, since $m_{h_1^0} \lesssim 110$ GeV.

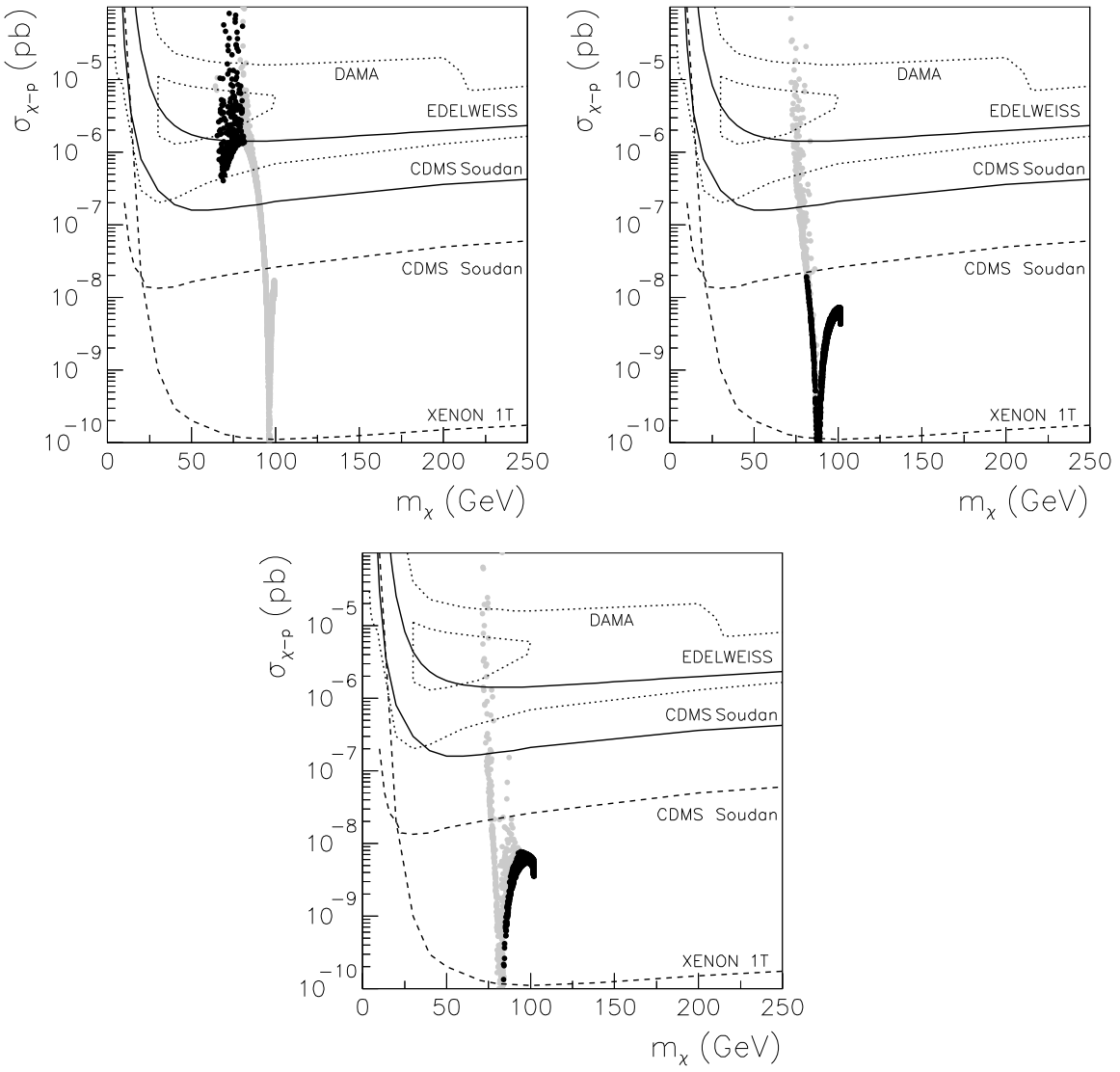

Figure 3.6: The same as in Fig. 3.3a but for the cases $A_\lambda = 200$, GeV $A_\kappa = -200$ GeV, $\mu = 110$ GeV, and $\tan\beta =$ 2, 4, 5, from left to right and top to bottom.

Similar examples, but for $A_\kappa = -200$ GeV can be found in Fig. 3.6, where the predictions for $\sigma_{\tilde{\chi}^0_1-p}$ are depicted as a function of the neutralino mass for $\tan\beta =$ 2, 4, 5. As already mentioned, small values of $\tan\beta$ favour lighter neutralinos with larger detection cross section.

Heavier neutralinos with a larger singlino composition can be obtained if the value of μ is increased. For this reason, the regions where direct neutralino production is not

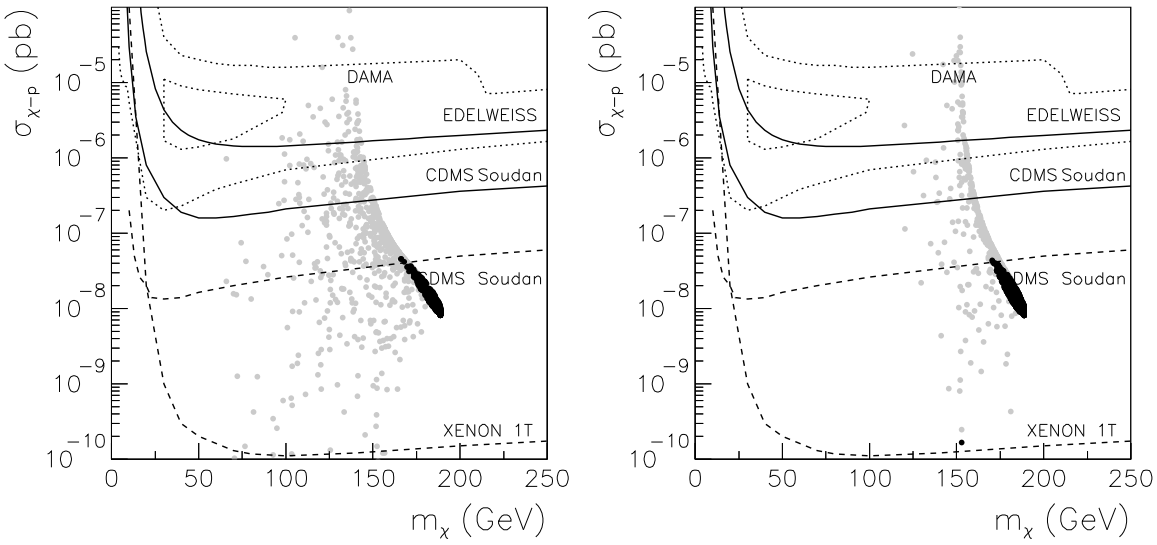

Figure 3.7: The same as in Fig. 3.3a but for the cases $A_\lambda = 200$ GeV, $\tan\beta = 3$, $\mu = 200$ GeV, and $A_\kappa = -50$, -200 GeV, from left to right.

in agreement with experimental bounds become much narrower. The mass of scalar Higgses also grows in this case, as well as their doublet character. Constraints on the Higgs sector are still strong enough to forbid those points where the neutralino is mostly singlino, and in the end $\tilde{\chi}_1^0$ preserves its mixed singlino-Higgsino character. In the remaining allowed area the predictions for $\sigma_{\tilde{\chi}_1^0-p}$ can vary, being typically smaller than in cases with low μ. This is shown in Fig. 3.7 for two examples with $\mu = 200$ GeV, $A_\lambda = 200$ GeV, $\tan\beta = 3$, and $A_\kappa = -50$, -200 GeV. In particular, in the case with $A_\kappa = -200$ GeV, the detection cross section is much smaller than in the analogous example with $\mu = 110$ GeV presented in Fig. 3.4.

Finally, variations in the value of A_λ also influence the theoretical predictions on $\sigma_{\tilde{\chi}_1^0-p}$. There is a range of A_λ for which the eigenvalues of the CP-even Higgs mass matrix are positive. However, for smaller or larger A_λ, off-diagonal terms may become large enough to ease the appearance of tachyons in the large λ regime. For instance, in Fig. 3.8 we have represented the (λ, κ) plane and the corresponding predictions for $\sigma_{\tilde{\chi}_1^0-p}$ in two cases with $A_\kappa = -50$ GeV, $\mu = 110$ GeV, $\tan\beta = 3$, and $A_\lambda = 50$, 450 GeV. We find that, in agreement with the discussion above, the tachyonic regions are larger than those for $A_\lambda = 200$ GeV in both cases. Also, the areas excluded by experimental constraints associated to IHDM and DHDM are more extensive, and in the case of $A_\lambda = 450$ GeV they forbid most of the parameter space. The neutralino is mostly

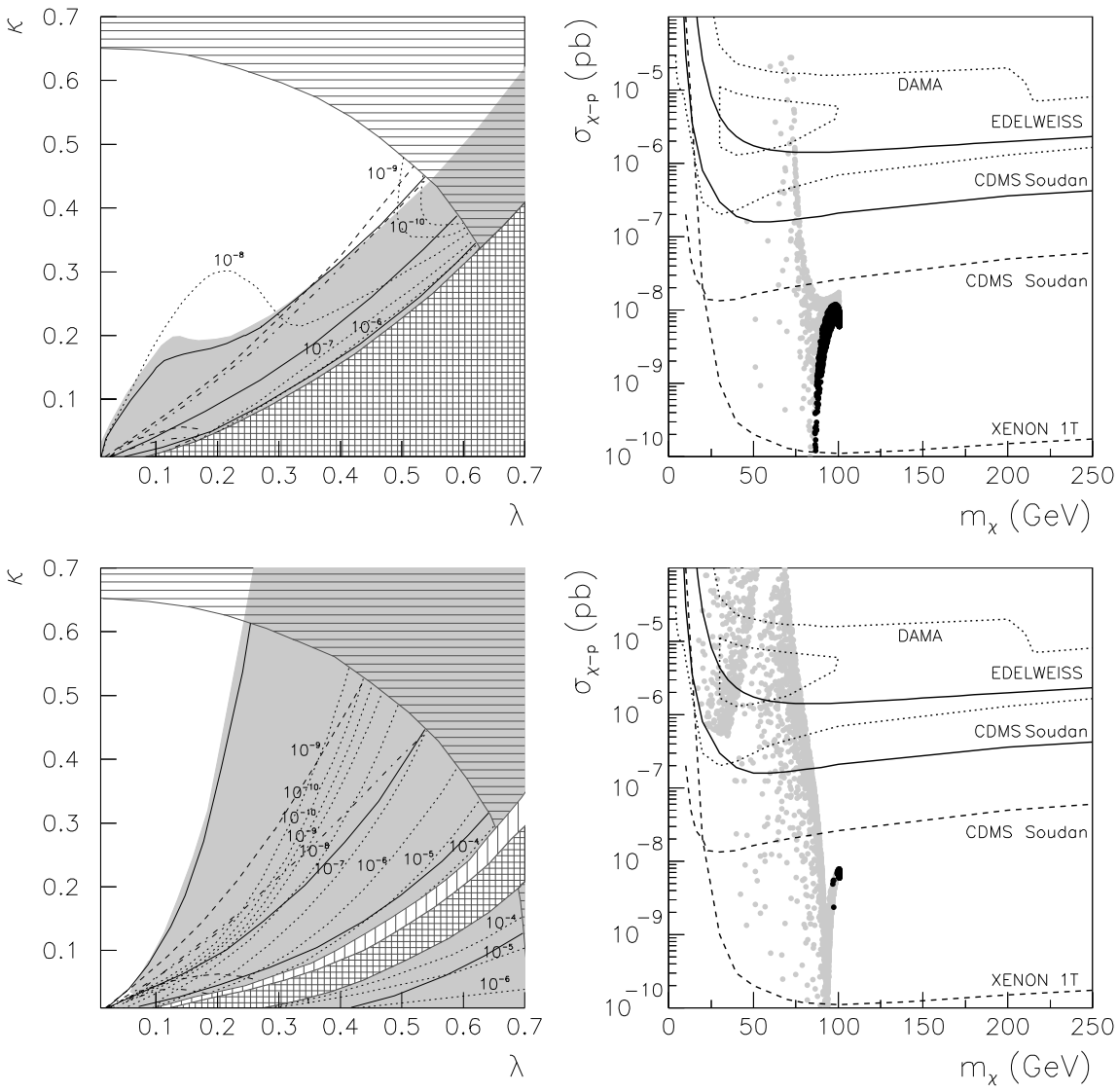

Figure 3.8: The same as in Fig. 3.4 but for the cases $A_\kappa = -50$ GeV, $\mu = 110$ GeV, $\tan\beta = 3$, and $A_\lambda = 50, 450$ GeV, from top to bottom.

Higgsino in the remaining allowed points, with $N_{15}^2 \lesssim 0.1(0.2)$ and $N_{13}^2 + N_{14}^2 \gtrsim 0.9(0.8)$ for $A_\lambda = 50(450)$ GeV, and there is a slight decrease in the predictions for $\sigma_{\tilde{\chi}_1^0 - p}$.

The range of values of A_λ for which the allowed area is more extensive is very dependent on the rest of the inputs. In particular, since large $\tan\beta$ and $|A_\kappa|$ increase the diagonal term, $\mathcal{M}^2_{P,22}$, in the CP-odd Higgs mass matrix, larger values of A_λ can be taken before $\mathcal{M}^2_{P,12}$ gets too big. For example, in the case with $A_\kappa = -200$ GeV one

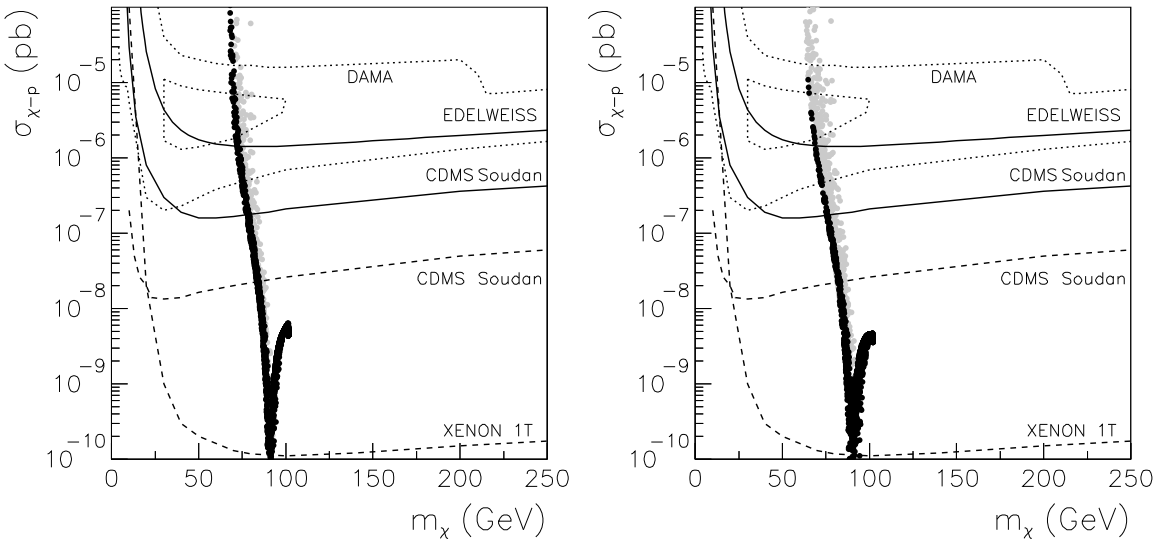

Figure 3.9: The same as in Fig. 3.3a but for the cases $A_\kappa = -200$ GeV, $\mu = 110$ GeV, $\tan\beta = 4$ and $A_\lambda = 300$ GeV, on the left, and $A_\kappa = -200$ GeV, $\mu = 110$ GeV, $\tan\beta = 5$ and $A_\lambda = 450$ GeV on the right.

can still obtain large accepted regions for $A_\lambda = 300 - 450$ GeV and $\tan\beta = 4 - 5$, as evidenced in Fig. 3.9, where points entering the sensitivities of the present dark matter detectors are obtained with $m_{\tilde{\chi}_1^0} \lesssim 75$ GeV.

To complete the analysis of the cases with $\mu A_\lambda > 0$ and $\mu A_\kappa < 0$, we must address the possibility of having μ, A_λ, $-A_\kappa < 0$. Note from (3.1.5) that the tree-level potential, $V^{\rm Higgs}_{\rm neutral}$, and therefore the Higgs mass matrices, are invariant under the exchange of the signs of μ, A_λ and A_κ, provided that the signs of μA_λ and μA_κ do not change. This implies that the above analysis regarding the Higgs sector is identical in this case. Differences arise, however, in the neutralino sector since the signs of $M_{1,2}$ were not altered. Therefore, the neutralino mass spectrum differs, as well as the lightest neutralino composition. Also the experimental constraints exhibit a slight variation. This case presents the same qualitative behaviour as the one formerly discussed in what the minimization of the Higgs potential is concerned. Nevertheless, differences arise regarding the theoretical predictions for $\sigma_{\tilde{\chi}_1^0-p}$ due to the experimental constraints and the different position of the accidental suppressions in the Higgs-exchange diagrams. These differences can be sizable for large $\tan\beta$. For instance, we have represented in Fig. 3.10 two examples with $A_\lambda = -200$ GeV, $\mu = -110$ GeV, $\tan\beta = 3$, and $A_\kappa = 50$, 200 GeV, where the suppression in $\sigma_{\tilde{\chi}_1^0-p}$ is found to occur

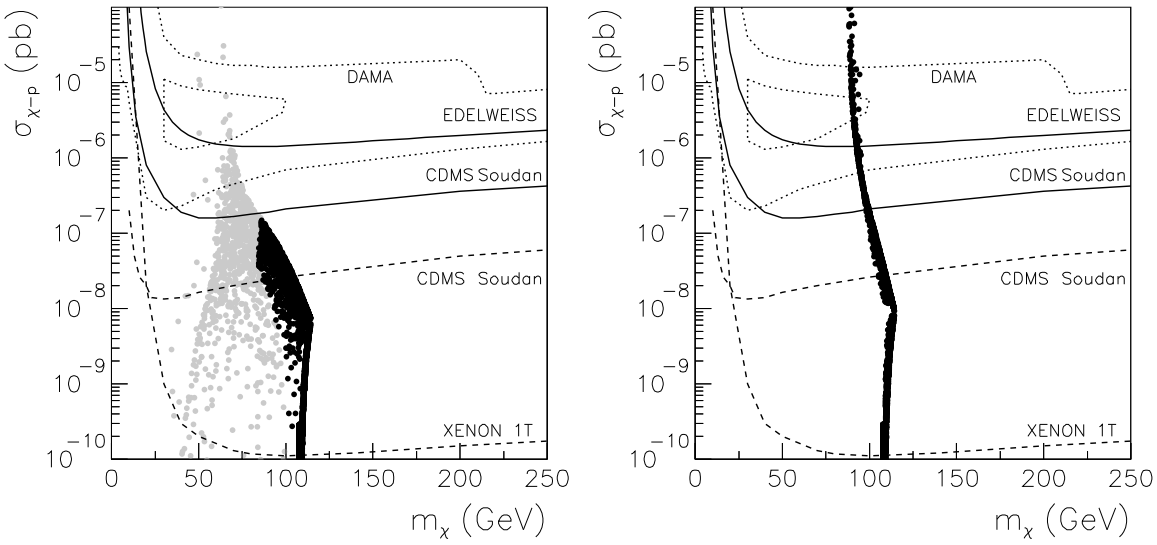

Figure 3.10: The same as in Fig. 3.3a but for the cases $A_\lambda = -200$ GeV, $\mu = -110$ GeV, $\tan\beta = 3$, and $A_\kappa = 50$, 200 GeV, from left to right.

for $m_{\tilde{\chi}_1^0} \approx 110$ GeV.

To sum up, we have found that large values of $\sigma_{\tilde{\chi}_1^0-p}$, even within the reach of dark matter detectors, can be obtained in the scenarios analysed in this Subsection. The NMSSM nature is evidenced in these examples by the compositions of the lightest neutralino (which is a singlino-Higgsino mixed state) and the scalar Higgs (which can be mostly singlet and as light as $m_{h_1^0} \gtrsim 20$ GeV).

3.3.2 $\mu A_\kappa < 0$ and $\mu A_\lambda < 0$ ($\kappa > 0$)

This choice comprises the cases μ, $-A_\lambda$, $-A_\kappa > 0$ and μ, $-A_\lambda$, $-A_\kappa < 0$.

We first address the possibility μ, $-A_\lambda$, $-A_\kappa > 0$. When compared with the cases discussed in the previous subection, the occurrence of tachyons in the Higgs sector gives rise to stronger constraints in this case, both in the CP-even and CP-odd Higgses.

For CP-even Higgses tachyons are now more likely to occur, due to the negative contributions in $\mathcal{M}^2_{S,33}$, induced by the terms proportional to μA_κ and A_λ/μ. Similarly, $\mathcal{M}^2_{S,11}$ receives a sizeable negative contribution from the term proportional to μA_λ which is particularly dangerous for large values of $\tan\beta$. In the CP-odd sector, an analogous study of the mass matrix shows that tachyons are more restrictive for large

values of λ and small values of κ. Actually, from the naive requirement $\mathcal{M}^2_{P,11} \geq 0$ the following constraint is obtained $\kappa \geq -\lambda A_\lambda/\mu$. In fact, this ensures the positiveness of the denominator in condition (ii) derived from the minimization of the Higgs potential in subection 3.1.2, and gives a qualitative idea on the dependence of the tachyonic region on the parameters A_λ and μ. When compared with the cases treated in the former subection, larger regions of the parameter space are now excluded. We found that tachyons in the CP-odd sector typically give rise to stronger constraints than those from CP-even sector, although the corresponding excluded regions practically coincide.

The experimental constraints from the neutralino sector are not very stringent in these examples, owing to the fact that the regions where the neutralino would have a small mass are typically excluded by the occurrence of tachyons.

As an example, the (λ, κ) plane is represented in Fig. 3.11 for $\tan\beta = 3$, $A_\lambda = -200$ GeV, $A_\kappa = -50$ GeV and $\mu = 110$ GeV. In this case, and in contrast with what was displayed in Fig. 3.2, there exists a very large region where one cannot find minima of $V^{\text{Higgs}}_{\text{neutral}}$. In particular, $\lambda \gtrsim 0.25$ is now excluded for this reason. In the rest of the parameter space, experimental constraints become very important in those regions with small values of the CP-even and CP-odd masses. Although the most important exclusion is due to DHDM constraints ($h^0 \to b\bar{b}$ and $h^0 \to \tau^+\tau^-$), some regions not fulfilling the bounds on APM ($h^0 a^0 \to 4b$'s) also appear. It is worth emphasizing that in the remaining allowed regions the lightest Higgs is doublet-like ($S^2_{13} \lesssim 0.003$) and its mass is never too small, $m_{h^0_1} \gtrsim 85$ GeV.

Regarding the composition of the lightest neutralino, it turns out to be Higgsino-like in all the allowed parameter space ($N^2_{13} + N^2_{14} \gtrsim 0.98$). As we already mentioned, those regions with small λ and κ that would lead to a singlino-like neutralino are excluded by absence of physical minima in the potential. For this reason the mass of the neutralino is dictated by the value of the μ term and we found $m_{\tilde{\chi}^0_1} \approx \mu$ throughout the allowed parameter space.

This is shown in Fig. 3.11, which represents the corresponding values of the neutralino-nucleon cross section as a function of the neutralino mass. The cross section ranges from 6×10^{-9} pb $\lesssim \sigma_{\tilde{\chi}^0_1 - p} \lesssim 7 \times 10^{-8}$ pb in this case. Once more, although higher values could be obtained, these are typically excluded due to the constraints on the CP-even Higgses.

Let us now address the relevance of variations in A_κ in the allowed regions of the parameter space and thus on the predictions for $\sigma_{\tilde{\chi}^0_1 - p}$. It can be seen that the increase

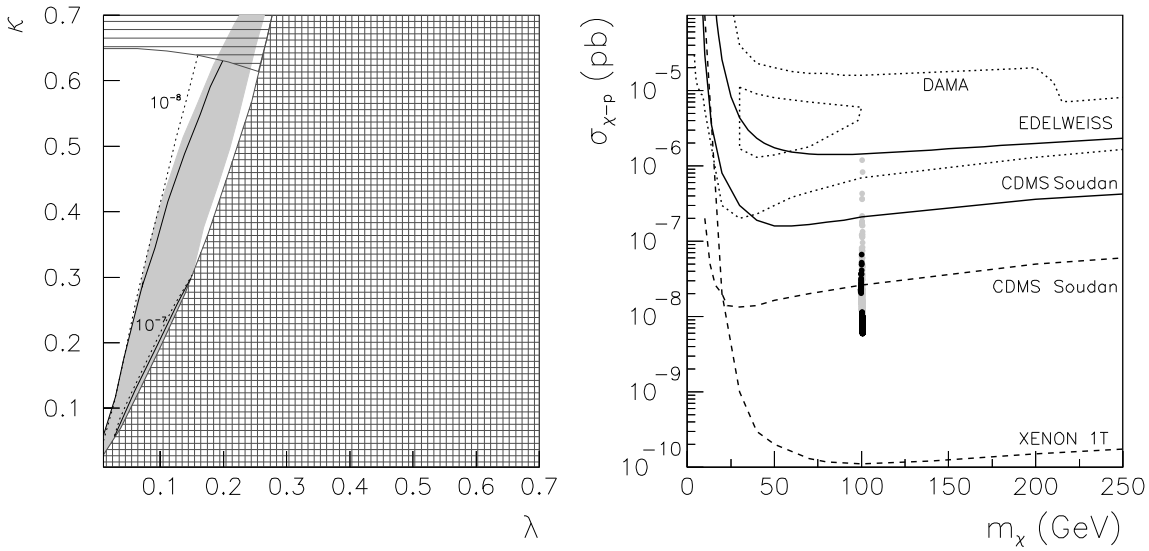

Figure 3.11: The same as in Fig. 3.4 but for $\tan\beta = 3$, $A_\lambda = -200$ GeV, $A_\kappa = -50$ Gev and $\mu = 110$ GeV. Only the lines with $m_{h_1^0} = 114$, 75 GeV are represented, and none of the lines showing the lightest scalar Higgs and neutralino composition is depicted, since $S_{13}^2 < 0.1$ and $N_{15}^2 < 0.1$ in all the plane.

in $|A_\kappa|$ (i.e., making it more negative) translates into an almost negligible enlargement in the allowed area, while the experimental constraints on CP-even Higgses become more restrictive. On the other hand, a decrease in the value of $|A_\kappa|$ leads to a lighter CP-odd Higgs and the tachyonic region increases, as can be easily understood from the mass matrix (3.1.10). For instance, in the particular case of $A_\kappa = 0$, and unless $|A_\lambda|$ is also very small, the entire parameter space can be excluded.

Regarding changes in A_λ and μ, these clearly affect the regions excluded by tachyons. Large values of μ and small $|A_\lambda|$ allow an increase in the accepted regions, in agreement with the condition on κ derived above, $\kappa \geq -\lambda A_\lambda/\mu$. Also, note that, since the masses of the Higgses increase, the associated experimental constraints become less restrictive and the allowed area is larger. Nevertheless, the region where the neutralino would have an important singlino composition is still typically excluded, and therefore in the allowed region $\tilde{\chi}_1^0$ is still Higgsino-like, with $m_{\tilde{\chi}_1^0} \approx \mu$. Despite the increase of $m_{\tilde{\chi}_1^0}$, the predictions for the cross section are essentially unaltered. An example with $\tan\beta = 3$, $A_\lambda = -200$ GeV, $A_\kappa = -50$ GeV and $\mu = 200$ GeV is represented in Fig. 3.12, displaying both the (λ, κ) plane and the neutralino-nucleon cross section versus the neutralino mass. We find $\sigma_{\tilde{\chi}_1^0-p} \lesssim 5 \times 10^{-8}$ pb, similar to what was found in Fig. 3.11, but now

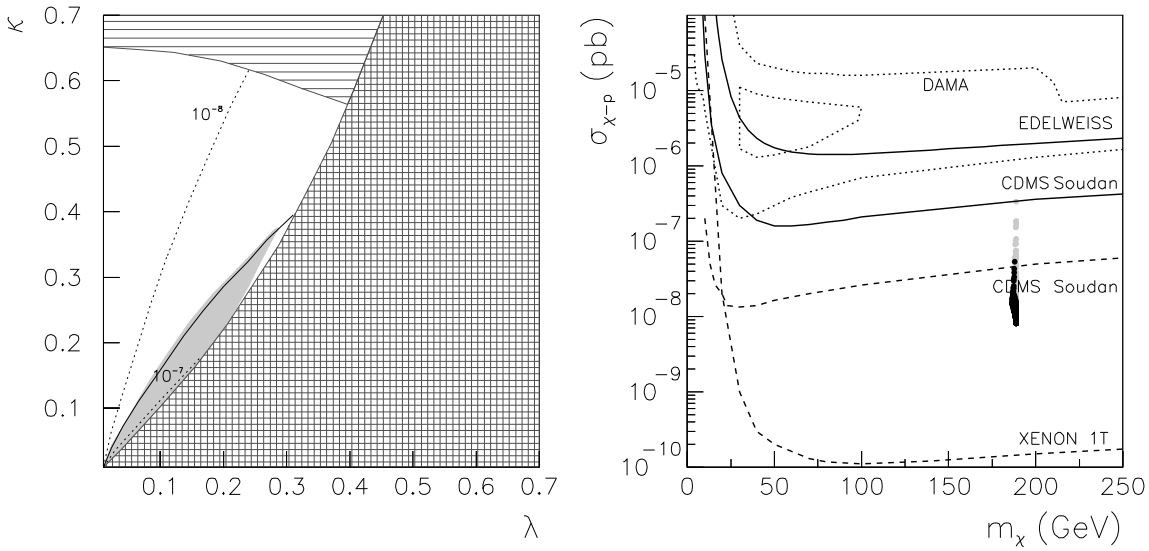

Figure 3.12: The same as in Fig. 3.4 but for $\tan\beta = 3$, $A_\lambda = -200$ GeV, $A_\kappa = -50$ Gev and $\mu = 200$ GeV. Only the line with $m_{h_1^0} = 114$ GeV is represented, and none of the lines showing the lightest scalar Higgs and neutralino composition is depicted, since $S_{13}^2 < 0.1$ and $N_{15}^2 < 0.1$ in all the plane.

with $m_{\tilde{\chi}_1^0} \approx 190$ GeV. The singlino component of $\tilde{\chi}_1^0$ is negligible ($N_{15}^2 \lesssim 0.006$) and the scalar Higgs is doublet-like ($S_{13}^2 \lesssim 0.001$).

Finally, regarding variations in the value of $\tan\beta$, these have little effect on the shape of the tachyonic region, whereas experimental constraints are more sensitive to them. As in the former scenario, for low values of $\tan\beta$ light scalar Higgses are obtained. Since these are predominantly doublet-like, experimental constraints (especially those associated with DHDM, namely, $h^0 \to b\bar{b}$ and $h^0 \to \tau^+\tau^-$) become very important and forbid, for instance, the whole parameter space in the case $\tan\beta = 2$. On the other hand, larger values of $\tan\beta$ are welcome in order to increase the value of $m_{h_1^0}$, obtaining also a moderate enhancement of the cross section. In order to illustrate this discussion, we represent in Fig. 3.13 two cases with $\tan\beta = 2, 5$, for $A_\lambda = -200$ GeV, $A_\kappa = -50$ GeV and $\mu = 110$ GeV. We find that the cross section can reach $\sigma_{\tilde{\chi}_1^0 - p} \approx 10^{-7}$ pb in the case where $\tan\beta = 5$. None of these examples displays any qualitative change regarding the neutralino and Higgs compositions.

To complete the analysis of the cases with $\mu A_\lambda < 0$ we still have to consider the case μ, $-A_\lambda$, $-A_\kappa < 0$. As we explained in the former Subsection, the analysis of the

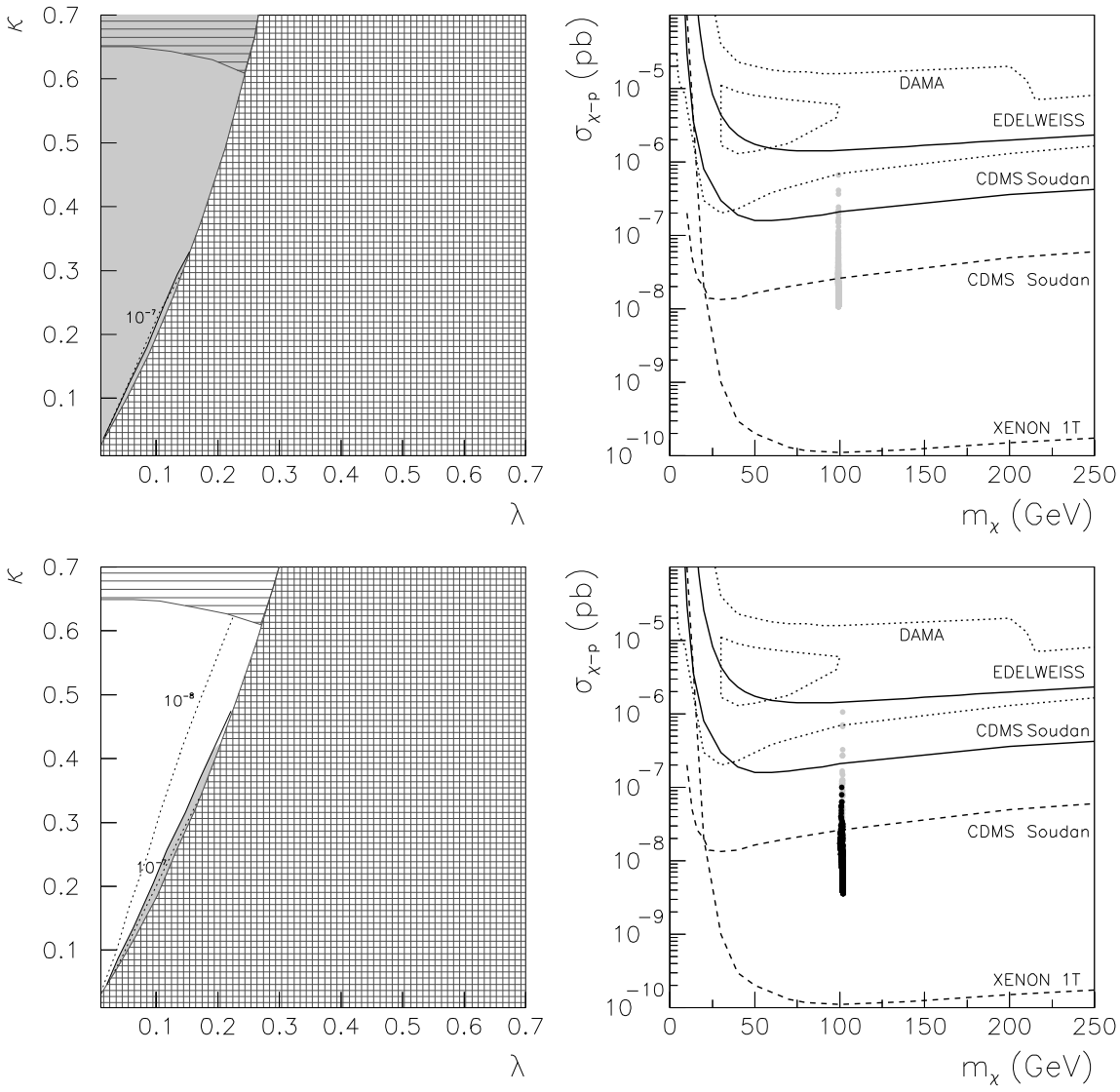

Figure 3.13: The same as in Fig. 3.4 but for the cases $A_\lambda = -200$ GeV, $A_\kappa = -50$ GeV, $\mu = 110$ GeV, and $\tan\beta = 2$, 5, from top to bottom. In the left frames, only the line with $m_{h_1^0} = 114$ GeV is represented, and none of the lines showing the lightest scalar Higgs and neutralino composition is depicted, since $S_{13}^2 < 0.1$ and $N_{15}^2 < 0.1$ in all the plane.

Higgs sector will be analogous to that of the case we have just studied. Despite the differences in the neutralino sector, its mass, composition and detection cross section will also be qualitatively equal to those previously discussed.

Summarizing, all the cases we have analysed in this Subsection present as common features the appearance of Higgsino-like neutralinos with a detection cross section which can be as large as $\sigma_{\tilde{\chi}_1^0-p} \lesssim 10^{-7}$ pb, and doublet-like Higgses.

3.3.3 $\mu A_\kappa > 0$ and $\mu A_\lambda > 0$ ($\kappa > 0$)

We consider now those cases where $\mu A_\kappa > 0$, and $\mu A_\lambda > 0$, conditions which are fulfilled in the cases μ, A_λ, $A_\kappa > 0$ and μ, A_λ, $A_\kappa < 0$.

We will begin with all μ, A_λ, and A_κ positive. As in the previous cases, a simple analysis of the tree-level Higgs mass matrices gives a qualitative understanding on the nature and extension of the tachyonic regions in the parameter space.

In this particular case tachyons in the CP-odd sector arise through the negative contribution $-\frac{3\kappa\mu}{\lambda}A_\kappa$ in $\mathcal{M}^2_{P,22}$. Since this is mainly compensated by the positive term $\frac{\lambda^2 v^2}{\mu}A_\lambda \sin 2\beta$, the tachyonic region occurs for small values of λ. The excluded region is obviously more important for small values of A_λ and large μ, A_κ, and $\tan\beta$. The occurrence of tachyons in the CP-even Higgses is analogous to the case $\mu A_\lambda > 0$, $\mu A_\kappa < 0$ discussed in Subsection 3.3.1, due to the increase of the off-diagonal terms in the mass matrix. As in that case, tachyons appear for large values of λ and small κ and become more stringent as $\tan\beta$ grows.

Experimental constraints play also a very relevant role in this case. Close to the tachyonic regions the experimental bounds on the Higgs sector are very severe. In particular IHDM, DHDM ($h^0 \to b\bar{b}$, $h^0 \to 2\,\text{jets}$) are responsible for the most important exclusions, although APM (mainly $h^0 a^0 \to 4\,b$'s) may also be violated. Finally, excluding those regions where the direct neutralino production is in disagreement with the experimental bounds leads to important constraints in the region with light $\tilde{\chi}_1^0$.

An example with $A_\lambda = 200$ GeV, $\mu = 110$ GeV, $A_\kappa = 50$ GeV and $\tan\beta = 3$ is represented in Fig. 3.14, depicting the constraints on the (λ, κ) plane and the corresponding predictions for $\sigma_{\tilde{\chi}_1^0-p}$ versus the neutralino mass. In the small experimentally allowed region the lightest neutralino is a mixed singlino-Higgsino state, with $N_{15}^2 \lesssim 0.4$ and $N_{13}^2 + N_{14}^2 \gtrsim 0.6$, and the lightest scalar Higgs can have an important singlet component ($S_{13}^2 \lesssim 0.8$). The experimental constraints impose $m_{\tilde{\chi}_1^0} \gtrsim 70$ GeV and $m_{h_1^0} \gtrsim 85$

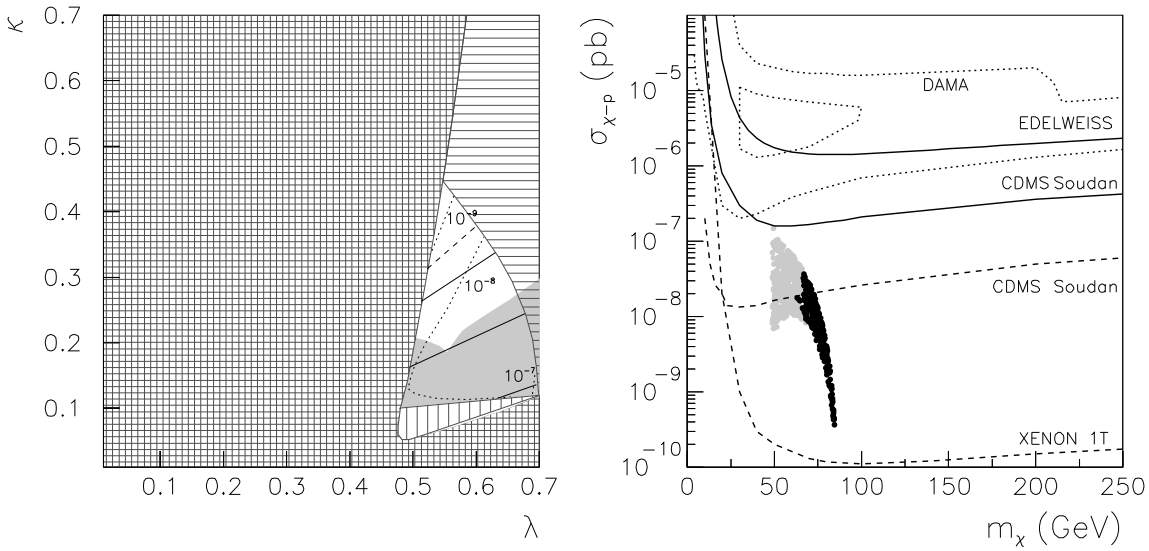

Figure 3.14: The same as in Fig. 3.4 but for $A_\lambda = 200$ GeV, $\mu = 110$ GeV, $A_\kappa = 50$ GeV, and $\tan\beta = 3$. Only the line with $S^2_{13} = 0.1$ is represented, and none of the lines showing the neutralino composition is depicted since $0.5 > N^2_{15} > 0.1$ in all the plane.

GeV, which set a limit on the theoretical predictions for the neutralino-nucleon cross section at $\sigma_{\tilde{\chi}^0_1 - p} \lesssim 4 \times 10^{-8}$ pb.

Variations of A_κ have an important impact on the allowed parameter space. As already commented, the region excluded due to tachyons in the CP-odd Higgs sector increases for larger values of A_κ. For instance, in the example with $A_\lambda = 200$ GeV, $\mu = 110$ GeV, and $\tan\beta = 3$, the allowed region completely disappears for $A_\kappa \gtrsim 110$ GeV. On the other hand, decreasing the value of A_κ the parameter space is enlarged. Recall that the minimal value $A_\kappa = 0$ has already been analysed in Subsection 3.3.1 in the context of a scenario with μ, $A_\lambda, -A_\kappa > 0$.

Decreasing the value of A_λ also leads to an increase of regions with a tachyonic pseudoscalar. If $\mu = 110$ GeV, $A_\kappa = 50$ and $\tan\beta = 3$, the whole parameter space is excluded for $A_\lambda \lesssim 50$ GeV. On the other hand, a moderate increase of A_λ helps avoiding tachyons, especially in the CP-even sector. An example with $A_\lambda = 300$ GeV can be found in Fig. 3.15, where the (λ, κ) plane and the theoretical predictions for $\sigma_{\tilde{\chi}^0_1 - p}$ are represented. Since in this case the experimental constraints from Higgs decays are less severe, we find that the regions with very light Higgs and $\tilde{\chi}^0_1$ are now experimentally viable. In particular, neutralinos with an important singlino composition, $N^2_{15} \lesssim 0.45$,

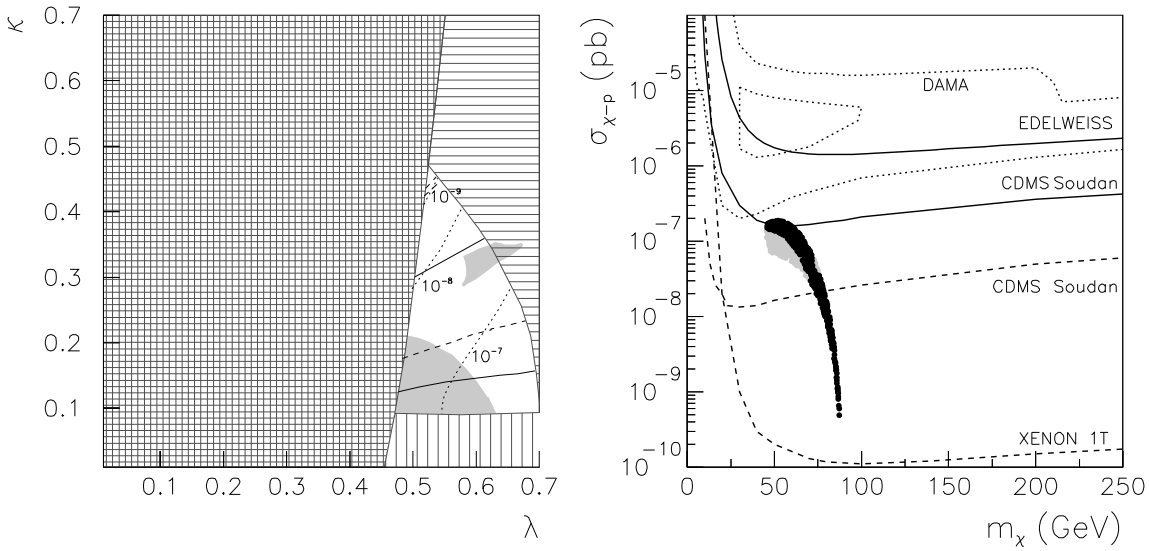

Figure 3.15: The same as in Fig. 3.4 but for $A_\lambda = 300$ GeV, $\mu = 110$ GeV, $A_\kappa = 50$ GeV, and $\tan\beta = 3$. Only the lines with $m_{h_1^0} = 114$, 75 GeV are represented. Regarding the neutralino composition, only the line with $N_{15}^2 = 0.1$ is shown in the upper corner of the allowed region, since in the rest of the parameter space $0.5 > N_{15}^2 > 0.1$.

can be obtained with $m_{\tilde{\chi}_1^0} \gtrsim 45$ GeV, whereas the lightest Higgses ($m_{h_1^0} \approx 65-90$ GeV) are all singlet-like. This in turn favours larger values of the cross section ($\sigma_{\tilde{\chi}_1^0-p} \lesssim 2 \times 10^{-6}$ pb), and compatibility with present experiments is almost obtained. Should we further increase the value of A_λ, the experimental constraints associated with the scalar Higgs would become again more important.

In order to prevent the occurrence of tachyons in the CP-odd Higgses, the value of μ has to be small. For instance, taking $\mu = 200$ GeV in the example with $A_\lambda = 200$ GeV, $A_\kappa = 50$ GeV and $\tan\beta = 3$, all the (λ, κ) plane would be excluded.

Regarding the value of $\tan\beta$, as already mentioned, the larger it is, the more extensive the regions excluded by $m_{h_1^0}^2 < 0$ become. In Fig. 3.16 we represent two examples with $A_\lambda = 200$ GeV, $A_\kappa = 50$ GeV, $\mu = 110$ GeV and $\tan\beta = 2$, 5. We find that low values of $\tan\beta$ still allow physical minima of the potential. Moreover, both the singlino component of $\tilde{\chi}_1^0$ and the singlet component of the scalar Higgs can be slightly enhanced. For example, for $\tan\beta = 2$ light neutralinos ($\tilde{\chi}_1^0 \gtrsim 60$ GeV) can be obtained with $N_{15}^2 \lesssim 0.55$, while Higgses in the mass range $m_{h_1^0} \approx 75 - 100$ GeV are singlet-like. However, the predictions for the detection cross section suffer a moderate decrease and

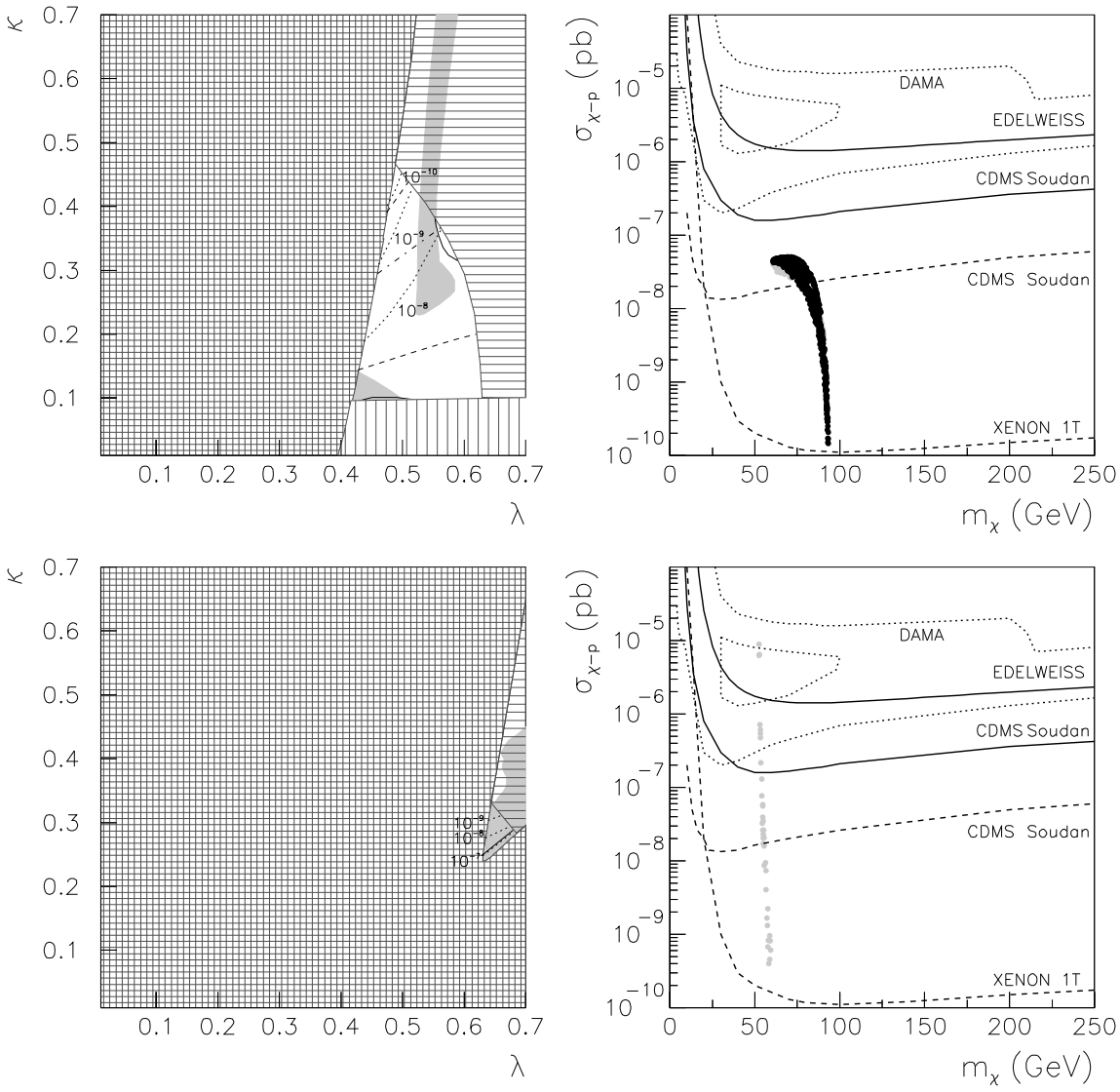

Figure 3.16: The same as in Fig. 3.4 but for the cases $A_\lambda = 200$ GeV, $\mu = 110$ GeV, $A_\kappa = 50$ GeV, and $\tan\beta = 2, 5$, from top to bottom. In the case with $\tan\beta = 2$ only the lines with $m_{h_1^0} = 114, 75$ GeV, and those with $S^2_{13} = 0.1$ and $N^2_{15} = 0.1$ are represented. Similarly, in the case with $\tan\beta = 5$ only the line with $m_{h_1^0} = 25$ GeV is drawn, and none of the lines showing the compositions of the lightest scalar Higgs and neutralino is depicted, since $0.7 > S^2_{13} > 0.1$ and $0.4 > N^2_{15} > 0.1$ in all the plane.

$\sigma_{\tilde{\chi}^0_1-p} \lesssim 5\times10^{-8}$ pb is obtained. On the other hand, for $\tan\beta \gtrsim 5$ the whole parameter space is in general excluded.

We should now address the complementary choice of the sign of the parameters, namely μ, A_λ, $A_\kappa < 0$, for which we already know that the analysis of the Higgs sector still holds. Once more, differences arise in the theoretical predictions for $\sigma_{\tilde{\chi}_1^0-p}$

To sum up, the choices for the signs of the parameters which have been considered in this Subsection also permit obtaining large values for the theoretical prediction of the neutralino-nucleon cross section, despite the fact that the parameter space is very constrained both experimentally and by the occurrence of tachyons. In particular, values of $\sigma_{\tilde{\chi}_1^0-p}$ close to the sensitivities of the present detectors can be found in some regions of the parameter space. The lightest neutralino displays a mixed singlino-Higgsino character, and the scalar Higgs is singlet-like and light in those regions with larger $\sigma_{\tilde{\chi}_1^0-p}$.

3.3.4 $\mu A_\kappa > 0$ and $\mu A_\lambda > 0$ ($\kappa < 0$)

We will now focus our attention on those cases with a negative value for κ, namely μ, A_λ, $A_\kappa > 0$ and μ, A_λ, $A_\kappa < 0$.

Let us therefore concentrate on the first of the two possibilities, μ, A_λ, $A_\kappa > 0$. The parameter space is in this case plagued with tachyons in both the CP-even and CP-odd Higgs sectors. On the one hand, regarding the CP-odd Higgses, large values of $|\kappa|$ and μ and small values of λ and A_λ may lead to negative values in the diagonal terms of the mass matrix, especially in $\mathcal{M}^2_{P,11}$. Nevertheless, large values of λ can also induce very large off-diagonal terms $\mathcal{M}^2_{P,12}$ if A_λ is large and a negative eigenvalue can be obtained in that case. Similar arguments lead to analogous conclusions concerning tachyons in the scalar sector, being the region with small λ the one facing the most severe restrictions.

Note that experimental constraints will play a very important role in the vicinity of these regions. Although the largest exclusions typically arise from the bounds on IHDM and DHDM (mainly in $h^0 \to b\bar{b}$, $h^0 \to 2\,\text{jets}$), APM can also exclude some regions with a small m_{a^0}. All these become particularly restrictive in the low $\tan\beta$ regime. In fact, in most of the cases with $\tan\beta \lesssim 3$ all of the parameter space is excluded. Experimental constraints in the neutralino sector can also be very stringent, especially for small values of μ, where $\tilde{\chi}_1^0$ is light and Higgsino-like.

In the remaining allowed regions of the parameter space, the lightest CP-even Higgs is mostly dominated by the doublet component. Concerning the lightest neutralino, it

turns out to be Higgsino-like. Owing to this, the predictions for $\sigma_{\tilde{\chi}_1^0-p}$ are very similar to those obtained in Subsection 3.3.2.

The above discussion can be illustrated with Fig. 3.17, where the (λ, κ) plane and the predictions for $\sigma_{\tilde{\chi}_1^0-p}$ are presented for a case with $A_\lambda = 450$ GeV, $\mu = 200$ GeV, $A_\kappa = 50$ GeV, and $\tan\beta = 5$. Light singlino-like neutralinos can only be obtained in the very small area with $|\kappa| \lesssim 0.06$, where the scalar Higgs may be as light as $m_{h_1^0} \gtrsim 50$ GeV with a large singlet component. In this particular region the predicted values for the detection cross section are not large, $\sigma_{\tilde{\chi}_1^0-p} \lesssim 10^{-9}$ pb. In the rest of the parameter space $\tilde{\chi}_1^0$ is Higgsino-like, which implies $m_{\tilde{\chi}_1^0} \approx \mu$, and the lightest scalar Higgs is a doublet with $m_{h_1^0} \gtrsim 112$ GeV. Slightly higher values for the cross section are obtained, which are bounded by the experimental constraints on the scalar Higgs at $\sigma_{\tilde{\chi}_1^0-p} \lesssim 6 \times 10^{-8}$ pb. This prediction can be slightly increased with larger values of $\tan\beta$. For instance, with $\tan\beta = 10$ one finds $\sigma_{\tilde{\chi}_1^0-p} \lesssim 2 \times 10^{-7}$ pb. None of the above remarks concerning the masses and compositions of the lightest neutralino and scalar Higgs would change in this case.

Variations in the rest of the parameters are very constrained due to the extensive tachyonic regions and the strong experimental bounds, especially those associated to the bounds on IHDM and DHDM. This is, for instance, what happens when the value of A_λ decreases. The very narrow region for small $|\kappa|$ where singlino-like neutralinos can be obtained is usually ruled out and the only surviving areas are those featuring heavy Higgsino-like neutralinos and doublet-like scalar Higgses. For this reason, the predictions for the detection cross section are always similar to those presented in the example of Fig. 3.17.

Finally, concerning the case μ, A_λ, $A_\kappa < 0$, nothing changes in the analysis of the Higgs sector. Once again, the differences in the neutralino sector and the slight changes in the experimental constraints can induce variations in the predicted $\sigma_{\tilde{\chi}_1^0-p}$. Nevertheless, a similar global upper bound of $\sigma_{\tilde{\chi}_1^0-p} \lesssim 10^{-7}$ pb is obtained.

The examples analysed in this Subsection feature a lightest neutralino which is Higgsino-like in most of the parameter space, together with a doublet-like lightest scalar Higgs. The neutralino-nucleon cross section is bounded by experimental constraints on the Higgs sector at $\sigma_{\tilde{\chi}_1^0-p} \lesssim 2 \times 10^{-7}$ pb. Singlino-like neutralinos can only be obtained in extremely small regions of the parameter space and predict smaller cross sections, $\sigma_{\tilde{\chi}_1^0-p} \lesssim 2 \times 10^{-9}$ pb.

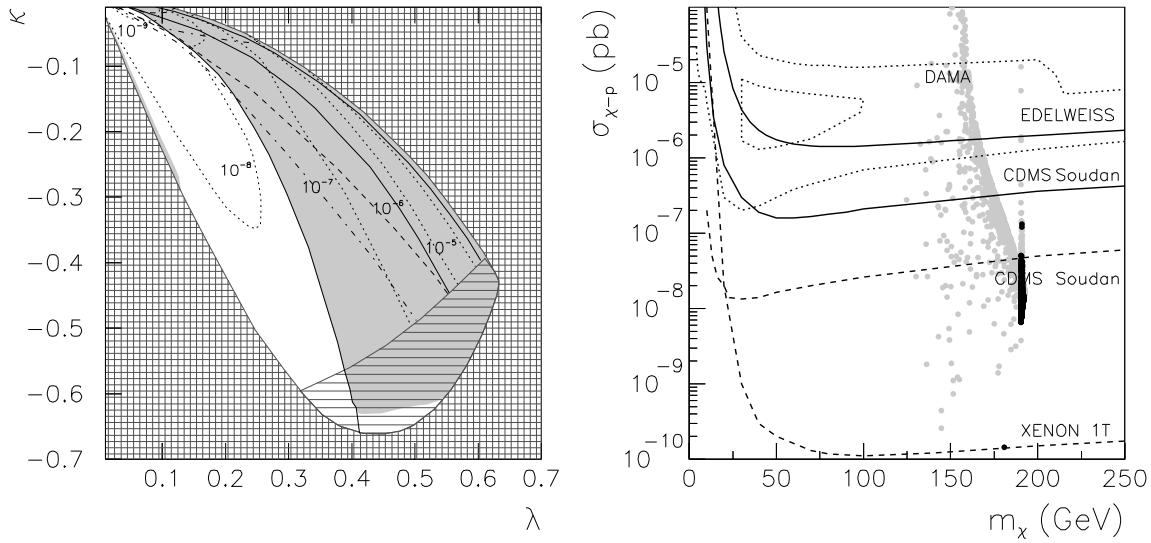

Figure 3.17: The same as in Fig. 3.4 but for positive κ, with $A_\lambda = 450$ GeV, $\mu = 200$ GeV, $A_\kappa = 50$ GeV and $\tan\beta = 5$

3.3.5 Overview of the results

In the previous Subsections we have presented a separate analysis of the distinct regions of the A_λ, A_κ, and $\tan\beta$ parameter space. This kind of approach was useful in order to comprehend the implications of individual variations of these parameters. We have thus computed the theoretical predictions for the scalar neutralino-proton cross section, $\sigma_{\tilde{\chi}_1^0-p}$, and compared it with the sensitivities of present and projected dark matter experiments. In the computation we have taken into account constraints on the parameter space from accelerator data.

We have found that large values of $\sigma_{\tilde{\chi}_1^0-p}$, even within the reach of present dark matter detectors, can be obtained in regions of the parameter space. This is essentially due to the exchange of very light Higgses, $m_{h_1^0} \lesssim 70$ GeV. The NMSSM nature is evidenced in this result, since such Higgses have a significant singlet composition, thus escaping detection and being in agreement with accelerator data. In fact, Higgses as light as 15 GeV can be obtained. The lightest neutralino in those regions exhibits a large singlino-Higgsino composition, and a mass in the range $50 \lesssim m_{\tilde{\chi}_1^0} \lesssim 100$ GeV.

On the other hand, in addition to LEP II and Tevatron limits on the spectrum, one should also take into account SUSY contributions to low-energy observables. The most stringent bounds arise from kaon and B decays, as well as from the muon anomalous

magnetic moment. Naturally, in order to be a viable dark matter candidate, the NMSSM lightest neutralino must also satisfy the present astrophysical bounds on the relic abundance. In the next Section we will complete the analysis, including these bounds, which may be very restrictive. For this, the analysis carried out in the previous Subsections is very useful, since we already know which regions of the parameter space give rise to large cross sections within the reach of dark matter detectors.

3.4 Including experimental and astrophysical constraints

In this Section, we continue studying the viability of the lightest NMSSM neutralino as a good dark matter candidate. Motivated by the results obtained in the previous Section, where large neutralino-nucleon cross sections were possible, we focus on these regions of the parameter space including other constraints. In particular, bounds from K- and B-meson decays, $a_\mu^{\rm SUSY}$, and the relic abundance are taken into account. Finally, we discuss the prospects of the experimentally viable regions regarding direct detection of dark matter.

Let us comment first in the next Subsection on the various constraints on the low-energy observables that will be included in the analysis.

3.4.1 Constraints on the parameter space

As discused in Section 3.1, in addition to ensuring the presence of a minimum of the potential, other constraints, both theoretical and experimental, must be imposed on the parameter space generated by the low-energy NMSSM degrees of freedom

$$\lambda,\ \kappa,\ \tan\beta,\ \mu,\ A_\lambda,\ A_\kappa\,. \tag{3.4.25}$$

The soft SUSY-breaking terms, namely gaugino masses $M_{1,2,3}$, scalar masses, $m_{Q,L,U,D,E}$, and trilinear parameters, $A_{Q,L,U,D,E}$, are also taken as free parameters and specified at low scale.

A comprehensive analysis of the low-energy NMSSM phenomenology can be obtained using the NMHDECAY 2.0 code [76]. After minimising the scalar potential, thus dismissing the presence of tachyons and/or false minima, the Higgs boson masses are computed, including 1- and 2-loop radiative corrections. Squark and slepton masses are also calculated, as well as the corresponding mixing angles for the third generation. Chargino and neutralino masses and mixings are evaluated and all the relevant couplings are derived.

Let us recall that even though the general analysis is performed at low-energy, a further theoretical constraint can be derived, namely the absence of a Landau pole for λ, κ, Y_t and Y_b below the GUT scale. Including logarithmic one-loop corrections to λ and κ, the latter constraint translates into $\lambda \lesssim 0.75$, $|\kappa| \lesssim 0.65$, with $1.7 \lesssim \tan\beta \lesssim 54$.

On the experimental side, NMHDECAY 2.0 includes accelerator (LEP and Tevatron) constraints, B-meson decays, and dark matter relic density through a link to micrOMEGAS [77]. In particular, direct bounds on the masses of the charged particles ($H^\pm$, $\tilde{\chi}^\pm$, $\tilde{q}$, $\tilde{l}$) and on the gluino mass are taken into account [78, 79]. Excessive contributions to the invisible decay width of the Z boson [68, 69], as those potentially arising from $Z \to \tilde{\chi}_i^0 \tilde{\chi}_j^0$ and $Z \to h^0 a^0$, are also excluded from the parameter space. Finally, in the neutral Higgs sector, one checks the constraints on the production rates for all the CP-even states h^0 and CP-odd states a^0, in all the channels studied at LEP [72]: $e^+e^- \to h^0 Z$, independent of the h^0 decay mode (IHDM); $e^+e^- \to h^0 Z$, dependent on the h^0 decay mode (DHDM), with the Higgs decaying via $h^0 \to b\bar{b}$, $h^0 \to \tau^+\tau^-$, $h^0 \to 2\,\text{jets}$ $h^0 \to \gamma\gamma$ and $h^0 \to$ invisible; associated production modes (APM), $e^+e^- \to h^0 a^0$, with $h^0 a^0 \to 4b$'s, $h^0 a^0 \to 4\tau$'s and $h^0 a^0 \to a^0 a^0 a^0 \to 6b$'s. In addition to the latter, one also takes into account the possible two body decays of all CP-even, CP-odd and charged Higgs bosons into squarks and sleptons, as well as radiatively induced decays of neutral Higgs bosons into two photons and two gluons.

Regarding B-meson decays, and although the NMHDECAY 2.0 code already contains a rough estimate of the $b \to s\gamma$ decay branching ratio (evaluated at the leading order in QCD), we include in our code a more precise computation of the $b \to s\gamma$ decay in the NMSSM [80], taking into account next-to-leading order (NLO) contributions [81, 82], following the results of [83]. However, we only include leading order (LO) SUSY contributions to the Wilson coefficients at the M_W scale[6]. The calculation within the context of the MSSM at LO and NLO can be found in [84] and [85], respectively. The most recent experimental world average for the branching ratio (BR) reported by the Heavy Flavour Averaging Group is [86, 68]

$$\text{BR}^{\text{exp}}(b \to s\gamma) = (3.55 \pm 0.27) \times 10^{-4}\,. \tag{3.4.26}$$

On the other hand, the current SM prediction for the branching ratio is [87]

$$\text{BR}^{\text{SM}}(b \to s\gamma) = (3.73 \pm 0.30) \times 10^{-4}\,, \tag{3.4.27}$$

where the charm-loop contribution has been included [82]. We have estimated the theoretical error that results from varying the scales in the $b \to s\gamma$ calculation within

[6] No charm-loop contributions were included in the analysis of Ref. [83], giving a SM central value of $\text{BR}^{\text{SM}}(b \to s\gamma) = 3.293 \times 10^{-4}$. This result is obtained by extrapolating the value of the branching ratio evaluated at $\delta = 0.9$ and $\mu_b = m_b$, where δ parameterises the photon energy cut $E_\gamma > (1-\delta)m_b/2$ and μ_b is the renormalisation scale. The corresponding new physics contribution has been implemented in our code by using the parameterisation of [83] evaluated at $\mu_b = m_b$ and $\delta = 0.9$.

the NMSSM, following the method described in [83]. We add to this the experimental error in quadrature. This procedure is performed at every point of the parameter space, typically leading to an error of about 10% of the total BR($b \to s\gamma$) value. Consistency at 2σ with the experimental central value of Eq. (3.4.26) is then demanded.

We have also included in our code other constraints coming from the contribution of a light pseudoscalar a^0 in NMSSM to the rare B- and K-meson decays [80]. When the pseudoscalar is very light it could be produced in meson decays and significantly affect the rates for $K - \bar{K}$ and $B - \bar{B}$ mixing and other SM decays. In particular, our code takes into account the constraints from the pseudo-scalar indirect contributions to $K - \bar{K}$ and $B - \bar{B}$ mixing, $B \to \mu^+\mu^-$, $B \to X_s\mu^+\mu^-$, $B^- \to K^-\nu\bar{\nu}$, $B \to K_S^0 X^0$, and by the direct production, at large $\tan\beta$, via $b \to sa^0$, $B \to Ka^0$, and $B \to \pi a^0$ decays.

Finally, in our analysis we will also include the constraints coming from the SUSY contributions to the muon anomalous magnetic moment, $a_\mu = (g_\mu - 2)$ [88]. Taking into account the most recent theoretical predictions for this quantity within the SM [89, 90, 91] and the measured experimental value [92], the observed excess in $a_\mu^{\rm exp}$ constrains a possible supersymmetric contribution to be $a_\mu^{\rm SUSY} = (27.6 \pm 8) \times 10^{-10}$, where theoretical and experimental errors have been combined in quadrature.

The evaluation of $a_\mu^{\rm SUSY}$ in the NMSSM has been included in our analysis, and consistency at the 2σ level imposed. Thus those regions of the parameter space not fulfilling $11.6 \times 10^{-10} \lesssim a_\mu^{\rm SUSY} \lesssim 43.6 \times 10^{-10}$ will be considered disfavoured.

3.4.2 Dark matter in the NMSSM

The new features of the NMSSM have an impact on the properties of the lightest neutralino as a dark matter candidate, affecting both its direct detection and relic abundance.

The computation of the spin-independent part of the neutralino-nucleon cross section was discussed in detail in the previous Section. It was pointed out there that the existence of a fifth neutralino state, together with the presence of new terms in the Higgs-neutralino-neutralino interaction (which are proportional to λ and κ), trigger new contributions to the spin-independent part of the neutralino-nucleon cross section, $\sigma_{\tilde{\chi}_1^0 - p}$. On the one hand, although the term associated with the s-channel squark exchange is formally identical to the MSSM case, it can be significantly reduced if

the lightest neutralino has a major singlino composition. On the other hand, and more importantly, the dominant contribution to $\sigma_{\tilde{\chi}_1^0-p}$, associated to the exchange of CP-even Higgs bosons on the t-channel can be largely enhanced when these are very light. In the NMSSM, the lightest CP-even Higgs can escape detection if its singlet composition is large. For instance, this makes possible the presence of scenarios with $m_{h_1^0} \lesssim 70$ GeV, thus considerably enhancing the neutralino-nucleon interaction. Consequently, large detection cross sections can be obtained, even within the reach of the present generation of dark matter detectors.

However, in order to be a good dark matter candidate, the lightest NMSSM neutralino must also comply with the increasingly stringent bounds on its relic density. As discussed in Chapter 2, astrophysical constraints, stemming from the analysis of galactic rotation curves [12]-[16], clusters of galaxies and large scale flows [18], suggest the following range for the WIMP relic abundance

$$0.1 \lesssim \Omega h^2 \lesssim 0.3\,, \tag{3.4.28}$$

which can be further reduced to

$$0.095 \lesssim \Omega h^2 \lesssim 0.112\,, \tag{3.4.29}$$

taking into account the recent three years data from the WMAP satellite [19].

Compared to what occurs in the MSSM, one would expect several alterations regarding the dominant processes. As discussed in [93], and as mentioned above regarding the direct detection cross section, the differences can be present at distinct levels. First, and given the presence of a fifth neutralino (singlino), the composition of the annihilating WIMPs can be significantly different from that of the MSSM in wide regions of the parameter space. Having the possibility of a singlino-like lightest supersymmetric particle (LSP), associated with the presence of new couplings in the interaction Lagrangian, in turn favours the coupling of the WIMPs to a singlet-like Higgs, whose mass can be substantially lighter that in the MSSM, given the more relaxed experimental constraints. Regarding the channels through which neutralino annihilation occurs, in the NMSSM we have new open channels, essentially due to the existence of light Higgs states. In summary, the presence of additional Higgs states (scalar and pseudoscalar) favours annihilation via s-channel resonances. On the other hand, having light h_1^0 and a_1^0 states that are experimentally viable means that new channels with annihilation into $Z\,h_1^0$, $h_1^0\,h_1^0$, $h_1^0\,a_1^0$ and $a_1^0\,a_1^0$ (either via s-channel Z, h_i^0, a_i^0 exchange or t-channel neutralino exchange) can provide important contributions the annihilation and co-annihilation cross-sections [94].

Noticing that important annihilation channels (s-channel) are related to the t-channel processes responsible for the most relevant contributions to $\sigma_{\tilde{\chi}_1^0-p}$, one should expect a strong interplay between a viable relic density, and promising prospects for the direct detection of the NMSSM dark matter candidate. In fact, there should be regions of the parameter space which provide new and interesting scenarios[7].

3.4.3 Results and discussion

In this Subsection we analyse the viability of the neutralino as a dark matter candidate. Motivated by the results obtained in Section 3.3, we focus on regions of the low-energy NMSSM parameter space where large direct detection cross sections are likely to be obtained. Building upon the previous analysis, we apply the new constraints K- and B-meson decays, $a_\mu^{\rm SUSY}$, and compatibility with the WIMP relic density. Finally, we discuss the prospects of the experimentally viable regions regarding direct detection of dark matter.

Let us just recall that the free parameters of the model, associated with the Higgs and neutralino sectors of the theory, are [8]

$$\lambda\,, \quad \kappa\,, \quad \mu(=\lambda s)\,, \quad \tan\beta\,, \quad A_\lambda\,, \quad A_\kappa\,, \quad M_1\,, \quad M_2\,, \quad M_3\,. \tag{3.4.30}$$

We assume that the gaugino mass parameters mimic, at low-energy, the values of a hypothetical GUT unification ($\frac{M_3}{6} = M_1 = \frac{M_2}{2}$).

It should be emphasised that in NMHDECAY 2.0 some of the input parameters are specified at a different scale than in the former version NMHDECAY 1.1 [62], which was used in the previous analysis done in Section 3.3 [1]. Although the difference between the values of λ (or κ) at the EW and the SUSY scales ($\approx$ 1 TeV) is very small, there is a substantial change in the value of the trilinear coupling A_λ. These variations are induced by the top trilinear coupling $A_{\rm top}$, and are approximately given by $A_\lambda^{\rm SUSY} \approx A_\lambda^{\rm EW} + 0.06\, A_{\rm top}^{\rm EW}$. Therefore, one needs to take this shift into account when comparing the present results with those of the previous Section.

As mentioned above, motivated by the results of Section 3.3 regarding the prospects for direct detection of dark matter, we will be interested in a regime of low $\tan\beta$, as

[7] As concluded in [93], it might even be possible to reconcile a very light neutralino with the experimental observations from DAMA, CDMS II, and WMAP.

[8] Although the soft gluino mass, M_3, is not directly related to the computation of the Higgs/neutralino masses and mixings, it plays a relevant role in contributing to the radiative corrections to the Higgs boson masses.

well as in values of $|\mu|$ in the range 110 GeV $\lesssim \mu \lesssim$ 200 GeV (the lower limit ensuring that in most cases one can safely avoid the LEP bound on the lightest chargino mass). Likewise, the following intervals for the trilinear couplings will be taken: -800 GeV $\lesssim A_\lambda \lesssim 800$ GeV, and -300 GeV $\lesssim A_\kappa \lesssim 300$ GeV (the optimal ranges will typically correspond to $|A_\lambda| \sim 400$ GeV and $|A_\kappa| \lesssim 200$ GeV, working in a small $\tan\beta$ regime).

Slepton and squark masses, as well as the corresponding trilinear parameters, do not significantly affect the neutralino detection properties, other than through the radiative corrections to the Higgs masses. However, low-energy observables are very sensitive to their specific values. In the following we will see, for instance, how the experimental constraint on $a_\mu^{\rm SUSY}$ favours light sleptons.

As already done in Section 3.3, we divide the scan of the low-energy NMSSM parameter space following the results of the minimisation with respect to the VEV phases, separately discussing each of the cases (i)-(iv) (see Subsection 3.1.2 and Section 3.3).

NMSSM parameter space: new constraints

We first discuss the new constraints on the parameter space arising from the improved analysis on the Higgs sector, the muon anomalous magnetic moment, and K- and B-meson decays.

Among the new features implemented in NMHDECAY 2.0, one finds additional radiative corrections to the Higgs boson masses, including corrections of order $g^2\, Y_{t,b}^2$ to the CP-even Higgs boson mass (induced by stop/sbottom D-term couplings). Regarding the logarithmic one-loop corrections of the order g^2, these are now dependent on the different masses of squarks/sleptons of distinct generations. Moreover, the corrections to fourth order in λ and κ are also taken into account. The computation of the sparticle spectrum is also complete in the new version, and all squark and gluino data is confronted with the constraints from both Tevatron and LEP. With respect to the results obtained in the previous analysis (Section 3.3), the latter improvements only translate into slight changes in the exclusion regions.

Concerning the evaluation of the supersymmetric contributions to the muon anomalous magnetic moment, the relevant processes comprise neutralino-sneutrino as well as chargino-smuon loops. The only change with respect to the MSSM is due to the fifth neutralino state and the corresponding modified neutralino-lepton-slepton coupling. Since we are interested in cases with very low $\tan\beta$, the contributions from neutralino and chargino loops are of similar magnitude, and very small. For example,

with $\tan\beta = 3$ and slepton mass parameters above $m_{E,L} \sim 1$ TeV one typically obtains $a_\mu^{\rm SUSY} \sim 10^{-11}$, which is disfavoured. In order to obtain compatibility with the experimental result an increase in the value of $\tan\beta$ is welcome, but this would then lead to regions of the parameter space where, from the dark matter point of view, the NMSSM resembles the MSSM. The other possibility is decreasing the slepton (and gaugino) masses. Furthermore, large values of the slepton trilinear couplings are needed in order to increase the LR mixing in the smuon mass matrix. The choice $\mu\, A_E < 0$ is optimal, since it makes the neutralino contribution positive and large. For example, with $\tan\beta \sim 5$, $A_E = -2500$ GeV and $m_{E,L} \lesssim 200$ GeV, one obtains $a_\mu^{\rm SUSY} \gtrsim 10^{-9}$ for $M_1 \lesssim 215$ GeV. The relevance of these changes is illustrated in Fig. 3.18, where the numerical results for $a_\mu^{\rm SUSY}$ are plotted versus the bino mass, M_1, for different combinations of slepton mass and trilinear couplings. For each case we have also varied A_λ and A_κ over a wide range and scanned the whole (λ, κ) plane, which as evidenced in the figure has virtually no effect on the resulting $a_\mu^{\rm SUSY}$. We have also included the various LEP and Tevatron constraints. For the rest of our analysis, we will assume $m_{E,L} = 150$ GeV and $A_E = -2500$ GeV. Also, and unless otherwise stated, we will set the bino mass to $M_1 = 160$ GeV, which, according to Fig. 3.18, leads to a sufficiently large $a_\mu^{\rm SUSY}$. The detection properties of the neutralino are in general quite insensitive to changes in the slepton sector. Notice however that if one does not wish to impose the bound on the muon anomalous magnetic moment, heavy sleptons (equal to squarks) can be taken which would not affect the dark matter predictions.

Regarding the bounds arising from K- and B-meson physics, the most important role is played by the $b \to s\,\gamma$ decay, which can in principle exclude important regions of the parameter space. Concerning the other K- and B-meson processes discussed in Subsection 3.4.1, we have verified that throughout the investigated NMSSM parameter space they are always in good agreement with experiment, so that we will make no further reference to the latter in the following discussion of the numerical results.

In the present analysis we will not take into account any source of flavour violation other than the Cabibbo-Kobayashi-Maskawa (CKM) matrix. Moreover, we will be systematically considering large values for the gluino mass (above 1 TeV). Under the latter assumptions, the most important contributions to ${\rm BR}(b \to s\,\gamma)$ arise in general from charged Higgs and chargino mediated diagrams [84].

On the one hand, when the dominant contributions are those stemming from charged Higgs exchange, the results for ${\rm BR}(b \to s\,\gamma)$ closely follow the behaviour

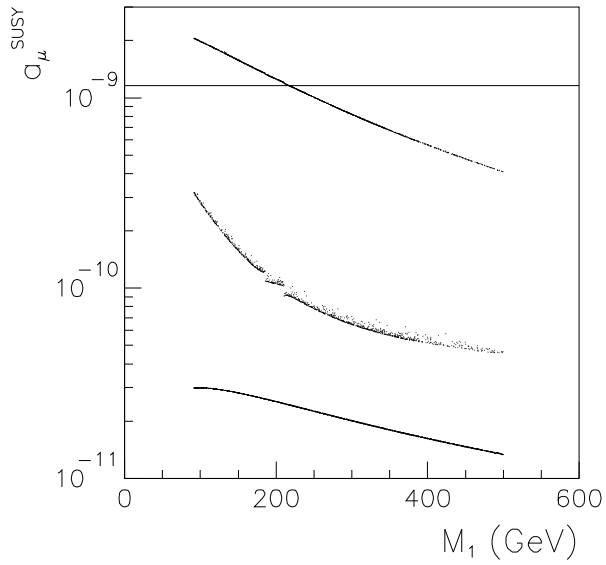

Figure 3.18: Supersymmetric contribution to the anomalous magnetic moment of the muon as a function of the bino mass, M_1, for $\tan\beta = 5$, $\mu = 150$ GeV, trilinear couplings in the range $-800 \lesssim A_\lambda \lesssim 800$ GeV, $-300 \lesssim A_\kappa \lesssim 300$ GeV. From bottom to top, the different bands correspond to the following values of the slepton mass and lepton trilinear terms, $m_{L,E} = 1$ TeV with $A_E = 1$ TeV, $m_{L,E} = 150$ GeV with $A_E = 1$ TeV, and $m_{L,E} = 150$ GeV with $A_E = -2.5$ TeV. A full scan on the (λ, κ) plane has been performed for each case, including LEP and Tevatron experimental constraints. The horizontal solid line indicates the lower bound of the allowed 2σ interval.

of the charged Higgs mass, which in the NMSSM is given by

$$m^2_{H^\pm} \;=\; \frac{2\,\mu^2}{\sin(2\beta)}\,\frac{\kappa}{\lambda} \;-\; v^2\,\lambda^2 \;+\; \frac{2\,\mu\,A_\lambda}{\sin(2\beta)} \;+\; M_W^2\,. \tag{3.4.31}$$

From the above, we expect that smaller values of $\mathrm{BR}(b \to s\,\gamma)$ should be obtained for large $m^2_{H^\pm}$, and therefore when κ/λ is sizable (for positive values of κ) or for small κ/λ (if $\kappa < 0$). In general, smaller values of the $\mathrm{BR}(b \to s\,\gamma)$ will be also associated to larger values of the product $\mu\,A_\lambda$. Furthermore, the leading term of the Wilson coefficient associated to the charged Higgs varies as $\tan^{-2}\beta$ [84]. As a consequence, one expects a decrease of this contribution as $\tan\beta$ increases. On the other hand, in a regime of $\mu \lesssim M_2$, the lightest chargino is Higgsino-dominated, so that its mass is also quite small ($m_{\tilde{\chi}_1^\pm} \sim \mu$). Thus, the chargino contributions (which are opposite in sign to those of the charged Higgs) are also expected to play a relevant role, although, in the cases analysed in this work ($\tan\beta \lesssim 10$), they are not dominant. Gluino contributions

are also very small, given the little flavour violation in the down squark sector, and the sizable values of M_3. Likewise, neutralino exchange contributions are almost negligible. We thus find that, in general, the NMSSM contribution to BR($b \to s\,\gamma$) at low $\tan\beta$ is large and mostly arising from charged Higgs loops. This leads to stringent constraints on the parameter space.

Let us study the effect of the experimental bound on BR($b \to s\,\gamma$), together with the updated accelerator constraints on the NMSSM parameter space. After this first survey we will no longer separately address the K- and B-meson constraints (and a_μ) from those arising from LEP/Tevatron data. Henceforth, experimentally allowed regions will be those that not only comply with the latter data, but that also exhibit BR($b \to s\,\gamma$) within 2σ from its central experimental value. As mentioned before, in order to satisfy the constraint on the muon anomalous magnetic moment, we take $M_1 = 160$ GeV in the following Subsubsection, for which, in the case with $\tan\beta = 5$, $a_\mu^{\rm SUSY} \approx 1.4 \times 10^{-9}$ (see Fig. 3.18).

$\mu A_\kappa < 0$ **and** $\mu A_\lambda > 0$ $(\kappa > 0)$

As discussed in Section 3.3, this is one of the most interesting areas of the parameter space, since although sizable regions are excluded due to the occurrence of tachyons in the CP-even Higgs sector (namely for larger values of $|A_\kappa|$), the possibility of having experimentally viable light scalar Higgs leads to potentially large values for $\sigma_{\tilde{\chi}_1^0 - p}$.

As an example, we represent on the left-hand side of Fig. 3.19 the (λ, κ) parameter space for an example with $\tan\beta = 3$, $A_\lambda = 200$ GeV, $A_\kappa = -200$ GeV and $\mu = 130$ GeV. The tachyonic region in the CP-even Higgs sector is depicted, as well as the region excluded due to the presence of false minima of the potential. An important part of the theoretically allowed region is also ruled out due to conflict with LEP and/or Tevatron data. This owes to the fact that the doublet component of the lightest scalar Higgs is very large and gives rise to excessive Higgs production rates, in particular, $e^+e^- \to h^0 Z$, IDHM and DHDM ($h^0 \to b\bar{b}$ and to a lesser extent, $h^0 \to 2$ jets). Once all these bounds are applied, a small area on the right of that experimentally excluded survives, remarkably exhibiting very light Higgses and neutralinos (associated with a singlet/singlino component above 90%) and therefore clearly characteristic of the NMSSM. We recall that these are the regions where one expects to find large theoretical predictions for $\sigma_{\tilde{\chi}_1^0 - p}$.

On the right-hand side of Fig. 3.19 we superimpose the results for the BR($b \to s\,\gamma$)

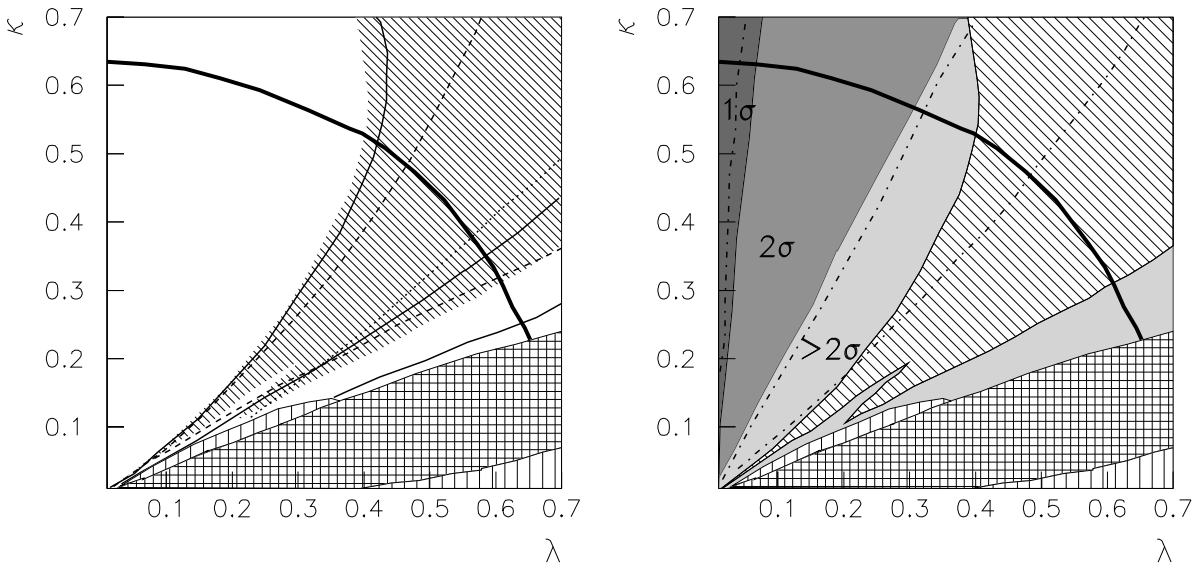

Figure 3.19: Effect of the experimental constraints on the (λ, κ) plane for an example with $\tan\beta = 3$, $A_\lambda = 200$ GeV, $A_\kappa = -200$ GeV and $\mu = 130$ GeV. In both cases, the gridded area is excluded due to the appearance of tachyons, while the vertically ruled area corresponds to the occurrence of unphysical minima. The oblique ruled area is associated with points that do not satisfy the LEP and/or Tevatron constraints or where (at least) the LEP bound on direct neutralino production is violated. The region above the thick black line is disfavoured due to the occurrence of a Landau pole below the GUT scale. On the left plot, from top to bottom, solid lines indicate different values of the lightest Higgs mass, $m_{h_1^0} = 114$, 75, 25 GeV. Dashed lines separate the regions where the lightest scalar Higgs has a singlet composition given by $S^2_{13} = 0.1$, 0.9 (from top to bottom). Finally in the area below the dotted line, the lightest neutralino has a singlino composition greater than $N^2_{15} = 0.1$. On the right, grey areas represent the theoretical predictions for $\mathrm{BR}(b \to s\,\gamma)$. From left to right, 1σ (dark), 2σ (medium) and excluded (light) regions are shown. Dot-dashed lines stand for the different values of the charged Higgs mass, $m_{H^\pm} = 1000$, 500, 450 GeV (from left to right).

on the (λ, κ) plane. As discussed in the previous Subsection, the resulting branching ratio is typically large, $\mathrm{BR}(b \to s\,\gamma) \gtrsim 3.5\times10^{-4}$, and increases to as much as $\sim 5\times10^{-4}$ in regions with small κ/λ, where the charged Higgs mass is smaller. Notice therefore that the regions of the (λ, κ) plane associated with larger values of $\mathrm{BR}(b \to s\,\gamma)$ typically correspond to those where the largest predictions for $\sigma_{\tilde{\chi}^0_1 - p}$ are found. In this example, only a small triangular region with $\lambda \lesssim 0.05$, for $\kappa < 0.7$, is within a 1σ

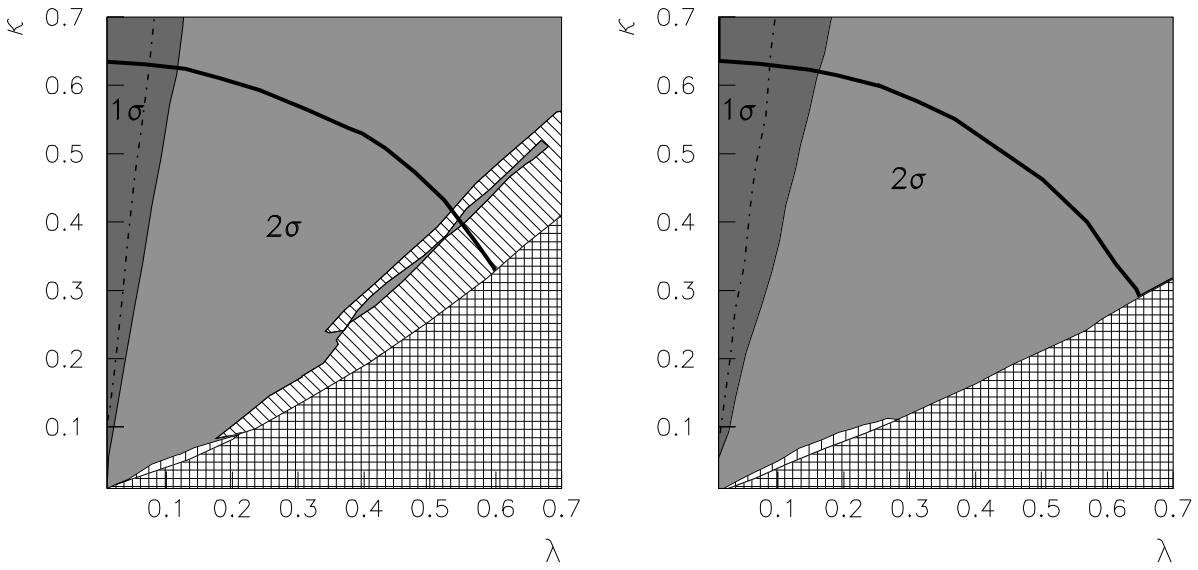

Figure 3.20: (λ, κ) parameter space for $\tan\beta = 5$, $A_\kappa = -200$ GeV, and $\mu = 130$ GeV. On the left we take $A_\lambda = 200$ GeV, while on the right we consider $A_\lambda = 400$ GeV. Line and colour code follow the conventions of Fig. 3.19. In this case, the single dot-dashed line corresponds to $m_{H^\pm} = 1000$ GeV.

deviation from the experimental bound of Eq. (3.4.26) and $\lambda \lesssim 0.35$ is needed in order to be within 2σ of that result. In the plot we also indicate with dot-dashed lines the different values of the charged Higgs mass, thus illustrating the correlation between its decrease and the increase in $\mathrm{BR}(b \to s\,\gamma)$.

The effect of the various experimental constraints on the parameter space is very sensitive to variations in the input parameters. We will now investigate how changes in $\tan\beta$ and A_λ affect the resulting $\mathrm{BR}(b \to s\,\gamma)$. On the one hand, as already mentioned, increasing the value of $\tan\beta$ leads to a reduction of the charged Higgs contribution. Since in our case this is the leading contribution to $\mathrm{BR}(b \to s\,\gamma)$, an enhancement in $\tan\beta$ enlarges the regions of the parameter space which are consistent with the experimental constraint. This is illustrated on the left-hand side of Fig. 3.20 with the same example of Fig. 3.19, but now taking $\tan\beta = 5$. The resulting charged Higgses are heavier ($m_{H^\pm} > 500$ GeV) and as a consequence the entire (λ, κ) plane fufils the experimental constraint on $\mathrm{BR}(b \to s\,\gamma)$. Notice that LEP and Tevatron constraints are also modified. On the other hand, an increase in the trilinear term A_λ also leads to heavier charged Higgses as seen in Eq. (3.4.31). Therefore, this can induce a further decrease in $\mathrm{BR}(b \to s\,\gamma)$. An example of this is shown on the right-hand side of

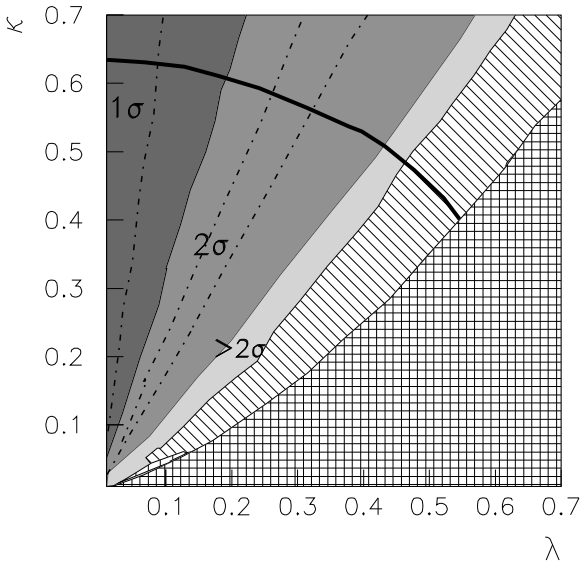

Figure 3.21: (λ, κ) parameter space for $\tan\beta = 5$, $A_\lambda = -200$ GeV, $A_\kappa = 200$ GeV and $\mu = -130$ GeV. Line and colour code following the conventions of Fig. 3.19.

Fig. 3.20, where in addition to $\tan\beta = 5$, $A_\lambda = 400$ GeV has been used. Again, the whole (λ, κ) plane is allowed due to the increase in $m_{H^\pm}$.

Let us finally comment on the possibility of changing the signs of μ, A_λ, and A_κ, while keeping $\mu A_\lambda > 0$ and $\mu A_\kappa < 0$. Although the Higgs potential is invariant under this change, the same does not occur for the chargino and neutralino sectors, so that both these spectra, as well as the experimental constraints are likely to be modified. As an illustrative example, we present in Fig. 3.21 the same case as in the left-hand side of Fig. 3.20 but with the opposite signs for μ, A_λ, and A_κ. There are some important alterations to the areas excluded by unphysical minima and experimental constraints, both of which are now more extensive. Finally, notice that the $\mathrm{BR}(b \to s\,\gamma)$ now excludes a larger area of the (λ, κ) plane, thereby disfavouring those areas which potentially lead to larger neutralino detection cross sections.

In the light of this analysis, the optimal areas of the parameter space correspond to those with μ, $A_\lambda > 0$, and $A_\kappa < 0$, and where $\tan\beta$ and A_λ are relatively large. In order to keep within the context where NMSSM-like dark matter scenarios can be obtained, we will use $\tan\beta \leq 5$.

$\mu A_\kappa < 0$ and $\mu A_\lambda < 0$ ($\kappa > 0$)

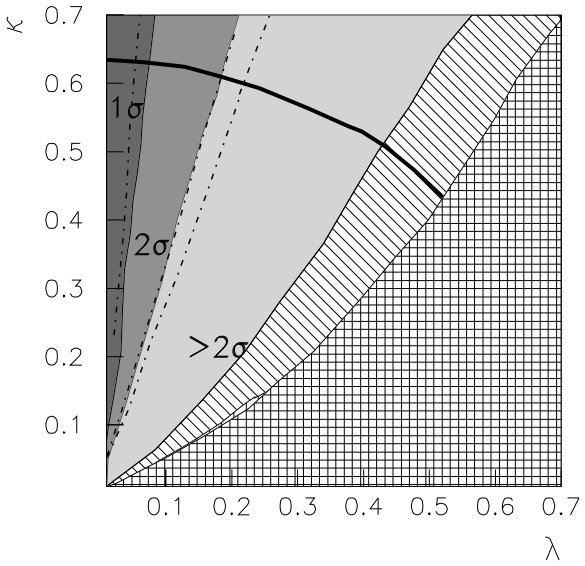

Figure 3.22: (λ, κ) parameter space for $\tan\beta = 5$, $A_\lambda = -200$ GeV, $A_\kappa = -200$ GeV and $\mu = 130$ GeV. Line and colour code following the conventions of Fig. 3.19.

Compared to the previous case, the presence of tachyons gives rise to far stronger constraints. Occurring now in both CP-even and CP-odd Higgs sectors, the non-physical (tachyonic) solutions exclude very large areas of the parameter space. Regarding the LEP experimental exclusions, these arise from excessive contributions to $h^0 \to b\bar{b}$ and $h^0 \to 2$ jets, and cover an area wider than what had been previously identified in Section [**?**] (a consequence of the improved computation of the Higgs spectrum). In addition, due to the lightness of the charged Higgs bosons, an important region is also excluded due to very large BR$(b \to s\,\gamma)$, so that the only surviving regions are those associated with $\lambda \lesssim 0.2$. As an example, Fig. 3.22 displays a case with $\tan\beta = 5$, $A_\lambda = -200$ GeV, $A_\kappa = -200$ GeV and $\mu = 130$ GeV. Let us remark that since the lower-right corner of the (λ, κ) plane is not accessible, one cannot find light neutral Higgs states, so that interesting prospects regarding the direct detection of dark matter should not be expected.

Although varying the several parameters results in modifications of the excluded areas (LEP/Tevatron, $b \to s\,\gamma$ and unphysical minima), in all cases these are sizable. Only very reduced regions, corresponding to small values of λ survive all the constraints. In these areas the singlet component of the lightest Higgs is negligible and the lightest neutralino is Higgsino-like, therefore resembling MSSM scenarios. The complementary region, with A_λ, $A_\kappa > 0$ and $\mu < 0$, leads to even more extensive tachyonic regions,

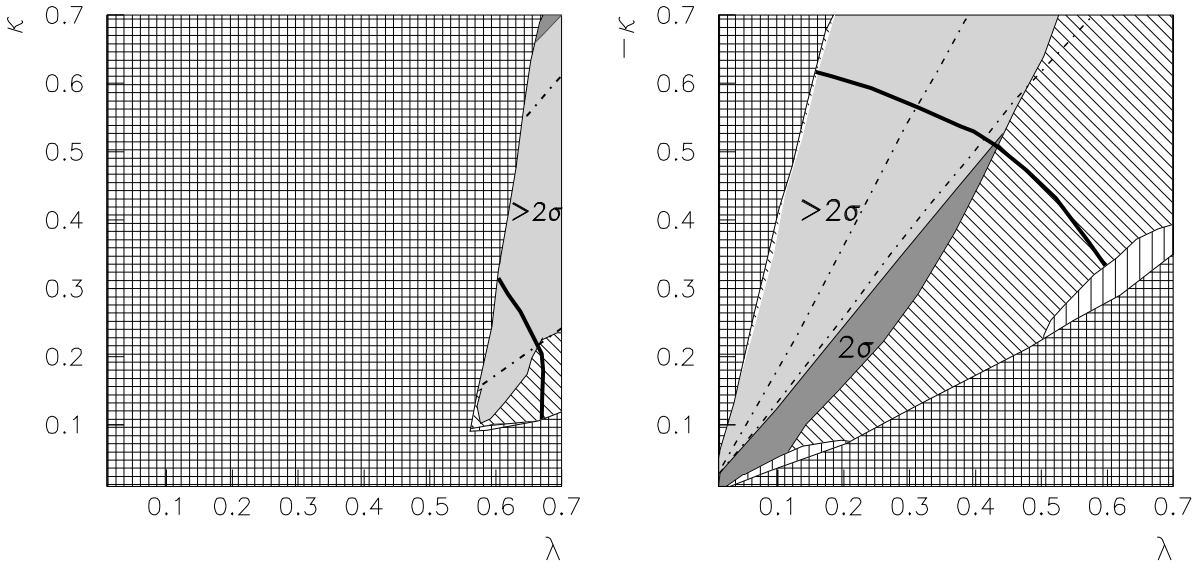

Figure 3.23: On the left (λ, κ) parameter space for $\tan\beta = 3$, $A_\lambda = 200$ GeV, $A_\kappa = 50$ GeV and $\mu = 160$ GeV. On the right $\tan\beta = 5$, $A_\lambda = 400$ GeV, $A_\kappa = 200$ GeV, and $\mu = 130$ GeV for $\kappa < 0$. Line and colour code following the conventions of Fig. 3.19.

and we will not further discuss it.

$\mu A_\kappa > 0$ **and** $\mu A_\lambda > 0$ $(\kappa > 0)$

This combination of signs leads to a parameter space which is plagued with tachyons, as discussed in Subsection 3.3.3, arising from both Higgs sectors. Contrary to what was noticed for the previous cases, here the unphysical minima occur for small values of λ. The remaining areas in the (λ, κ) plane are also very affected by experimental constraints. As a consequence, only very reduced areas of the parameter space survive.

For example, considering the choice $A_\lambda = 200$ GeV, $A_\kappa = 50$ GeV and $\mu = 160$ GeV, with $\tan\beta = 3$, we observe that once the areas corresponding to the occurrence of tachyons are excluded, the small surviving region is still plagued by false minima as well as by the violation of several experimental constraints. In particular, lower values of κ are ruled out due to conflict with LEP ($h^0 \to b\bar{b}$ and $h^0 \to 2$ jets) and excessive contributions to the BR$(b \to s\,\gamma)$. This is illustrated on the left-hand side of Fig. 3.23.

Although reducing the values of A_κ and $\tan\beta$ enlarges the areas where physical minima can be found, the addition of the experimental constraint on BR$(b \to s\gamma)$ to

the LEP and Tevatron bounds typically rules out the whole (λ, κ) plane. Increasing $\tan\beta$ in order to reduce the contribution to BR($b \to s\gamma$) is also highly disfavoured since the tachyonic region becomes more important. As a consequence, no interesting implications for neutralino dark matter detection are expected in this case.

$\mu A_\kappa > 0$ **and** $\mu A_\lambda > 0$ $(\kappa < 0)$

The only viable combination of signs associated with negative values of κ is also plagued by the appearance of tachyons, both in the CP-even and CP-odd Higgs sectors, towards the regions with small λ, as discussed in Subsection 3.3.4. In addition, experimental constraints also exclude large portions of the parameter space in the vicinity of the tachyonic regions. As an example, let us mention that for the case $A_\lambda = 100$ GeV, $A_\kappa = 50$ GeV and $\mu = 130$ GeV, with $\tan\beta = 3$, all the parameter space associated with physical minima is ruled out, since either DHDM constraints ($h^0 \to b\bar{b}$ and $h^0 \to 2$ jets) are violated or consistency with the BR($b \to s\,\gamma$) bound is not achieved. Increasing A_λ, A_κ, and $\tan\beta$ leads to a significant improvement. For example, with $A_\lambda = 400$ GeV, $A_\kappa = 200$ GeV, $\mu = 130$ GeV with $\tan\beta = 5$ some allowed areas are found, as shown on the right-hand side of Fig. 3.23. Nevertheless, LEP/Tevatron experimental constraints together with the bound on BR($b \to s\,\gamma$) rule out those parts of the parameter space where the Higgs is light and more singlet-like, and in which $\sigma_{\tilde{\chi}_1^0 - p}$ can be sizable. The remaining allowed regions correspond to a rather small area, in which the lightest Higgs is essentially doublet-like, while the lightest neutralino exhibits a strong Higgsino dominance.

Neutralino relic density

The next step in our analysis is to take into account the available experimental data on the WIMP relic density. In order to be a viable dark matter candidate, the lightest NMSSM neutralino must have an abundance within the ranges presented in Eqs. (3.4.28,3.4.29). Similar to what occurs in the MSSM, this additional constraint further reduces the regions of the low-energy parameter space. Moreover, and as hinted before, one expects that $\Omega_{\tilde{\chi}_1^0} h^2$ will in general lie below the experimental ranges.

A thorough analysis of the relic density of dark matter in the NMSSM has been carried out in [94]. It was found that compatibility with the WMAP constraint is possible in the regions where the lightest Higgs is dominated by the doublet components

and the lightest neutralino is a bino-Higgsino mixture. Apart from possible Higgs resonances, compatible values of $\Omega_{\tilde{\chi}_1^0} h^2$ are found for two distinct regions: $\mu \gg M_2$ and $\mu \gtrsim M_1$ (similar to the MSSM for small to intermediate values of $\tan\beta$). Also note that, for regions with $\mu \lesssim M_1$, Higgsino-singlino neutralinos with masses below M_W can give a relic density within the WMAP range (or larger) essentially because the annihilation into Z and W gauge bosons is kinematically forbidden. It is also worth noticing that a pure bino LSP also offers interesting scenarios, with a remarkable role being played by s-channel Higgs resonances (else $\Omega_{\tilde{\chi}_1^0} h^2$ tends to be above the experimental bound). Additional LSP annihilation via scalar or pseudoscalar Higgses can also play a relevant role.

In order to understand the results for $\Omega_{\tilde{\chi}_1^0} h^2$ one needs to take into account the variations in the mass and composition of the lightest neutralino in the (λ, κ) plane, as well as in the Higgs sector. In general, the neutralino relic density will be too small in those regions of the parameter space where it is Higgsino-like and increases when the neutralino becomes more singlino-like. In addition, one should consider the possible existence of resonant annihilation (when twice the neutralino mass equals the mass of one of the mediating particles in an s-channel) and the kinematic thresholds for the various channels (e.g., annihilations into ZZ, WW, Zh_i^0, $h_i^0 h_j^0$, $a_i^0 a_j^0$, and $a_i^0 h_j^0$).

Since the goal of our present study is to discuss the potential of NMSSM-like scenarios regarding the theoretical predictions for $\sigma_{\tilde{\chi}_1^0 - p}$, in this Subsubsection we focus on those examples of the parameter space having large neutralino detection cross section. We investigate to which extent the inclusion of the bound of the relic density further constrains the parameter space. As pointed out in Section 3.3, these scenarios typically occur in association to singlet-like h_1^0, with singlino-Higgsino neutralinos. Let us study one example in detail.

We begin by taking $M_1 = 160$ GeV, $A_\lambda = 400$ GeV, $A_\kappa = -200$ GeV, and $\mu = 130$ GeV, with $\tan\beta = 5$, which according to Figs. 3.18 and 3.20 is consistent with the bounds on $a_\mu^{\rm SUSY}$ and BR$(b \to s\,\gamma)$, respectively. The results for the neutralino relic density are depicted in the (λ, κ) plane on the left-hand side of Fig. 3.24. On the experimentally allowed area, grey dots stand for points which, in addition to experimental constraints, fulfil $0.1 \leq \Omega_{\tilde{\chi}_1^0} h^2 \leq 0.3$, whereas black dots represent points in agreement with the WMAP constraint. Notice that in this case, no points are excluded by LEP or Tevatron bounds.

For large values of κ and small λ (i.e., on the upper left corner of the plots), the lightest neutralino is relatively heavy and has a mixed bino-Higgsino composition, since

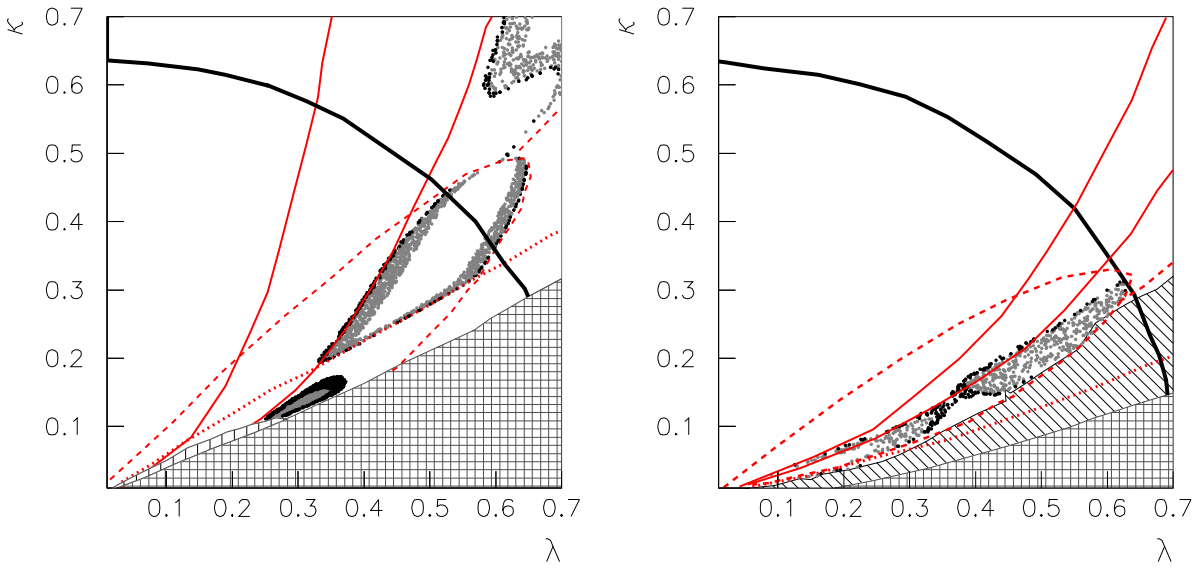

Figure 3.24: (λ, κ) parameter space with information about the neutralino relic density. On the left, an example with $M_1 = 160$ GeV, $\tan\beta = 5$, $A_\lambda = 400$ GeV, $A_\kappa = -200$ GeV, and $\mu = 130$ GeV. The gridded area is excluded due to the appearance of tachyons, while the vertically ruled area corresponds to the occurrence of unphysical minima. The region above the thick black line is disfavoured because of the occurrence of a Landau pole below the GUT scale. The oblique ruled area is associated to those points that do not satisfy LEP/Tevatron and/or BR$(b \to s\,\gamma)$ constraints, whereas the bound on $a_\mu^{\rm SUSY}$ is fulfilled in the whole plane. The dark shaded (cyan) area corresponds to points which are experimentally viable, and whose relic density complies with the astrophysical bound of Eq. (3.4.28). Points in black are those in agreement with experimental constraints and WMAP bounds (c.f. Eq. (3.4.29)). The dashed red lines indicate the resonances of the lightest neutralino annihilation channels through the second lightest CP-even Higgs, $2\,m_{\tilde{\chi}_1^0} = m_{h_2^0}$. In the region below the red dotted line the lightest neutralino mass is larger than the mass of the lightest Higgs. Along the red solid lines the neutralino mass is equal to the Z and W mass (from left to right, respectively). On the right, the same example is shown, but with $A_\kappa = 0$ and $\mu = 150$ GeV.

we have chosen $\mu \sim M_1$. Due to the large Higgsino component, the neutralino relic density is very small, and cannot account for the observed amount of dark matter. As we move in the (λ, κ) plane towards smaller values of κ and larger values of λ, the neutralino becomes lighter and has a larger singlino component (in this example $N_{15}^2 \lesssim 0.35$), and as a consequence, $\Omega_{\tilde{\chi}_1^0} h^2$ increases. As the neutralino mass decreases, some annihilation channels become kinematically forbidden, such as annihilation into a pair of Z or W bosons when $m_{\tilde{\chi}_1^0} < M_Z$ or $m_{\tilde{\chi}_1^0} < M_W$, respectively. We have indicated these two thresholds in the figure with red solid lines. Below these the resulting relic density can be large enough to fulfil the WMAP constraint. Variations in the Higgs sector also affect the calculation of the neutralino abundance. On the one hand, the mass and composition of the lightest Higgs also vary throughout the (λ, κ) plane. Lighter Higgses with a larger singlet composition are obtained for small values of κ. In our case, $m_{\tilde{\chi}_1^0} < m_{h_1^0}$ for large κ and small λ, but eventually, the Higgs becomes lighter and new annihilation channels (the most important being $\tilde{\chi}_1^0 \tilde{\chi}_1^0 \to h_1^0 h_1^0$ and $Z h_1^0$) are available for the neutralino, thus decreasing its relic density. The points where $m_{\tilde{\chi}_1^0} = m_{h_1^0}$ are indicated with a dotted red line in the plot. On the other hand, one also needs to take into account the existence of rapid neutralino annihilation with the second-lightest CP-even Higgs, when $2\, m_{\tilde{\chi}_1^0} = m_{h_2^0}$, which is responsible for a further decrease in $\Omega_{\tilde{\chi}_1^0} h^2$. This is indicated in the plot with a red dashed line.

As we can see, in the present example the correct relic density is only obtained when either the singlino composition of the neutralino is large enough or when the annihilation channels into Z, W, or h_1^0 are kinematically forbidden. Interestingly, some allowed areas are very close to the tachyonic border. The neutralino-nucleon cross section can be very large in these regions, due to the presence of very light singlet-like Higgses (in this example $S_{13}^2 \approx 0.99$).

The same example, but now with $A_\kappa = 0$ and $\mu = 150$ GeV is shown on the right-hand side of Fig. 3.24. Once more, in order to reproduce the correct $\Omega_{\tilde{\chi}_1^0} h^2$ the neutralino has to be either sufficiently light so that some annihilations channels are closed or have a large singlino component. In this particular case the singlino component of $\tilde{\chi}_1^0$ can be even larger, with $N_{15}^2 \sim 0.9$ in the allowed area with very low κ. Notice, however, that the region in the vicinity of the tachyonic area is excluded by experimental bounds.

In order to study the importance of the neutralino composition, we will now consider variations in the gaugino masses. To begin with, we increase the bino mass and take $M_1 = 330$ GeV, thereby decreasing the bino component of the lightest neutralino.

Such an increase of the gaugino masses implies a reduced contribution to the muon anomalous magnetic moment. We obtain $a_\mu^{\rm SUSY} \approx 7.2 \times 10^{-10}$ (see Fig. 3.18), more than 2σ away from the central value and therefore disfavoured. The resulting (λ, κ) plane is represented on the left-hand side of Fig. 3.25. Since the Higgsino component has increased with respect to the previous examples, the resulting relic density for the neutralino in the region with large κ and small λ is even smaller. Once more, in order to have the correct $\Omega_{\tilde{\chi}_1^0} h^2$ we need to go to regions of the parameter space where some annihilation channels are not kinematically allowed and/or the neutralino is singlino-like. Notice also that the neutralino is in general heavier in this example and therefore the lines with $m_{\tilde{\chi}_1^0} = M_Z$ and $m_{\tilde{\chi}_1^0} = M_W$ are shifted to lower values of κ. Also, the region with $m_{\tilde{\chi}_1^0} < m_{h_1^0}$ is modified and now corresponds to the area on the right of the dotted red line. Finally, we must take into account the possible resonances along which $\Omega_{\tilde{\chi}_1^0} h^2$ decreases. In this example, rapid annihilation of neutralinos occurs via CP-even Higgs exchange when $2m_{\tilde{\chi}_1^0} = m_{h_1^0}$, which takes place along the two upper red dashed lines. There is also a resonance with the Z boson when $2m_{\tilde{\chi}_1^0} = M_Z$ which occurs along the lower red dashed line. It is worth noticing that, once more, a part of the region allowed by experimental and astrophysical constraints lies close to the tachyonic area, and could have a large $\sigma_{\tilde{\chi}_1^0 - p}$.

Finally on the right-hand side of Fig. 3.25 we show another example where the bino mass has been further increased to $M_1 = 500$ GeV. The contribution to the muon anomalous magnetic moment is also too low. As shown in Fig. 3.18, $a_\mu^{\rm SUSY} \approx 4 \times 10^{-10}$, more than 2σ away from the experimental value. Due to the further increase of the Higgsino component and mass of the lightest neutralino, its relic density is even smaller and compatibility with WMAP is only obtained when the neutralino is lighter than the lightest Higgs and, at least, the W boson. Notice that in this example there is also a resonant annihilation through the lightest CP-odd Higgs when $2\, m_{\tilde{\chi}_1^0} \approx m_{a_1^0}$, which further decreases $\Omega_{\tilde{\chi}_1^0} h^2$. This constrains the allowed region to small values of λ, in which the neutralino is mostly singlino, $N_{15}^2 \lesssim 0.8$.

To summarise, in these scenarios, neutralinos typically have a very small relic density (insufficient to account for the dark matter in the Universe) as a consequence of their large Higgsino composition. Only when one moves towards regions of the parameter space where the singlino composition is enhanced or the neutralino mass is decreased (such that some annihilation channels become forbidden) can the WMAP result be reproduced.

We have not yet addressed the other areas of the parameter space (ii)-(iv). These

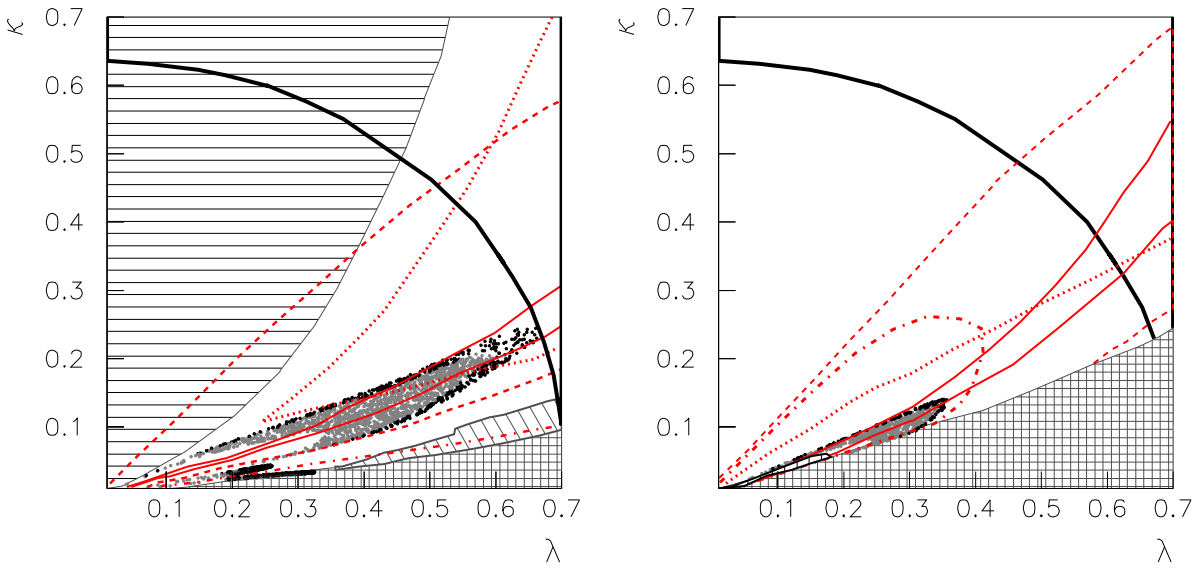

Figure 3.25: On the left, the same as in Fig. 3.24 but with $M_1 = 330$ GeV, $\tan\beta = 5$, $A_\lambda = 570$ GeV, $A_\kappa = -60$ GeV, with $\mu = 160$ GeV. The area to the right of the red dotted line has $m_{\tilde{\chi}_1^0} < m_{h_1^0}$. Along the red dot-dashed line, $2\,m_{\tilde{\chi}_1^0} = M_Z$, leading to rapid neutralino annihilation. On the right, the same with $M_1 = 500$ GeV, $\tan\beta = 5$, $A_\lambda = 400$ GeV, $A_\kappa = -150$ GeV, with $\mu = 130$ GeV. In this example the red dot-dashed line indicates resonances on the neutralino annihilation mediated by the lightest pseudoscalar when $2\,m_{\tilde{\chi}_1^0} = m_{a_1^0}$. In both examples the resulting $a_\mu^{\rm SUSY}$ is outside the experimental 2σ region.

other choices of signs for the different parameters are associated to less favourable scenarios. First, in cases (ii) and (iv) the experimental constraints rule out the regions where $\tilde{\chi}_1^0$ has a large singlino component. Therefore, the lightest neutralino is in general Higgsino-like throughout all the allowed (λ, κ) plane and, consequently, its relic abundance is much below the favoured values, i.e., $\Omega_{\tilde{\chi}_1^0} h^2 \ll 0.1$. In case (iii), where large areas are excluded because of the occurrence of tachyons, it is extremely complicated to find regions that simultaneously fulfil the experimental and astrophysical constraints. For this reason, in the following Subsection we will limit our analysis to case (i).

As a next step of our analysis, we will bring together all the constraints so far explored, and after having ensured that we are indeed in the presence of a viable NMSSM scenario (namely with the correct relic density), we will investigate to which extent the lightest neutralino can be detectable in dark matter experiments.

Neutralino direct detection prospects

After having discussed the new and the improved constraints on the low-energy parameter space, we will now address whether or not NMSSM neutralinos with a relic density in agreement with current limits are likely to be detected by the present or the next generation of dark matter detectors.

Although in our survey of the low-energy NMSSM parameter space we have scanned over all combinations of signs (i)-(iv), as we already mentioned, cases (ii)-(iv) present far less interesting situations regarding the neutralino relic density. Even though one can find in the latter three cases some challenging situations regarding direct detection prospects, as discussed in Section 3.3, the new imposed constraints imply that finding experimentally viable areas, with a sizable $\sigma_{\tilde{\chi}_1^0-p}$, becomes nearly impossible. Thus, for the present study we will focus on case (i). We will go through the same examples as above.

Let us start with the regime where $M_1 \approx \mu$, and as an example ensuring compatibility with WMAP, choose $A_\lambda = 400$ GeV, $A_\kappa = -200$ GeV, $\mu = 130$ GeV, with $\tan\beta = 5$ (corresponding to what was already depicted on the right panel of Fig. 3.20 and the left of Fig. 3.24). As shown in the previous Subsubsection, there exist regions in the parameter space where the neutralino fulfils all experimental constraints and has the correct relic density. The latter are characterised by neutralinos with a significant singlino fraction and/or a small mass. In this case, one of the allowed regions is close to the tachyonic area and exhibits very light singlet-like Higgses, potentially leading to large detection cross sections. This is indeed the case, as evidenced on the left-hand side of Fig. 3.26, where the theoretical predictions for $\sigma_{\tilde{\chi}_1^0-p}$ are plotted versus the lightest neutralino mass. The resulting $\sigma_{\tilde{\chi}_1^0-p}$ spans several orders of magnitude, but, remarkably, areas with $\sigma_{\tilde{\chi}_1^0-p} \gtrsim 10^{-7}$ pb are found. These correspond to the above mentioned regions of the parameter space with very light singlet-like Higgses ($25\,\text{GeV} \lesssim m_{h_1^0} \lesssim 50\,\text{GeV}$ with $S^2_{13} \gtrsim 0.99$). The neutralino is a mixed singlino-Higgsino state with $N^2_{15} \approx 0.35$ and a mass around 75 GeV.

The sensitivities of present and projected dark matter experiments are also depicted for comparison. The small area bounded by dotted lines is allowed by the DAMA experiment in the simple case of an isothermal spherical halo model [41]. The larger area also bounded by dotted lines represents the DAMA region when uncertainties to this simple model are taken into account [44]. For the other experiments in the figure only the spherical halo has been considered in their analyses. In particular, the (upper)

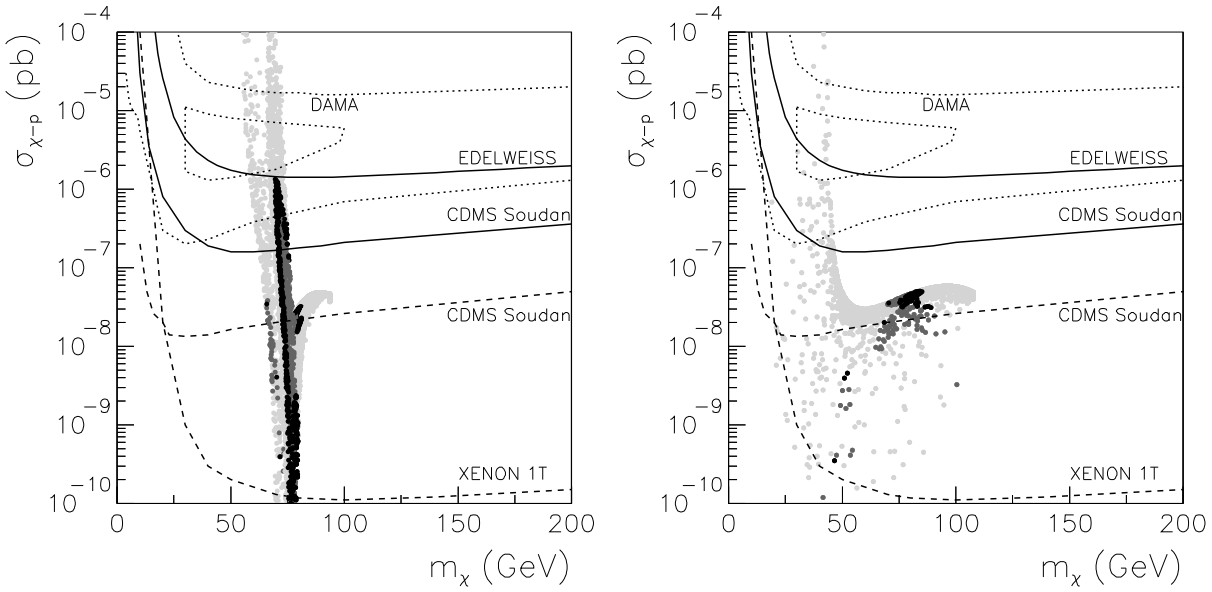

Figure 3.26: Scatter plot of the scalar neutralino-nucleon cross section as a function of the lightest neutralino mass. On the left, an example with $M_1 = 160$ GeV, $\tan\beta = 5$, $A_\lambda = 400$ GeV, $A_\kappa = -200$ GeV, and $\mu = 130$ GeV. All the points represented are in agreement with LEP/Tevatron, $a_\mu^{\rm SUSY}$, and BR($b \to s\,\gamma$) bounds. Dark gray dots represent points which, in addition, fulfil $0.1 \leq \Omega_{\tilde\chi_1^0} h^2 \leq 0.3$, whereas black dots are those in agreement with the WMAP constraint. The sensitivities of present and projected experiments are also depicted, with solid and dashed lines, respectively. On the right we show the same example but with $\mu = 150$ GeV and $A_\kappa = 0$.

areas bounded by solid lines are excluded by EDELWEISS [48][9] and CDMS Soudan [47]. Finally, the dashed lines represent the sensitivities of the projected CDMS Soudan and XENON 1T [51] experiments.

On the right-hand side of Fig. 3.26 we show the resulting $\sigma_{\tilde\chi_1^0-p}$ when the μ parameter and A_κ are varied to $\mu = 150$ GeV, $A_\kappa = 0$, for which the effect of the different constraints on the (λ, κ) plane were represented on the right-hand side of Fig. 3.24. Since the areas of the parameter space with very light Higgses are ruled out by experimental constraints the detection cross section is not as large as in the previous examples. In the regions consistent with both experimental and astrophysical constraints the lightest Higgs mass is in the range $80\,\text{GeV} \lesssim m_{h_1^0} \lesssim 120\,\text{GeV}$, thus leading to $\sigma_{\tilde\chi_1^0-p} \lesssim 5 \times 10^{-8}$ pb, within the sensitivity of projected dark matter experiments,

[9] Since the exclusion area due to ZEPLIN I [49] is similar to EDELWEISS we have not depicted it here, nor in any subsequent plot.

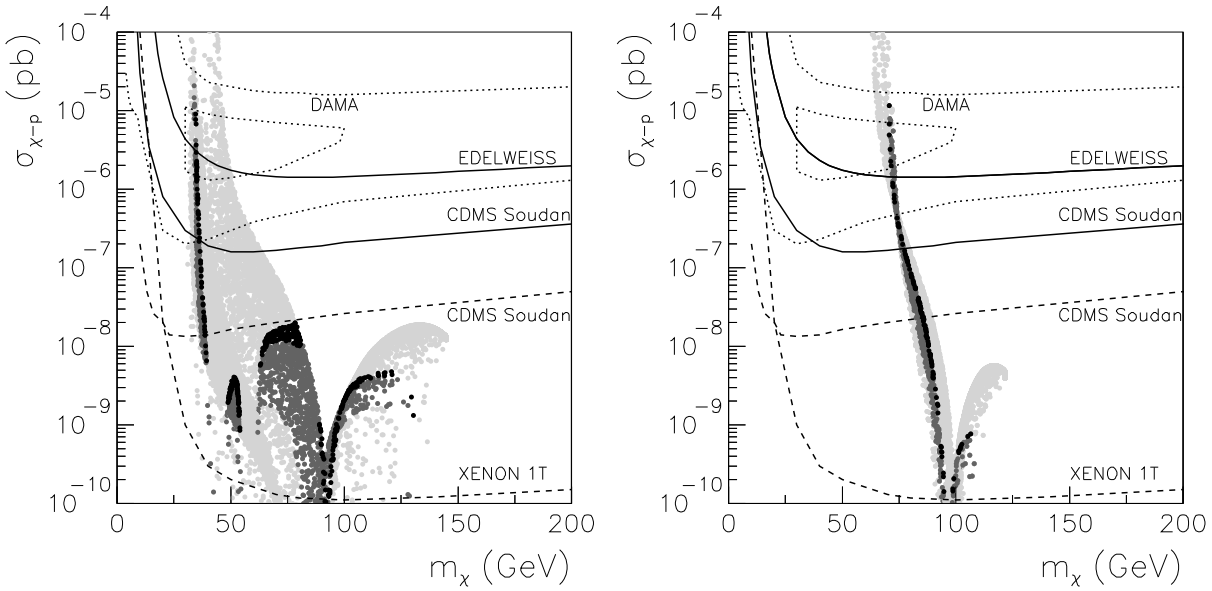

Figure 3.27: The same as in Fig. 3.26 but for an example with $M_1 = 330$ GeV, $\tan\beta = 5$, $A_\lambda = 570$ GeV, $A_\kappa = -60$ GeV, with $\mu = 160$ GeV (left) and $M_1 = 500$ GeV, $\tan\beta = 5$ $A_\lambda = 400$ GeV, $A_\kappa = -150$ GeV, with $\mu = 130$ GeV (right). In both examples, the resulting $a_\mu^{\rm SUSY}$ is outside the experimental 2σ region.

such as CDMS Soudan.

Let us now investigate the effect of changing the neutralino composition by modifying the bino mass. As commented in Subsection 3.3, the largest values of the neutralino detection cross section were obtained for a mixed singlino-Higgsino composition, when $\mu \lesssim M_1 < M_2$. In order to enhance the Higgsino composition we will consider examples where M_1 is increased with respect to the μ-parameter. Such neutralinos annihilate more efficiently, thus leading to a reduced $\Omega_{\tilde\chi_1^0} h^2$, so that the astrophysical constraint becomes more stringent. Nevertheless, as seen in the previous Subsubsection, it is still possible to find areas of the parameter space with the correct relic density while simultaneously fulfilling all experimental constraints. These regions corresponded to light singlet-like Higgses, which can potentially lead to sizable detection cross sections.

First, $M_1 = 330$ GeV will be taken, for an example with $\mu = 160$ GeV, $A_\lambda = 570$ GeV, $A_\kappa = -60$ GeV, and $\tan\beta = 5$. The parameter space for this case was represented in Fig. 3.25, were we showed the effect of resonant annihilation channels on the allowed regions. The theoretical predictions for neutralino direct detection are shown in Fig. 3.27. In this plot, the various resonances appear as funnels in the

predicted $\sigma_{\tilde{\chi}_1^0-p}$ for the regions with the correct $\Omega_{\tilde{\chi}_1^0}\,h^2$ at the corresponding values of the neutralino mass ($m_{\tilde{\chi}_1^0} \approx M_Z/2$ and $m_{\tilde{\chi}_1^0} \approx m_{h_1^0}/2$). Below the resonance with the Z boson, light neutralinos are obtained $m_{\tilde{\chi}_1^0} \lesssim M_Z/2$ with a large singlino composition which have the correct relic abundance. The lightest Higgs is also singlet-like and very light, leading to a very large detection cross section, $\sigma_{\tilde{\chi}_1^0-p} \gtrsim 10^{-6}$ pb. This corresponds to the allowed area of the (λ, κ) plane which lies in the vicinity of the tachyonic region in Fig. 3.25.

Remember however that these two examples with a larger bino mass were disfavoured by the resulting muon anomalous magnetic moment, as it was illustrated in Fig. 3.18.

One more example, this time for $M_1 = 500$ GeV, $\mu = 130$ GeV, $A_\lambda = 400$ GeV, $A_\kappa = -150$ GeV, and $\tan\beta = 5$ is represented in Fig. 3.27 and shows how large detection cross sections can also be achieved for heavier neutralinos. In this case (whose parameter space was illustrated and discussed in Fig. 3.25) neutralino detection cross sections as large as $\sigma_{\tilde{\chi}_1^0-p} \approx 10^{-5}$ pb are possible while fulfilling experimental and astrophysical constraints. Once more, the occurrence of light singlet-like Higgses is crucial for enhancing $\sigma_{\tilde{\chi}_1^0-p}$ and the sizable singlino component of the lightest neutralino ($N_{15}^2 \approx 0.9$) reduces the annihilation cross section and ensures the correct relic density.

Finally, we show in Fig. 3.28 a scatter plot of the theoretical predictions for the neutralino-nucleon cross section as a function of the neutralino mass and the lightest Higgs mass when λ, κ, M_1, the μ parameter and the trilinear terms, A_λ and A_κ are varied while keeping $\tan\beta = 5$. In order to satisfy the $a_\mu^{\rm SUSY}$ constraint, a small slepton mass, $m_{L,E} = 150$ GeV, has been used. Only the points which are in agreement with LEP/Tevatron, BR($b \to s\,\gamma$), and $a_\mu^{\rm SUSY}$ limits and which, in addition, are consistent with the astrophysical bound or the WMAP constraint on the relic density are plotted. We clearly see how large detection cross sections are correlated to the presence of very light Higgses ($m_{h_1^0} \lesssim 50$ GeV). Neutralinos fulfilling all constraints and within the reach of dark matter experiments are possible with $50\,\text{GeV} \lesssim m_{\tilde{\chi}_1^0} \lesssim 130\,\text{GeV}$. The upper bound on the neutralino mass is due to the lightest stau becoming the LSP. If the slepton mass is increased, heavier neutralinos can be found but the resulting $a_\mu^{\rm SUSY}$ is soon outside the experimentally allowed range.

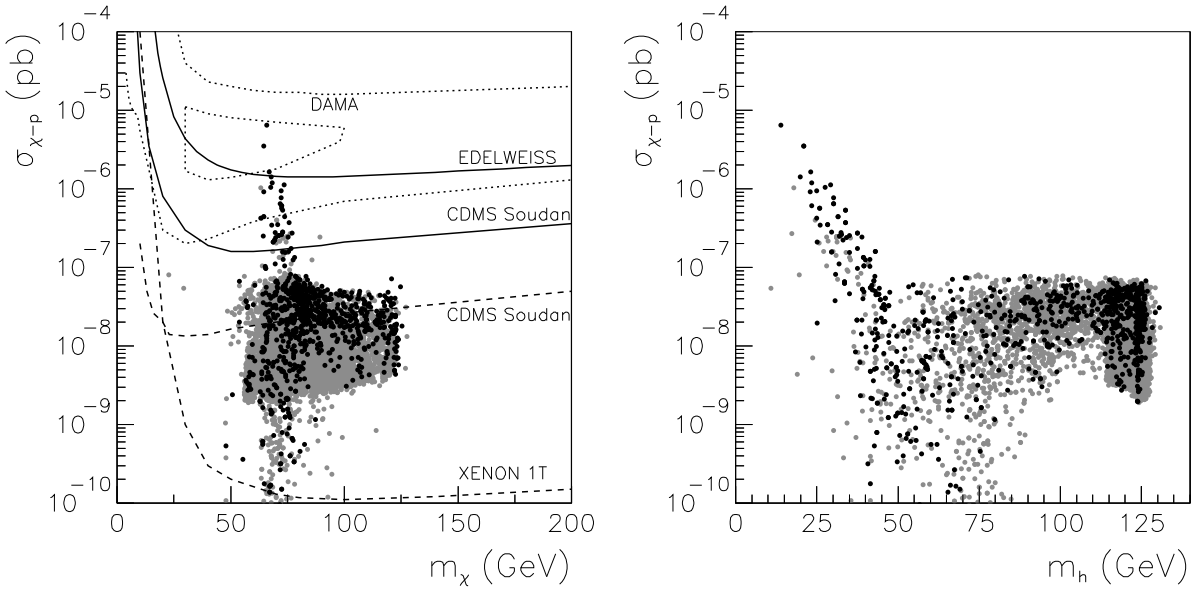

Figure 3.28: Scatter plot of the neutralino-nucleon cross section as a function of the neutralino mass (left) and as a function of the lightest CP-even Higgs mass (right) for an example with $\tan\beta = 5$, and the remaining parameters in the ranges $0.01 \leq \lambda, \kappa \leq 0.7$, 110 GeV $\lesssim M_2 \lesssim$ 430 GeV, -300 GeV $\lesssim A_\kappa \lesssim$ 300 GeV, -800 GeV $\lesssim A_\lambda \lesssim$ 800 GeV, and 110 GeV $< \mu <$ 300 GeV. All the points represented are in agreement with LEP/Tevatron, $a_\mu^{\rm SUSY}$, and BR($b \to s\,\gamma$) constraints, and have a relic density in agreement with the astrophysical bound (grey dots) or the WMAP constraint (black dots).

3.4.4 Conclusions

We have extended the systematic analysis of Section 3.3 of the low-energy parameter space of the Next-to-Minimal Supersymmetric Standard Model (NMSSM), studying the implications of experimental and astrophysical constraints on the direct detection of neutralino dark matter. We have computed the theoretical predictions for the scalar neutralino-proton cross section, $\sigma_{\tilde{\chi}_1^0-p}$, and compared it with the sensitivities of present and projected dark matter experiments. In the computation we have taken into account all available experimental bounds from LEP and Tevatron, including constraints coming from B and K physics, as well as the supersymmetric contribution to the muon anomalous magnetic moment, $a_\mu^{\rm SUSY}$. Finally, the relic abundance of neutralinos has also been computed and consistency with astrophysical constraints imposed.

We have found very stringent constraints on the parameter space coming from low-energy observables. On the one hand, $a_\mu^{\rm SUSY}$ is generally very small unless very light slepton ($m_{L,E} \lesssim 200$ GeV) and gaugino masses ($M_1 \lesssim 210$ GeV) are considered, and slepton trilinear couplings modified in order to increase the LR mixing in the smuon mass matrix. On the other hand, the contribution to BR($b \to s\gamma$) is sizable, mostly due to the smallness of the charged Higgs mass, so that regions with $\tan\beta \lesssim 3$ are disfavoured.

Regarding the neutralino relic density, regions of the parameter space can be found where $\Omega_{\tilde{\chi}_1^0} h^2$ is in agreement with the WMAP constraint. This is possible when either the neutralino mass is small enough for some annihilation channels to be kinematically forbidden or when the singlino component of the lightest neutralino is large enough to suppress neutralino annihilation.

Remarkably, some of the regions fulfilling all the experimental and astrophysical constraints display very light Higgses, $m_{h_1^0} \sim 50$ GeV, which are singlet-like, $S_{13}^2 \gtrsim 0.9$, thus allowing a sizable increase of the neutralino-nucleon cross section. Neutralinos with a detection cross-section within the reach of dark matter experiments are therefore possible, and have a mass in the range $50\,\text{GeV} \lesssim m_{\tilde{\chi}_1^0} \lesssim 130\,\text{GeV}$. These neutralinos have a mixed singlino-Higgsino composition and are therefore characteristic of the NMSSM.

Chapter 4

Beyond the MSSM and the NMSSM

4.1 Why beyond the MSSM and the NMSSM?

In the last few years we have learned a great deal about neutrinos. Two very small mass splittings have been measured and an unexpected pattern of mixing angles has been uncovered [95]. Theorists have struggled with different ideas trying to explain such structure but progress is difficult. Nevertheless, many models have been proposed that can accommodate the observed neutrino spectrum with different degrees of plausibility. Still, there is room for novel models, and it is of some interest to examine new proposals, especially if they have some virtue like simplicity, and some measurable implications in the not so distant future. We refer to the extensive bibliography in neutrinos physics, for example see [96] and reference thereim.

In the context of models with low-energy SUSY, like the MSSM, the best motivated model for neutrino masses is the SUSY version of the see-saw (which is actually the natural version of the see-saw). Besides explaining in a simple and elegant way the smallness of neutrino masses the model scores some success in being able to explain the baryon asymmetry through leptogenesis. The only drawback (not for the model but rather for us being able to test it) is that the scale of masses involved in the mechanism is too high ($\geq 10^{11}$ GeV) to probe directly in any conceivable way.

Many alternatives to the "standard" see-saw have been studied. We proposed in [3] a novel SUSY model for neutrino masses in a very economical extension of the MSSM,

the $\mu\nu SSM$. The new model introduces three gauge-singlet neutrino superfields (like the usual see-saw) but forbids all mass terms in the superpotential, both for the Higgses (therefore there is no μ term) and for the singlet neutrinos (no Majorana mass for them). In addition it allows cubic couplings among the singlet neutrinos and a Yukawa coupling to the Higgs doublets. The model then uses non-zero VEVs for the sneutrinos to generate both an effective μ term (solving the μ-problem like in the NMSSM) and a Majorana mass for the singlet neutrinos (at the TeV scale rather than at 10^{11} GeV). Another salient feature of the model is that it breaks R-parity explicitly and spontaneously. Needless to say, the phenomenology of the model is quite different from the MSSM or the NMSSM and offers the exciting possibility of testing at colliders the physics associated to neutrino masses. We introduce our proposal, the $\mu\nu SSM$ in the next Section.

We would like to mention here that there is and extensive literature with different proposals for models with R-parity violation. For example, see Ref. [96, 97] and references therein. Nevertheless, the novel point of our proposal is the fact that in our model the neutrino right-handed supermultiplets solve the μ-problem in a very natural way without the introduction of any extra field.

4.2 The $\mu\nu SSM$ proposal

As we have already mention in the previous Section, neutrino experiments have confirmed during the last years that neutrinos are massive [95]. As a consequence, it is natural in the context of the MSSM [5] to supplement the ordinary neutrino superfields, $\hat{\nu}_i$, $i = 1, 2, 3$, contained in the $SU(2)_L$-doublet, $\hat{L}_i$, with gauge-singlet neutrino superfields, $\hat{\nu}^c_i$. Once experiments induce us to introduce these new superfields, and given the fact that sneutrinos are allowed to get vacuum expectation values (VEVs), we may wonder why not to use terms of the type $\hat{\nu}^c \hat{H}_1 \hat{H}_2$ to produce an effective μ term. This would allow us to solve the naturalness problem of the MSSM, the so-called μ problem [53], without having to introduce an extra singlet superfield as in case of the NMSSM [55]. It is true that in the model with Bilinear R-parity Violation (BRpV) [98], the bilinear terms $\hat{H}_2 \hat{L}_i$ induce neutrino masses through the mixing with the neutralinos (actually only one mass at tree level and the other two at one loop) without using the superfields $\hat{\nu}^c_i$, however the μ problem is augmented with the three new bilinear terms.

Thus the aim of this Section is to analyse the "μ from ν" Supersymmetric Standard Model ($\mu\nu$SSM) arising from this proposal: natural particle content without μ problem [3]. In addition to the MSSM Yukawa couplings for quarks and charged leptons, the $\mu\nu$SSM superpotential contains Yukawa couplings for neutrinos, and two additional type of terms involving the Higgs doublet superfields, $\hat{H}_1$ and $\hat{H}_2$, and the three neutrino superfields, $\hat{\nu}^c_i$,

$$\begin{aligned} W = \quad & \epsilon_{ab} \left(Y_u^{ij} \, \hat{H}_2^b \, \hat{Q}_i^a \, \hat{u}_j^c + Y_d^{ij} \, \hat{H}_1^a \, \hat{Q}_i^b \, \hat{d}_j^c + Y_e^{ij} \, \hat{H}_1^a \, \hat{L}_i^b \, \hat{e}_j^c + Y_\nu^{ij} \, \hat{H}_2^b \, \hat{L}_i^a \, \hat{\nu}_j^c \right) \\ & - \epsilon_{ab} \lambda^i \, \hat{\nu}_i^c \, \hat{H}_1^a \hat{H}_2^b + \tfrac{1}{3} \kappa^{ijk} \hat{\nu}_i^c \hat{\nu}_j^c \hat{\nu}_k^c \, , \end{aligned} \tag{4.2.1}$$

where we take $\hat{H}_1^T = (\hat{H}_1^0, \hat{H}_1^-)$, $\hat{H}_2^T = (\hat{H}_2^+, \hat{H}_2^0)$, $\hat{Q}_i^T = (\hat{u}_i, \hat{d}_i)$, $\hat{L}_i^T = (\hat{\nu}_i, \hat{e}_i)$, a, b are $SU(2)$ indices, and $\epsilon_{12} = 1$. In this model, the usual MSSM bilinear μ term is absent from the superpotential, and only dimensionless trilinear couplings are present in W. For this to happen we can invoke a Z_3 symmetry as is usually done in the NMSSM. On the other hand, let us recall that this is actually what happens in the low energy limit of string constructions: only trilinear couplings are present in the superpotential. Since string theory seems to be relevant for the unification of interactions, including gravity, this argument in favour of the absence of a bare μ term in the superpotential is robust.

When the scalar components of the superfields $\hat{\nu}^c_i$, denoted by $\tilde{\nu}^c_i$, acquire VEVs of order the EW, an effective interaction $\mu \hat{H}_1 \hat{H}_2$ is generated through the fifth term in

(4.2.1), with $\mu \equiv \lambda^i \langle \tilde{\nu}_i^c \rangle$. The last type of terms in (4.2.1) is allowed by all symmetries, and avoids the presence of an unacceptable axion associated to a global $U(1)$ symmetry. In addition, it generates effective Majorana masses for neutrinos at the EW scale. These two type of terms replace the two NMSSM terms $\hat{S}\hat{H}_1\hat{H}_2$, $\hat{S}\hat{S}\hat{S}$, with $\hat{S}$ an extra singlet superfield.

It is worth noticing that these terms break explicitly lepton number, and therefore, after spontaneous symmetry breaking, a massless Goldstone boson (Majoron) does not appear. On the other hand, R-parity (+1 for particles and -1 for superpartners) is also explicitly broken and this means that the phenomenology of the $\mu\nu$SSM is going to be very different from the one of the MSSM. Needless to mention, the lightest R-odd particle is not stable. Obviosly, the neutralino is no longer a candidate for dark matter. Nevertheless, other candidates can be found in the literature, such as the gravitino [99], the well-known axion, and many other (exotic) particles [10]. It is also interesting to realise that the Yukawa couplings producing Dirac masses for neutrinos, the fourth term in (4.2.1), generate through the VEVs of $\tilde{\nu}_i^c$, three effective bilinear terms $\hat{H}_2\hat{L}_i$. As mentioned above these characterize the BRpV.

Let us finally remark that the superpotential (4.2.1) has a Z_3 symmetry, just like the NMSSM, under which all chiral superfields transform as $\Phi \to e^{2i\pi/3}\Phi$. Therefore, one expects to have also a cosmological domain wall problem [100, 57] in this model. Nevertheless, the usual solutions to this problem [58] will also work in this case: non-renormalizable operators [100] in the superpotential can break explicitly the dangerous Z_3 symmetry, lifting the degeneracy of the three original vacua, and this can be done without introducing hierarchy problems. In addition, these operators can be chosen small enough as not to alter the low-energy phenomenology. An alternative solution to this Z_3 problem could be to introduce an additional $U(1)'$ gauge group under which ν^c carries some non-zero charge (this forbids the cubic coupling of ν^c in W, but the Goldstone that appears after ν^c takes a VEV is now eaten by the Z' boson to get its mass). We have tried this option paying particular attention to the cancellation of anomalies with the new $U(1)'$. Such cancellation requires the introduction of new fermions charged under the SM group which would complicate the model and therefore we have not pursued this route.

Working in the framework of gravity mediated SUSY breaking, we will discuss now in more detail the phenomenology of the $\mu\nu$SSM. Let us write first the soft terms appearing in the Lagrangian $\mathcal{L}_{\rm soft}$, which in our conventions is given by

$$-\mathcal{L}_{\rm soft} = (m^2_{\tilde{Q}})^{ij}\,\tilde{Q}^{a\,*}_i\,\tilde{Q}^a_j + (m^2_{\tilde{u}^c})^{ij}\,\tilde{u}^{c\,*}_i\,\tilde{u}^c_j + (m^2_{\tilde{d}^c})^{ij}\,\tilde{d}^{c\,*}_i\,\tilde{d}^c_j + (m^2_{\tilde{L}})^{ij}\,\tilde{L}^{a\,*}_i\,\tilde{L}^a_j + (m^2_{\tilde{e}^c})^{ij}\,\tilde{e}^{c\,*}_i\,\tilde{e}^c_j$$

$$
\begin{aligned}
&+ \; m_{H_1}^2\, H_1^{a*}\, H_1^a + m_{H_2}^2\, H_2^{a*} H_2^a + (m_{\tilde{\nu}^c}^2)^{ij}\, \tilde{\nu}_i^{c*} \tilde{\nu}_j^c \\
&+ \; \epsilon_{ab} \Big[(A_u Y_u)^{ij}\, H_2^b\, \tilde{Q}_i^a\, \tilde{u}_j^c + (A_d Y_d)^{ij}\, H_1^a\, \tilde{Q}_i^b\, \tilde{d}_j^c + (A_e Y_e)^{ij}\, H_1^a\, \tilde{L}_i^b\, \tilde{e}_j^c \\
&+ \; (A_\nu Y_\nu)^{ij}\, H_2^b\, \tilde{L}_i^a\, \tilde{\nu}_j^c + \text{H.c.} \Big] \\
&+ \; \left[-\epsilon_{ab} (A_\lambda \lambda)^i\, \tilde{\nu}_i^c\, H_1^a H_2^b + \frac{1}{3} (A_\kappa \kappa)^{ijk} \tilde{\nu}_i^c \tilde{\nu}_j^c \tilde{\nu}_k^c \; + \text{H.c.} \right] \\
&- \; \frac{1}{2} \left(M_3\, \tilde{\lambda}_3\, \tilde{\lambda}_3 + M_2\, \tilde{\lambda}_2\, \tilde{\lambda}_2 + M_1\, \tilde{\lambda}_1\, \tilde{\lambda}_1 + \text{H.c.} \right) . \qquad (4.2.2)
\end{aligned}
$$

In addition to terms from $\mathcal{L}_{\text{soft}}$, the tree-level scalar potential receives the usual D and F term contributions. Once the EW symmetry is spontaneously broken, the neutral scalars develop in general the following VEVs:

$$
\langle H_1^0 \rangle = v_1 \,, \quad \langle H_2^0 \rangle = v_2 \,, \quad \langle \tilde{\nu}_i \rangle = \nu_i \,, \quad \langle \tilde{\nu}_i^c \rangle = \nu_i^c \,. \qquad (4.2.3)
$$

In what follows it will be enough for our purposes to neglect mixing between generations in (4.2.1) and (4.2.2), and to assume that only one generation of sneutrinos gets VEVs, ν, ν^c. The extension of the analysis to all generations is straightforward, and the conclusions are similar. We then obtain for the tree-level neutral scalar potential:

$$
\begin{aligned}
\langle V_{\text{neutral}} \rangle \;&=\; \frac{g_1^2 + g_2^2}{8} \left(|\nu|^2 + |v_1|^2 - |v_2|^2 \right)^2 \\
&+ \; |\lambda|^2 \left(|\nu^c|^2 |v_1|^2 + |\nu^c|^2 |v_2|^2 + |v_1|^2 |v_2|^2 \right) + |\kappa|^2 |\nu^c|^4 \\
&+ \; |Y_\nu|^2 \left(|\nu^c|^2 |v_2|^2 + |\nu^c|^2 |\nu|^2 + |\nu|^2 |v_2|^2 \right) \\
&+ \; m_{H_1}^2 |v_1|^2 + m_{H_2}^2 |v_2|^2 + m_{\tilde{\nu}^c}^2 |\nu^c|^2 + m_{\tilde{\nu}}^2 |\nu|^2 \\
&+ \; \left(-\lambda \kappa^* v_1 v_2 \nu^{c*2} - \lambda Y_\nu^* |\nu^c|^2 v_1 \nu^* - \lambda Y_\nu^* |v_2|^2 v_1 \nu^* + k Y_\nu^* v_2^* \nu^* \nu^{c2} \right. \\
&- \; \left. \lambda A_\lambda \nu^c v_1 v_2 + Y_\nu A_\nu \nu^c \nu v_2 + \frac{1}{3} \kappa A_\kappa \nu^{c3} + \text{H.c.} \right) . \qquad (4.2.4)
\end{aligned}
$$

In the following, we assume for simplicity that all parameters in the potential are real. One can derive the four minimization conditions with respect to the VEVs v_1, v_2, ν^c, ν, with the result:

$$
\begin{aligned}
\frac{1}{4}(g_1^2 + g_2^2)(\nu^2 + v_1^2 - v_2^2) v_1 + \lambda^2 v_1 \left(\nu^{c2} + v_2^2 \right) + m_{H_1}^2 v_1 - \lambda \nu^c v_2 \left(\kappa \nu^c + A_\lambda \right) \\
- \lambda Y_\nu \nu \left(\nu^{c2} + v_2^2 \right) = 0 \,, \\
-\frac{1}{4}(g_1^2 + g_2^2)(\nu^2 + v_1^2 - v_2^2) v_2 + \lambda^2 v_2 \left(\nu^{c2} + v_1^2 \right) + m_{H_2}^2 v_2 - \lambda \nu^c v_1 \left(\kappa \nu^c + A_\lambda \right) \\
+ Y_\nu^2 v_2 \left(\nu^{c2} + \nu^2 \right) + Y_\nu \nu \left(-2\lambda v_1 v_2 + \kappa \nu^{c2} + A_\nu \nu^c \right) = 0 \,, \\
\lambda^2 \left(v_1^2 + v_2^2 \right) \nu^c + 2\kappa^2 \nu^{c3} + m_{\tilde{\nu}^c}^2 \nu^c - 2\lambda \kappa v_1 v_2 \nu^c - \lambda A_\lambda v_1 v_2 + \kappa A_\kappa \nu^{c2}
\end{aligned}
$$

$$
\begin{aligned}
&+Y_\nu^2\nu^c\left(v_2^2+\nu^2\right)+Y_\nu\nu\left(-2\lambda\nu^c v_1+2\kappa v_2\nu^c+A_\nu v_2\right)=0\,,\\
&\frac{1}{4}(g_1^2+g_2^2)(\nu^2+v_1^2-v_2^2)\nu+m_{\tilde{\nu}}^2\nu+Y_\nu^2\nu\left(v_2^2+\nu^{c2}\right)\\
&+Y_\nu\left(-\lambda\nu^{c2}v_1-\lambda v_2^2 v_1+\kappa v_2\nu^{c2}+A_\nu\nu^c v_2\right)=0\,. \quad (4.2.5)
\end{aligned}
$$

As discussed in the context of R-parity breaking models with extra singlets [101], the VEV of the left-handed sneutrino, ν, is in general small. Here we can use the same argument. Notice that in the last equation in (4.2.15) $\nu\to 0$ as $Y_\nu\to 0$, and since the coupling Y_ν determines the Dirac mass for the neutrinos, $m_D\equiv Y_\nu v_2$, ν has to be very small. Using this rough argument we can also get an estimate of the value, $\nu\lesssim m_D$. This also implies that we can approximate the other three equations as follows:

$$
\begin{aligned}
\frac{1}{2}M_Z^2\cos 2\beta+\lambda^2\left(\nu^{c2}+v^2\sin^2\beta\right)+m_{H_1}^2-\lambda\nu^c\tan\beta\left(\kappa\nu^c+A_\lambda\right)&=\ 0\,,\\
-\frac{1}{2}M_Z^2\cos 2\beta+\lambda^2\left(\nu^{c2}+v^2\cos^2\beta\right)+m_{H_2}^2-\lambda\nu^c\cot\beta\left(\kappa\nu^c+A_\lambda\right)&=\ 0\,,\\
\lambda^2v^2+2\kappa^2\nu^{c2}+m_{\tilde{\nu}^c}^2-\lambda\kappa v^2\sin 2\beta-\frac{\lambda A_\lambda v^2}{2\nu^c}\sin 2\beta+\kappa A_\kappa\nu^c&=\ 0\,, \quad (4.2.6)
\end{aligned}
$$

where $\tan\beta\equiv v_2/v_1$, $2M_W^2/g_2^2=v_1^2+v_2^2+\nu^2\approx v_1^2+v_2^2\equiv v^2$, and we have neglected terms proportional to Y_ν. It is worth noticing that these equations are the same as the ones defining the minimization conditions for the NMSSM, with the substitution $\nu^c\leftrightarrow s$. Thus one can carry out the analysis of the model similarly to the NMSSM case, where many solutions in the parameter space $\lambda,\kappa,\mu(\equiv\lambda s),\tan\beta,A_\lambda,A_\kappa$, can be found [1].

Once we know that solutions are available in this model, we have to discuss in some detail the important issue of mass matrices. Concerning this point, the breaking of R-parity makes the $\mu\nu$SSM very different from the MSSM and the NMSSM. In particular, neutral gauginos and Higgsinos are now mixed with the neutrinos. Not only the fermionic component of $\tilde{\nu}^c$ mixes with the neutral Higgsinos (similarly to the fermionic component of S in the NMSSM), but also the fermionic component of $\tilde{\nu}$ enters in the game, giving rise to a sixth state. Of course, now we have to be sure that one eigenvalue of this matrix is very small, reproducing the experimental results about neutrino masses. In the weak interaction basis defined by $\Psi^{0T}\equiv\left(\tilde{B}^0=-i\tilde{\lambda}',\tilde{W}_3^0=-i\tilde{\lambda}_3,\tilde{H}_1^0,\tilde{H}_2^0,\nu^c,\nu\right)$, the neutral fermion mass terms in the Lagrangian are $\mathcal{L}_{\rm neutral}^{\rm mass}=-\frac{1}{2}(\Psi^0)^T\mathcal{M}_{\rm n}\Psi^0+{\rm H.c.}$, with $\mathcal{M}_{\rm n}$ a 6×6 (10×10 if we include all generations of neutrinos) matrix,

$$
\mathcal{M}_{\rm n}=\begin{pmatrix} M & m\\ m^T & 0\end{pmatrix}, \quad (4.2.7)
$$

where

$$M = \begin{pmatrix} M_1 & 0 & -M_Z \sin\theta_W \cos\beta & M_Z \sin\theta_W \sin\beta & 0 \\ 0 & M_2 & M_Z \cos\theta_W \cos\beta & -M_Z \cos\theta_W \sin\beta & 0 \\ -M_Z \sin\theta_W \cos\beta & M_Z \cos\theta_W \cos\beta & 0 & -\lambda\nu^c & -\lambda v_2 \\ M_Z \sin\theta_W \sin\beta & -M_Z \cos\theta_W \sin\beta & -\lambda\nu^c & 0 & -\lambda v_1 + Y_\nu \nu \\ 0 & 0 & -\lambda v_2 & -\lambda v_1 + Y_\nu \nu & 2\kappa\nu^c \end{pmatrix}, \tag{4.2.8}$$

is very similar to the neutralino mass matrix of the NMSSM (substituting $\nu^c \leftrightarrow s$ and neglecting the contributions $Y_\nu \nu$), and

$$m^T = \begin{pmatrix} -\frac{g_1 \nu}{\sqrt{2}} & \frac{g_2 \nu}{\sqrt{2}} & 0 & Y_\nu \nu^c & Y_\nu v_2 \end{pmatrix}. \tag{4.2.9}$$

Matrix (4.2.7) is a matrix of the see-saw type that will give rise to a very light eigenvalue if the entries of the matrix M are much larger than the entries of the matrix m. This is generically the case since the entries of M are of order the EW scale, but for the entries of m, ν is small and $Y_\nu v_2$ is the Dirac mass for the neutrinos m_D as discussed above ($Y_\nu \nu^c$ has the same order of magnitude of m_D). We have checked numerically that correct neutrino masses can easily be obtained. For example, using typical EW scale values in (4.2.8), and a Dirac mass of order 10^{-4} GeV in (4.2.9), one obtains that the lightest eigenvalue of (4.2.7) is of order 10^{-2} eV. Including the three generations in the analysis we can obtain different neutrino mass hierarchies playing with the hierarchies in the Dirac masses.

The possibility of using a see-saw at the EW scale has not been considered in much detail in the literature [For a recent work see ref. [102], where an extension of the NMSSM is considered with Majorana masses for neutrinos generated dynamically through the VEV of the singlet S. R-parity may be broken in this extension, although spontaneously], although this avoids the introduction of ad-hoc high energy scales. Of course, with a see-saw at the scale of a GUT one can have Yukawa couplings of order one for neutrinos. However, since we know that the Yukawa coupling of the electron has to be of order 10^{-6}, why the one of the neutrino should be six orders of magnitude larger? As mentioned above, with the EW scale see-saw a Yukawa coupling of order of the one of the electron is sufficient to reproduce the neutrino mass. Notice also that a purely Dirac mass for the neutrino would imply a Yukawa coupling of order 10^{-13}, i.e. seven orders of magnitude smaller than the one we need with a EW scale see-saw. It is worth mentioning here that in some string constructions, where SUSY standard-like

models can be obtained without the necessity of a GUT, and Yukawa couplings can be explicitly computed, those for neutrinos cannot be as small as 10^{-13}, and therefore the presence of a see-saw at the EW scale is helpful [103]. In any case, let us remark that in our model the see-saw is dynamical and unavoidable, since the matrix of eq. (4.2.7) producing such a see-saw is always present.

It has been noted in the literature that the sneutrino-antisneutrino mixing effect generates a loop correction to the neutrino mass, which depends on the mass-splitting of the sneutrino mass eigenstates [104]. In the case of assuming a large Majorana mass this correction is negligible if all parameters are of order the SUSY scale. We have checked that the same result is obtained in our model with a see-saw at the EW scale, unless a fine tune of the parameters is forced producing a too large sneutrino mass difference.

On the other hand, the charginos mix with the charged leptons and therefore in a basis where $\Psi^{+T} \equiv \left(-i\tilde{\lambda}^+, \tilde{H}_2^+, e_R^+\right)$ and $\Psi^{-T} \equiv \left(-i\tilde{\lambda}^-, \tilde{H}_1^-, e_L^-\right)$, one obtains the matrix

$$\begin{pmatrix} M_2 & g_2 v_2 & 0 \\ g_2 v_1 & \lambda\nu^c & -Y_e\nu \\ g_2\nu & -Y_\nu\nu^c & Y_e v_1 \end{pmatrix}. \tag{4.2.10}$$

Here we can distinguish the 2×2 submatrix which is similar to the chargino mass matrix of the NMSSM (substituting $\nu^c \leftrightarrow s$). Clearly, given the vanishing value of the 13 element of the matrix (4.2.10), and the extremely small absolute value of the 23 element, there will always be a light eigenvalue corresponding to the electron mass $Y_e v_1$. The extension of the analysis to three generations is again straightforward.

Of course, other mass matrices are also modified. This is the case for example of the Higgs boson mass matrices. The presence of the VEVs ν, ν^c, leads to mixing of the neutral Higgses with the sneutrinos. Concerning the Higgs phenomenology, since basically the ν^c plays the role of the singlet S, this will be similar to the one of the NMSSM [1]. For example, two CP-odd Higgses are present, and we have checked that one of them can in principle be light. Likewise the charged Higgses will be mixed with the charged sleptons. On the other hand, when compared to the MSSM case, the structure of squark mass terms is essentially unaffected, provided that one uses $\mu = \lambda\nu^c$, and neglects the contribution of the fourth term in (4.2.1).

In the next Section we will analyse a particular limit of our model where R-parity is still conserved, and therefore the usual candidates for dark matter are still present.

4.2.1 Constraining the $\mu\nu SSM$ with R-parity conservation

In this Section we go one step further and, willing to keep R-parity unbroken, we forbid some of the superpotential couplings of the $\mu\nu SSM$ [4]. Let us call the three singlet neutrino superfields $\hat{S}$ and $\hat{S}_\alpha$ with $\alpha = 1, 2$. We assume that $\hat{S}$ has even parity: $R(\hat{S}) = +1$, while $R(\hat{S}_\alpha) = -1$. For quark, lepton and Higgs superfields one has $R(\hat{Q}_i) = R(\hat{u}^c_j) = R(\hat{L}_i) = R(\hat{e}^c_j) = -1$ and $R(\hat{H}_{1,2}) = +1$. With this R-parity assignments and still forbidding mass terms, the R-preserving superpotential reads

$$\begin{aligned} W &= Y_u^{ij}\,\hat{Q}_i\cdot\hat{H}_2\,\hat{u}^c_j + Y_d^{ij}\,\hat{H}_1\cdot\hat{Q}_i\,\hat{d}^c_j + Y_e^{ij}\,\hat{H}_1\cdot\hat{L}_i\,\hat{e}^c_j + Y_\nu^{i\alpha}\,\hat{L}_i\cdot\hat{H}_2\,\hat{S}_\alpha \\ &+ \lambda\,\hat{S}\,\hat{H}_1\cdot\hat{H}_2 + \frac{1}{2}\kappa^{\alpha\beta}\hat{S}\,\hat{S}_\alpha\hat{S}_\beta + \frac{1}{3}\kappa\hat{S}^3\,, \end{aligned} \tag{4.2.11}$$

where $\cdot$ stands for the $SU(2)$ invariant product. The main differences with respect to the $\mu\nu SSM$ are: only $\hat{S}_\alpha$ have neutrino Yukawa couplings while only $\hat{S}$ is allowed to couple to $\hat{H}_1\cdot\hat{H}_2$. In addition, not all cubic couplings between the $\hat{S}$ and $\hat{S}_\alpha$ are allowed.

With this superpotential one finds that the scalar components of $\hat{S}_\alpha$ do not take VEVs while the scalar component of $\hat{S}$ does take a non-zero VEV. As a result of this VEV an effective μ parameter is generated at the same time as Majorana neutrino masses for the fermionic components of the two $\hat{S}_\alpha$. In this way R-parity is not broken, either explicitly or spontaneously, and the model, therefore still has a candidate for dark matter in the LSP. This could be e.g. the neutralino, as is the usual situation in SUSY models where R-parity is unbroken.

Without R-parity conservation (or another symmetry that can discriminate between neutrinos and singlinos) the singlino and the neutrino supermultiplets are essentially the same. In models with R-parity one is odd and the other is even under this symmetry. In this sense, this model, the constraint $\mu\nu SSM$, can be identified with an R-parity conserved extension of the NMSSM with two right-handed neutrinos.

In order to discuss in more detail the phenomenology of this model let us write first the soft SUSY-breaking terms appearing in the Lagrangian $\mathcal{L}_{\rm soft}$ and relevant for the breaking of the EW symmetry. In our conventions this is given by

$$\begin{aligned} -\mathcal{L}_{\rm soft} &= m^2_{H_1}\,|H_1|^2 + m^2_{H_2}|H_2|^2 + m^2_{S_1}\,|S_1|^2 + m^2_{S_2}|S_2|^2 + m^2_S\,|S|^2 \\ &+ \left[(A_\lambda\lambda)SH_1\cdot H_2 + \frac{1}{2}(A_\kappa\kappa)^{\alpha\beta}SS_\alpha S_\beta + \frac{1}{3}(A_\kappa\kappa)S^3 + \text{H.c.}\right]. \end{aligned} \tag{4.2.12}$$

In addition to terms from $\mathcal{L}_{\rm soft}$, the tree-level scalar potential receives the usual D and

F term contributions. We then obtain for the tree-level neutral scalar potential:

$$\begin{aligned} V_0 &= m_{H_1}^2 |H_1^0|^2 + m_{H_2}^2 |H_2^0|^2 + m_{S_1}^2 |S_1|^2 + m_{S_2}^2 |S_2|^2 + m_S^2 |S|^2 \\ &+ \left[(A_\lambda \lambda) S H_1^0 H_2^0 + \frac{1}{2} (A_\kappa \kappa)^{\alpha\beta} S S_\alpha S_\beta + \frac{1}{3} (A_\kappa \kappa) S^3 + \text{H.c.} \right] \\ &- \left| \lambda H_1^0 H_2^0 + \frac{1}{2} \kappa^{\alpha\beta} S_\alpha S_\beta + \kappa S^2 \right|^2 + |\lambda|^2 |S|^2 \left(|H_1^0|^2 + |H_2^0|^2 \right) \\ &+ \kappa^{\alpha\beta} \kappa^{\alpha\gamma *} |S|^2 S_\beta S_\gamma^* + \frac{g_1^2 + g_2^2}{2} \left(|H_1^0|^2 - H_2^0|^2 \right)^2 . \end{aligned} \tag{4.2.13}$$

As usual, we expect $m_{H_2}^2 < 0$ by radiative effects, and this triggers a cascade of other VEVs. In general one gets the following non-zero VEVs:

$$\langle H_1^0 \rangle = \frac{v_1}{\sqrt{2}} , \quad \langle H_2^0 \rangle = \frac{v_2}{\sqrt{2}} , \quad \langle S \rangle = \frac{v_s}{\sqrt{2}} . \tag{4.2.14}$$

Inspection of the potential (4.2.13) immediately shows that the S_α do not develop VEVs, provided $m_{S_\alpha}^2 > 0$. That is, even in the presence of the VEVs of (4.2.14) no tadpole is generated for the S_α. In the following, we assume for simplicity that all parameters in the potential are real. One can derive the minimization conditions for the VEVs v_1, v_2, v_s, with the result:

$$\begin{aligned} &m_{H_1}^2 v_1 + \frac{1}{8}(g_1^2 + g_2^2)(v_1^2 - v_2^2) v_1 + \frac{1}{2} \lambda^2 v_1 \left(v_2^2 + v_s^2 \right) + \lambda v_2 v_s \left(\frac{1}{4} \kappa v_s + \frac{1}{\sqrt{2}} A_\lambda \right) = 0 , \\ &m_{H_2}^2 v_2 + \frac{1}{8}(g_1^2 + g_2^2)(v_2^2 - v_1^2) v_2 + \frac{1}{2} \lambda^2 v_2 \left(v_1^2 + v_s^2 \right) + \lambda v_1 v_s \left(\frac{1}{4} \kappa v_s + \frac{1}{\sqrt{2}} A_\lambda \right) = 0 , \\ &m_S^2 v_s + \frac{1}{2} \lambda^2 v_s \left(v_1^2 + v_2^2 \right) + \lambda v_1 v_2 \left(\frac{1}{2} \kappa v_s + \frac{1}{\sqrt{2}} A_\lambda \right) + \frac{1}{2} \kappa v_s^2 \left(\frac{1}{2} \kappa v_s + \frac{1}{\sqrt{2}} A_\kappa \right) = 0 , \end{aligned} \tag{4.2.15}$$

where we have neglected the neutrino Yukawa couplings, which have to be very small to reproduce the neutrino masses. Notice that as happened in the previous Section, these minimization equations are the same as the ones of the NMSSM, and therefore the same comment applies: one can carry out the analysis of the model similarly to the NMSSM case, where many solutions in the parameter space can be found [1].

Unlike what happened in the $\mu\nu SSM$, neutrinos and neutralinos do not mix in this model. The neutralino mass matrix resembles that of the NMSSM while now the full neutrino mass matrix is 5×5. In the basis $\{\nu_i, \tilde{S}_\alpha\}$, this matrix takes the form

$$\mathcal{M}_\nu = \begin{pmatrix} 0 & m_D \\ m_D^T & M \end{pmatrix} , \tag{4.2.16}$$

where the 3×2 Dirac matrix reads

$$(m_D)_{i\alpha} = \frac{1}{\sqrt{2}} Y_\nu^{i\alpha} v_2 \ , \tag{4.2.17}$$

while the 2×2 Majorana mass matrix is

$$M_{\alpha\beta} = \frac{1}{\sqrt{2}} \kappa^{\alpha\beta} v_s \ . \tag{4.2.18}$$

Assuming that the typical mass scales in $M_{\alpha\beta}$ are of order 1 TeV and therefore much larger than the typical mass scales in m_D (which we assume to be of the same order as the masses of the charged leptons), we have a see-saw mechanism working at the TeV scale and producing very small neutrino masses. One salient feature of the present setup with only two Majorana neutrinos is that, of the three light active neutrinos, only two are massive while one remains massless.

More explicitly, the effective mass matrix for the three light neutrinos is

$$\mathcal{M}_{\nu L} = m_D M^{-1} m_D^T \, , \tag{4.2.19}$$

or, in components:

$$(\mathcal{M}_{\nu L})_{ij} = \frac{1}{\sqrt{2}} \frac{v_2^2}{v_s} Y_\nu^{i\alpha} (\kappa^{-1})_{\alpha\beta} Y_\nu^{\beta j} \ . \tag{4.2.20}$$

Going to a basis of the S_α that makes $\kappa_{\alpha\beta}$ diagonal [$\kappa_{\alpha\beta} = \kappa_{(\alpha)} \delta_{\alpha\beta}$] we get

$$(\mathcal{M}_{\nu L})_{ij} = \frac{1}{\sqrt{2}} \frac{v_2^2}{v_s} Y_\nu^{i\alpha} \frac{1}{\kappa_{(\alpha)}} Y_\nu^{\alpha j} \, , \tag{4.2.21}$$

that is,

$$\mathcal{M}_{\nu L} = \frac{1}{\sqrt{2}} \frac{v_2^2}{v_s} \sum_{\alpha=1,2} \frac{1}{\kappa_{(\alpha)}} \begin{pmatrix} Y^{1\alpha} \\ Y^{2\alpha} \\ Y^{3\alpha} \end{pmatrix} (Y^{1\alpha}, Y^{2\alpha}, Y^{3\alpha}) \, . \tag{4.2.22}$$

This formula makes it explicit that $\mathcal{M}_{\nu L}$ is rank 2. The two non-zero eigenvalues are

$$\begin{aligned} m_\nu \ = \ & \frac{1}{2\sqrt{2}} \frac{v_2^2}{v_s \kappa_{(1)} \kappa_{(2)}} \Big\{ \|Y_\nu^{i2}\|^2 \kappa_{(1)} + \|Y_\nu^{i1}\|^2 \kappa_{(2)} \\ & \sqrt{(\|Y_\nu^{i2}\|^2 \kappa_{(1)} - \|Y_\nu^{i1}\|^2 \kappa_{(2)})^2 + 4 (Y_\nu^{i1} Y_\nu^{i2})^2 \kappa_{(1)} \kappa_{(2)}} \Big\} \ . \end{aligned} \tag{4.2.23}$$

There are basically two options to accomodate the observed neutrino mass splittings with only two non-zero eigenvalues. In both one necessarily has a hierarchical neutrino

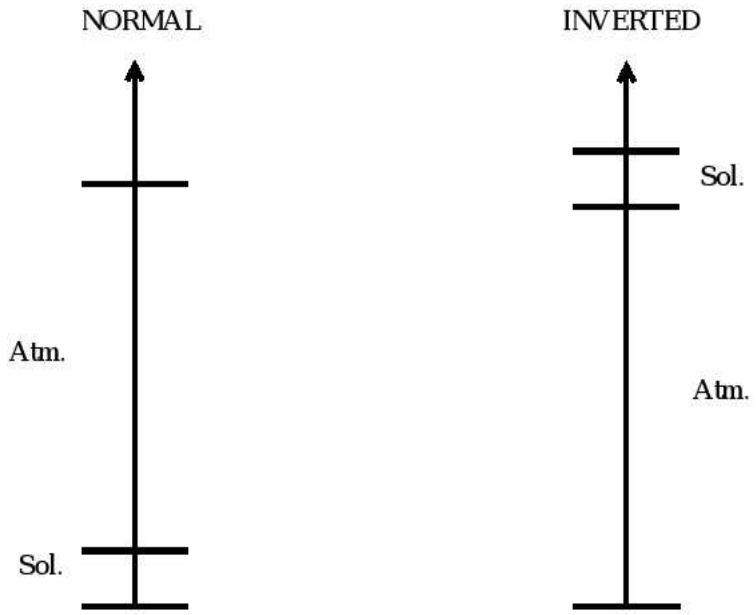

Figure 4.1: Neutrino masses squared, showing the two types of spectra with normal or inverted hierarchy.

spectrum, either with normal hierarchy, when

$$\begin{aligned} m^2_{\nu-} &= \Delta m^2_{sol} \ , \\ m^2_{\nu+} &\simeq \Delta m^2_{atm} \ , \end{aligned} \tag{4.2.24}$$

in which case, the small solar neutrino splitting is below the larger atmospheric one; or with inverted hierarchy, when

$$\begin{aligned} m^2_{\nu-} &\simeq \Delta m^2_{atm} \ , \\ m^2_{\nu+} - m^2_{\nu-} &= \Delta m^2_{sol} \ , \end{aligned} \tag{4.2.25}$$

and the solar splitting is on top of the atmospheric one, see Fig 4.1. It is simple to arrange things so that the neutrino mixing angles also come out right (*i.e.* $\theta_2 \sim 0$; $\theta_1, \theta_3 \sim \pi/4$). From eq. (4.2.22) it is clear for instance that choosing appropriate values of $\kappa_{(1)}$ and $\kappa_{(2)}$ so as to reproduce the neutrino masses, the angles come out right simply

choosing the Yukawa couplings to satisfy

$$\begin{aligned} Y_\nu^{11} : Y_\nu^{21} : Y_\nu^{31} &\sim 1 : 1/\sqrt{2} : -1/\sqrt{2} \ , \\ Y_\nu^{12} : Y_\nu^{22} : Y_\nu^{32} &\sim 0 : 1 : 1 \ . \end{aligned} \tag{4.2.26}$$

4.3 Outlook

The $\mu\nu SSM$ is a new proposal for a SUSY SM. We use the couplings of the right-handed neutrino superfields to the two Higgs doublets in order to generate spontaneously the μ term of the MSSM. In this way we connect this term and its origin to neutrino physics.

Obviously, since R-parity and lepton number are not conserved, the phenomenology of the $\mu\nu$SSM is very rich and different from other models, and therefore many more issues can be addressed in the future. This is the case of an analysis of the parameter space including possible experimental constraints [105], implications for accelerator physics, analysis of the (modified) renormalization group equations, study of the neutrino masses in detail, generation of baryon asymmetry, etc. Needless to say, the starting of the LHC offers the exciting possibility of testing this model soon.

On the other hand, unlike the case of the MSSM and NMSSM, the neutralino cannot be a candidate for dark matter. Nevertheless, other candidates can be found in the literature such as the gravitino or the axion. Another possibility arises from constraining the $\mu\nu$SSM. As discussed above, if one forbids some of the superpotential couplings R-parity is conserved again, and a different phenomenology is obtained. For example, the neutralino is again a good candidate for dark matter, the μ-term is generated as in the NMSSM, and only two neutrinos are massive.

Chapter 5

Conclusiones Finales

En este último capítulo exponemos las conclusiones generales del trabajo de tesis.

En esta tesis hemos realizado en primer lugar un análisis fenomenológico del Next to Minimal Supersymmetric Standard Model (NMSSM), estudiando en detalle su espacio de parámetros. Así mismo, hemos discutido la viabilidad de que el neutralino del NMSSM constituya la materia oscura del universo [1, 2]. En el análisis hemos tenido en cuenta todas las restricciones relevantes que vienen dadas por la física de aceleradores, incluyendo el análisis del momento magnético anómalo del muón a_μ y la física de mesones (siendo el cálculo más relevante el BR($b \to s\gamma$)). también se calculó la densidad reliquia del neutralino comparandola con las últimas observaciones de WMAP, y se analizó la detección directa del neutralino teniendo en cuenta el rango experimentalmente alcanzable.

En segundo lugar se propuso un nuevo modelo supersimétrico publicado con el nombre de $\mu\nu SSM$ [3]. Con este modelo resolvemos el problema μ del Minimal Supersymmetric Standard Model (MSSM) sin la necesidad de introducir un nuevo supercampo como se hace en el NMSSM. Esencialmente la idea es usar los supercampos neutrinos *right-handed*, que incorporamos a la teoría al haberse demostrado que los neutrinos son masivos, para generar dinámicamente el término μ.

Con respecto al análisis del neutralino del NMSSM como candidato a constituir la materia oscura del universo, éste se ha llevado a cabo en el Capítulo 3. En primer término hemos identificado en el modelo las regiones del espacio de parámetros que dan como resultado una sección eficaz neutralino-nucleon dentro del rango asequible a los detectores existentes. Se concluyó que se podian obtener secciones eficaces muy

altas, $\sigma_{\tilde{\chi}_1^0-p} \gtrsim 10^{-7}$ pb, gracias al intercambio de Higgses muy ligeros $m_{h_1^0} \lesssim 70$ GeV. Esto último es posible debido a que el Higgs más ligero en estos casos tiene una alta composición de singlete, evitando por tanto su detección en los experimentos que se han llevado a cabo hasta el momento. Recordemos finalmente que la obtención de estos resultados se ve favorecida para valores de $\tan\beta \lesssim 10$.

En un segundo paso hemos incorporado en el análisis el cálculo del momento magnético anómalo del muón, a_μ, física de mesones y el cálculo de la densidad reliquia de neutralinos.

En cuanto al a_μ, el cálculo teórico en el modelo estándar y los resultados experimentales actuales discrepan en 3.4 sigmas. Aunque todavía es prematuro afirmar que esta es una señal de nueva física, no es descartable que así sea. El avance tanto en el campo teórico como en el experimental abrirá la posibilidad de corroborar este resultado que parece ir más allá del modelo estándar. También será posible corroborar (o refutar) las distintas extensiones supersimétricas. En el caso del NMSSM hemos sido los primeros en hacer el cálculo de a_μ y hemos verificado que existe una zona del espacio de parámetros dentro del intervalo de 2σ de compatibilidad entre el resultado teórico y el experimental. Hemos encontrado que para $\tan\beta \lesssim 10$ el valor de a_μ no está en general dentro de la región de 2σ por ser demasiado pequeño, a menos que la masa de los sleptones sea $m_{L,E} \lesssim 200$ GeV y la de los gauginos $M_1 \lesssim 210$ GeV. Por tanto, hemos encontrado en este contexto una cota experimental para $m_{L,E}$ y M_1, para $\tan\beta$ pequeño.

Con respecto a física de mesones K y B, el proceso dominante es $b \to s\gamma$. Hemos obtenido que para $\tan\beta \lesssim 3$ el BR($b \to s\gamma$) discrepa en más de 2σ del valor experimental. Por tanto, estos valores de $\tan\beta$ se encuentran desfavorecidos.

Finalmente, para que el neutralino sea realmente un candidato a constituir la materia oscura del universo debemos constatar que la densidad reliquia calculada en el modelo se encuentra dentro del rango observacionalmente aceptado. Gracias a las últimas observaciones de WMAP, este valor esta medido con gran precisión, $0.095 < \Omega\, h^2 < 0.112$. Hemos confirmado que es posible obtener resultados dentro de este intervalo cuando la masa del neutralino es lo suficientemente pequeña como para que algunos canales de aniquilación estén cinemáticamente prohibidos o cuando la composición de singlino del neutralino es lo suficientemente grande como para suprimir su aniquilación.

Comprobamos por último que es posible encontrar regiones que satisfacen todas

las cotas experimentales y astrofísicas anteriores y poseen Higgses muy ligeros, $m_{h^0} \sim 50$ GeV, estando dominados en su composición por el singlete $S^2_{13} \gtrsim 0.9$. Esto nos ha permitido obtener secciones eficaces altas. De hecho, es posible obtener neutralinos con una sección eficaz de detección dentro del alcance de los experimentos de materia oscura y con masas comprendidas en el rango $50\,\text{GeV} \lesssim m_{\tilde{\chi}^0_1} \lesssim 130\,\text{GeV}$. Estos neutralinos son principalmente una mezcla Higgsino-singlino y por tanto característicos del NMSSM.

En el cuarto capítulo de la tesis nos hemos fijado en el hecho experimental de que los neutrinos tienen masa. Este hecho sugiere la existencia del neutrino right-handed. Recordemos que el neutrino es el único fermión que en el modelo estándar no posee parte right-handed, motivado porque en un principio se creía que el neutrino no era masivo. Una vez aceptada la inclusión de esta componente nos preguntamos *¿cuál es el modelo supersimétrico mínimo, libre del problema μ, y con tres familias de neutrinos right-handed?* Este planteamiento nos llevó a proponer el nuevo modelo $\mu\nu SSM$.

La principal característica del modelo es la existencia en el superpotencial de términos $\nu^c\, H_1\, H_2$. Éstos generan el parámetro μ de forma dinámica mediante el valor esperado en el vacío del sneutrino right handed ν^c. Al mismo tiempo, términos del tipo $(\nu^c)^3$ prohíben la presencia de un bosón de Goldstone y generan masas efectivas de Mayorana a la escala electrodébil. La presencia de estos términos implica que la simetría discreta llamada R-parity está rota explícitamente. Para masas de Dirac de los neutrinos del orden de 10^{-4} GeV podemos reproducir, usando el mecanismo de see-saw que se genera a la escala electrodebil en este modelo, una masa del neutrino más pesado del orden de 0.01 eV. Dicho de otra manera, con un acoplo de Yukawa del neutrino del orden del Yukawa del electron, es posible reproducir en nuestro modelo la física de neutrinos observada experimentalmente (para generar las masas de los neutrinos más ligeras sólo tenemos que jugar con las jerarquías en los restantes Yukawas). Si bien se suelen asumir masas de Majorana mucho más altas basadas en la idea GUT, para que sea suficiente para reproducir la masa del neutrino más pesado un Yukawa de orden uno, podemos preguntarnos *¿por qué este Yukawa va a ser seis órdenes de magnitud mayor que el análogo asociado al electrón?* El Yukawa del neutrino en el $\mu\nu$SSM es al menos tan natural como el del electrón. No hace falta decir que al estar todo formulado a la escala electrodébil en este modelo, no hace falta introducir ninguna escala *ad hoc*.

El $\mu\nu SSM$ tiene una motivación teórica muy importante, la solución del problema μ, y origina una rica fenomenología. El LHC brindará en un futuro muy próximo la posibilidad de contrastar las predicciones del modelo con la realidad.

Evidentemente, dado que R-parity no se conserva el neutralino no puede ser en el $\mu\nu SSM$ el candidato a materia oscura al decaer muy rápidamente. Sin embargo, es bien sabido que otros candidatos son posibles, tales como el gravitino o el axión. Otra alternativa interesante consiste en suprimir algunos parámetros del $\mu\nu$SSM para obtener un modelo que conserva R-Parity [4]. En este caso el resultado que obtenemos es básicamente el NMSSM extendido con dos neutrinos right-handed, y donde la masa de Majorana de los mismos se genera dinámicamente a través del valor esperado del singlete. La diferencia fundamental con nuestra propuesta original, es que en esta versión restringida el neutrino y el singlino son dos campos distinguibles por el número cuántico asociado a R-parity. Como consecuencia poseen distintos acoplos que hacen que solo el supercampo que contiene al singlino genere el término μ.

Appendix A

Relevant NMSSM interaction vertices

A.1 Higgs-quark-quark Yukawa coupling

Parameterising the interaction of neutral CP-even Higgs fields with quarks as

$$\mathcal{L}_{qqh} = -\bar{q}_i \left[C^i_{YL} P_L + C^i_{YR} P_R \right] q_i \, h^0_a \,, \tag{A.1.1}$$

where h^0_a denotes the physical (mass) Higgs eigenstates and $i = 1, 2$ up- and down-type quarks, one has

$$C^i_{YL} = C^i_{YR} = C^i_Y \,; \qquad C^1_Y = -\tfrac{g m_u}{2 M_W \sin\beta} S_{a2} \,, \quad C^2_Y = -\tfrac{g m_d}{2 M_W \cos\beta} S_{a1} \,, \tag{A.1.2}$$

where we have omitted the quark generations and S is the unitary matrix that diagonalises the scalar Higgs mass matrix, defined in Eq. (3.1.9).

A.2 Neutralino-neutralino-Higgs interaction

The interaction of scalar Higgs and neutralinos can be parametrised as

$$\mathcal{L}_{h\tilde{\chi}^0\tilde{\chi}^0} = \frac{1}{4} h^0_a \bar{\tilde{\chi}}^0_\alpha \left[C^{a\alpha\beta}_{HL} P_L + C^{a\alpha\beta}_{HR} P_R \right] \tilde{\chi}^0_\beta \,, \tag{A.2.3}$$

where $a = 1 - 3$ refers to the Higgs mass eigenstate, $\alpha, \beta = 1 - 5$ denote the physical neutralino states, and the couplings are defined as

$$C^{a\alpha\beta}_{HL} = \qquad \left\{ -g \left(N^*_{\alpha 2} - \tan\theta_W N^*_{\alpha 1} \right) \left(S_{a1} N^*_{\beta 3} - S_{a2} N^*_{\beta 4} \right) + \right.$$

$$+\sqrt{2}\lambda\left[S_{a3}N^*_{\alpha3}N^*_{\beta4}+N^*_{\beta5}\left(S_{a2}N^*_{\alpha3}+S_{a1}N^*_{\alpha4}\right)\right]+(\alpha\to\beta)\Big\}$$
$$-2\sqrt{2}\kappa S_{a3}N^*_{\alpha5}N^*_{\beta5}\,, \tag{A.2.4}$$
$$C^{a\alpha\beta}_{HR}=\left(C^{a\alpha\beta}_{HL}\right)^*\,. \tag{A.2.5}$$

In the text, and since we have exclusively analysed interactions involving the lightest neutralino states (i.e. $\alpha=\beta=1$), we have simplified the above as $C^{a11}_{HL}=C^a_{HL}$ and $C^{a11}_{HR}=C^a_{HR}$.

A.3 Neutralino-squark-quark interaction

In terms of the mass eigenstates, the Lagrangian reads

$$\mathcal{L}_{q\tilde{q}\tilde{\chi}^0}=\bar{q}_i\left[C^{\alpha Xi}_L P_L+C^{\alpha Xi}_R P_R\right]\tilde{\chi}^0_\alpha\tilde{q}^X_i\,, \tag{A.3.6}$$

where $i=1,2$ denotes an up- or down-type quark and squark, $X=1,2$ the squark mass eigenstates, and $\alpha=1,\ldots,5$ the neutralino states. Since we have neglected flavour violation in the squark sector, only LR mixing occurs, and squark physical and chiral eigenstates are related as

$$\begin{pmatrix}\tilde{q}_1\\ \\ \tilde{q}_2\end{pmatrix}=\begin{pmatrix}\eta^{\tilde{q}}_{11} & \eta^{\tilde{q}}_{12}\\ \\ \eta^{\tilde{q}}_{21} & \eta^{\tilde{q}}_{22}\end{pmatrix}\begin{pmatrix}\tilde{q}_L\\ \\ \tilde{q}_R\end{pmatrix}\,. \tag{A.3.7}$$

One can also make the usual redefinition $\eta^{\tilde{q}}_{11}=\eta^{\tilde{q}}_{22}=\cos\theta_{\tilde{q}}$ and $\eta^{\tilde{q}}_{12}=-\eta^{\tilde{q}}_{21}=\sin\theta_{\tilde{q}}$ Therefore, for the up sector, and again omitting quark and squark generation indices, the coefficients $C^{\alpha Xi}_{L,R}$ are given by:

$$C^{\alpha11}_L=-\sqrt{2}g\left[\tfrac{Y_u}{2}\tan\theta_W N^*_{\alpha1}\sin\theta_{\tilde{u}}+\tfrac{m_u}{2M_W\sin\beta}N^*_{\alpha4}\cos\theta_{\tilde{u}}\right]\,, \tag{A.3.8}$$
$$C^{\alpha11}_R=-\sqrt{2}g\left\{\left[N^*_{\alpha2}T^u_3+\tfrac{Y_Q}{2}\tan\theta_W N^*_{\alpha1}\right]\cos\theta_{\tilde{u}}+\tfrac{m_u}{2M_W\sin\beta}N^*_{\alpha4}\sin\theta_{\tilde{u}}\right\}\,, \tag{A.3.9}$$
$$C^{\alpha21}_L=-\sqrt{2}g\left[\tfrac{Y_u}{2}\tan\theta_W N^*_{\alpha1}\cos\theta_{\tilde{u}}-\tfrac{m_u}{2M_W\sin\beta}N^*_{\alpha4}\sin\theta_{\tilde{u}}\right]\,, \tag{A.3.10}$$
$$C^{\alpha21}_R=-\sqrt{2}g\left\{\left[-N^*_{\alpha2}T^u_3+\tfrac{Y_Q}{2}\tan\theta_W N^*_{\alpha1}\right]\sin\theta_{\tilde{u}}+\tfrac{m_u}{2M_W\sin\beta}N^*_{\alpha4}\cos\theta_{\tilde{u}}\right\} \tag{A.3.11}$$

In the above, $Y_{Q(u)}$ denotes the hypercharge of the $SU(2)_L$ quark doublet (up-singlet) and T^u_3 the isospin of the u_L field. The analogous for the down sector is trivially obtained by the appropriate replacements ($Y_u\to Y_d$, $T^u_3\to T^d_3$, $m_u\to m_d$, $\theta_{\tilde{u}}\to\theta_{\tilde{d}}$, $\sin\beta\to\cos\beta$ and $N_{\alpha4}\to N_{\alpha3}$). In this work, and since only $q-\tilde{q}-\tilde{\chi}^0_1$ interactions have been considered, we have always used $C^{1Xi}_{L,R}=C^{Xi}_{L,R}$, i.e., setting $\alpha=1$ in the above.

Bibliography

[1] D. G. Cerdeño, C. Hugonie, D. E. López-Fogliani, C. Muñoz and A. M. Teixeira, 'Theoretical predictions for the direct detection of neutralino dark matter in the NMSSM', *J. High Energy Phys. (JHEP)* **12** (2004) 048 [arXiv:hep-ph/0408102].

[2] D. G. Cerdeño, E. Gabrielli, D. E. López-Fogliani C. Muñoz and A. M. Teixeira, 'Phenomenological viability of neutralino dark matter in the NMSSM', to be published in *J. Cosmol. and Astrop. Phys. (JCAP)*, arXiv:hep-ph/0701271.

[3] D. E. López-Fogliani and C. Muñoz, 'Proposal for a supersymmetric standard model', *Phys. Rev. Lett.* **97** (2006) 041801 [arXiv:hep-ph/0508297].

[4] J. R. Espinosa, D. E. López-Fogliani and C. Muñoz, 'Constraining the $\mu\nu SSM$ with R-parity conservation', to be published in *Phys. Lett. B.*

[5] For reviews, see H.P. Nilles, 'Supersymmetry, supergravity and particle physics' *Phys. Rept.* **110** (1984) 1;

H.E. Haber and G.L. Kane, 'The search for supersymmetry: probing physics beyond the standard model', *Phys. Rept.* **117** (1985) 75;

S. P. Martin, 'A Supersymmetric primer', arXiv:hep-ph/9709356.

[6] F. Zwicky, *Helv. Phys. Acta* **6** (1933) 110.

[7] M.W. Goodman and E. Witten, 'Detectability of certain dark-matter candidates', *Phys. Rev.* **D31** (1985) 3059.

[8] I. Wasserman, 'Possibility of detecting heavy neutral fermions in the Galaxy', *Phys. Rev.* **D33** (1986) 2071.

[9] H. Goldberg, 'Constraint on the photino mass from cosmology', *Phys. Rev. Lett.* **50** (1983) 1419;

J. Ellis, J.S. Hagelin, D.V. Nanopoulos and M. Srednicki, 'Search for supersymmetry at the $\bar{p}p$ collider', *Phys. Lett.* **B127** (1983) 233;

L.M. Krauss 'New constraints on "INO" masses from cosmology (I). Supersymmetric "inos"', *Nucl. Phys.* **B227** (1983) 556;

J. Ellis, J.S. Hagelin, D.V. Nanopoulos, K.A. Olive and M. Srednicki, 'Supersymmetric relics from the Big Bang', *Nucl. Phys.* **B238** (1984) 453.

[10] For a recent review, see C. Muñoz, 'Dark Matter Detection in the Light of Recent Experimental Results', *Int. J. Mod. Phys.* **A19** (2004) 3093 [arXiv:hep-ph/0309346].

[11] D.P. Roy, 'Basic constituents of the visible and invisible matter–a microscopic view of the Universe' [physics/0007025].

[12] A detailed analysis can be found in M. Persic, P. Salucci and F. Stel, 'The universal rotation curve of spiral galaxies: I. The dark matter connection', *Mon. Not. Roy. Astron. Soc.* **281** (1996) 27 [astro-ph/9506004].

[13] For a review, see Y. Sofue and V. Rubin, 'Rotation curves of spiral galaxies', *Ann. Rev. Astron. Astrophy.* **39** (2001) 137 [astro-ph/0010594].

[14] For a recent review, see M. Roncadelli, 'Searching for dark matter', astro-ph/0307115.

[15] A detailed analysis can be found in P. Salucci and M. Persic, 'Dark matter halos around galaxies', Proceedings of the Sesto DM1996 Conference, astro-ph/9703027.

[16] For a review, see E. Battaner and E. Florido, 'The rotation curve of spiral galaxies and its cosmological implications', *Fund. Cosmic Phys.* **21** (2000) 1 [astro-ph/0010475].

[17] See e.g. J. Binney and S. Tremaine, 'Galactic dynamics', Princeton University Press (1988).

[18] W. L. Freedman, 'Determination of cosmological parameters', *Phys. Scripta* **T85** (2000) 37 [arXiv:astro-ph/9905222].

[19] D. N. Spergel et al., 'Wilkinson Microwave Anisotropy Probe (WMAP) Three Year Results: Implications for Cosmology', arXiv:astro-ph/0603449;

C. L. Bennett et al., 'First Year Wilkinson Microwave Anisotropy Probe (WMAP) observations: Preliminary maps and basic results', *Astrophys. J. Suppl.* **148** (2003) 1 [arXiv:astro-ph/0302207];

D. N. Spergel et al. [WMAP Collaboration], 'First Year Wilkinson Microwave Anisotropy Probe (WMAP) observations: Determination of cosmological parameters', *Astrophys. J. Suppl.* **148** (2003) 175 [arXiv:astro-ph/0302209];

L. Verde et al., 'First Year Wilkinson Microwave Anisotropy Probe (WMAP) observations: Parameter estimation methodology", *Astrophys. J. Suppl.* **148** (2003) 195 [arXiv:astro-ph/0302218].

[20] For critical reviews, see D. Scott, M. White, J.D. Cohn and E. Pierpaoli, 'Cosmological difficulties with Modified Newtonian Dynamics (or, la fin du MOND?)', arXiv:astro-ph/0104435;

A. Aguirre, C.P. Burgess, A. Friedland and D. Nolte, 'Astrophysical constraints on modifying gravity at large distances', *Class. Quant. Grav.* **18** (2001) 223 [arXiv:hep-ph/0105083];

A. Lue and G.D. Starkman, 'Squeezing MOND into a cosmological scenario' *Phys. Rev. Lett.* **92** (2004) 131102 [arXiv:astro-ph/0310005].

[21] F. Prada et al., 'Observing the dark matter density profile of isolated galaxies', *Astrophys. J.* **598** (2003) 260-271 [arXiv:astro-ph/0301360].

[22] D. Clowe et al., 'A direct empirical proof of the existence of dark matter', astro-ph/0608407.

[23] R. Cowsik and J. McClelland, 'An upper limit on the neutrino rest mass', *Phys. Rev. Lett.* **29** (1972) 669.

[24] R.D. Peccei and H.R. Quinn, 'CP conservation in the presence of instantons', *Phys. Rev. Lett.* **38** (1977) 1440; 'Constraints imposed by CP conservation in the presence of instantons', *Phys. Rev.* **D16** (1977) 1791.

[25] J. Ipser and P. Sikivie, 'Are galactic halos made of axions?', *Phys. Rev. Lett.* **50** (1983) 925;

F.W. Stecker and Q. Shafi, 'The evolution of structure in the Universe from axions', *Phys. Rev. Lett.* **50** (1983) 928;

M.S. Turner, F. Wilczek and A. Zee, 'Formation of structure in an axion dominated Universe', *Phys. Lett.* **B125** (1983) 35, erratum *ibid.* **B125** (1983) 519;

For a review, see M.S. Turner, 'Windows on the axion', *Phys. Rept.* **197** (1990) 67.

[26] For a review, see G. Jungman, M. Kamionkowski and K. Griest, 'Supersymmetric dark matter', *Phys. Rept.* **267** (1996) 195 [arXiv:hep-ph/9506380].

[27] J. Ellis, J.S. Hagelin, D.V. Nanopoulos, K.A. Olive and M. Srednicki, 'Supersymmetric relics from the Big Bang', *Nucl. Phys.* **B238** (1984) 453.

[28] K. Griest, 'Calculations of rates for direct detection of neutralino dark matter', *Phys. Rev. Lett.* **61** (1988) 666; 'Cross-sections, relic abundance and detection rates for neutralino dark matter', *Phys. Rev.* **D38** (1988) 2357, erratum *ibid.* **D39** (1989) 3802.

[29] K. Griest, M. Kamionkowski and M.S. Turner, 'Supersymmetric dark matter above the W mass', *Phys. Rev.* **D41** (1990) 3565.

[30] J. Ellis, L. Roszkowski and Z. Lalak, 'Higgs effects on the relic supersymmetric particle density', *Phys. Lett.* **B245** (1990) 545.

[31] M. Drees and M.M. Nojiri, 'The neutralino relic density in minimal N=1 supergravity', *Phys. Rev.* **D47** (1993) 376 [arXiv:hep-ph/9207234].

[32] K.A. Olive and M. Srednicki, 'New limits on parameters of the supersymmetric standard model from cosmology', *Phys. Lett.* **B230** (1989) 78; 'Cosmological limits on massive LSP's', *Nucl. Phys.* **B355** (1991) 208.

[33] M. Kamionkowski, 'Energetic neutrinos from heavy neutralino annihilation in the sun', *Phys. Rev.* **D44** (1991) 3021;

L. Roszkowski, 'Light neutralino as dark matter', *Phys. Lett.* **B262** (1991) 59;

J. McDonald, K.A. Olive and M. Srednicki, ' Relic densities of neutralinos', *Phys. Lett.* **B283** (1992) 80.

[34] K. Griest and D. Seckel, 'Three exceptions in the calculation of relic abundandes', *Phys. Rev.* **D43** (1991) 3191.

[35] P. Gondolo and G. Gelmini, 'Cosmic abundances of stable particles: improved analysis', *Nucl. Phys.* **B360** (1991) 145;

R. Arnowitt and P. Nath, 'Susy mass spectrum in $SU(5)$ supergravity grand unification', *Phys. Rev. Lett.* **69** (1992) 725;

J.L. Lopez, D.V. Nanopoulos and K. Yuan, 'Accurate neutralino relic density computations in supergravity models', *Phys. Rev.* **D48** (1993) 2766 [arXiv:hep-ph/9304216];

M. Drees and A. Yamada, 'A decisive test of superstring inspired E_6 models', *Phys. Rev.* **D53** (1996) 1586 [arXiv:hep-ph/9508254];

M. Srednicki, R. Watkins and K.A. Olive, 'Calculations of relic densities in the early Universe', *Nucl. Phys.* **B310** (1988) 693;

T. Nihei, L. Roszkowski and R. Ruiz de Austri, 'Towards an accurate calculation of the neutralino relic density', *J. High Energy Phys.* **05** (2001) 063 [arXiv:hep-ph/0102308]; 'Exact cross sections for the neutralino WIMP pair-annihilation', *J. High Energy Phys.* **07** (2002) 024 [arXiv:hep-ph/0206266].

[36] See e.g. the discussion in the Introduction of the review by P.F. Smith and J.D. Lewin, 'Dark matter detection', *Phys. Rept.* **187** (1990) 203, and in particular Fig. 1.1.

[37] S.P. Ahlen et al., 'Limits on cold dark matter candidates from an ultralow background germanium spectrometer', *Phys. Lett.* **B195** (1987) 603;

D.O. Caldwell et al., 'Laboratory limits on galactic cold dark matter', *Phys. Rev. Lett.* **61** (1988) 510;

D. Reusser et al., 'Limits on cold dark matter from the Gotthard Ge experiment', *Phys. Lett.* **B255** (1991) 143;

J. Morales et al., 'Filtering microphonics in dark matter germanium experiments', *Nucl. Instrum. Meth.* **A321** (1992) 410;

E. García et. al., 'Dark matter searches with a germanium detector at the Canfranc tunnel', *Nucl. Phys. B (Proc. Suppl.)* **28A** (1992) 286; 'Results of a dark matter search with a germanium detector in the Canfranc tunnel', *Phys. Rev.* **D51** (1995) 1458;

A.K. Drukier et al., 'Progress report on the search for cold dark matter using ultralow-background germanium detectors at Homestake', *Nucl. Phys. B (Proc. Suppl.)* **28A** (1992) 293;

M. Beck et al., 'Searching for dark matter with the enriched detectors of the Heidelberg-Moscow double beta decay experiment', *Phys. Lett.* **B336** (1994) 141.

[38] Heidelberg-Moscow Collaboration, L. Baudis et al., 'New limits on dark-matter weakly interacting particles from the Heidelberg-Moscow experiment', *Phys. Rev.* **D59** (1999) 022001 [arXiv:hep-ex/9811045].

[39] IGEX Collaboration, A. Morales et al., 'New constraints on WIMPs from the Canfranc IGEX dark matter search', *Phys. Lett.* **B489** (2000) 268 [arXiv:hep-ex/0002053].

[40] A.K. Drukier, K. Freese and D.N. Spergel, 'Detecting cold dark-matter candidates', *Phys. Rev.* **D33** (1986) 3495;

K. Freese, J. Frieman and A. Gould, 'Signal modulation in cold-dark matter detection', *Phys. Rev.* **D37** (1988) 3388;

K. Griest, 'Effect of the Sun's gravity on the distribution and detection of dark matter near the Earth', *Phys. Rev.* **D37** (1988) 2703.

[41] DAMA Collaboration, R. Bernabei et al., 'Search for WIMP annual modulation signature: results from DAMA/NaI-3 and DAMA/NaI-4 and the global combined analysis', *Phys. Lett.* **B480** (2000) 23.

[42] DAMA Collaboration, R. Bernabei et al., 'Dark matter search', *Riv. N. Cim.* **26** (2003) 1 [astro-ph/0307403].

[43] DAMA Collaboration, R. Bernabei et al., 'New limits on WIMP search with large-mass low-radioactivity NaI(Tl) set-up at Gran Sasso', *Phys. Lett.* **B389** (1996) 757.

[44] P. Belli, R. Cerulli, N. Fornengo and S. Scopel, 'Effect of the galactic halo modeling on the DAMA/NaI annual modulation result: an extended analysis of the data for WIMPs with a purely spin-independent coupling', *Phys. Rev.* **D66** (2002) 043503 [arXiv:hep-ph/0203242].

A.M. Green, 'The WIMP annual modulation signal and non-standard halo models', *Phys. Rev.* **D63** (2001) 043005 [astro-ph/0008318]; 'A potential WIMP signature for the caustic ring halo model', *Phys. Rev.* **D63** (2001) 103003 [arXiv:astro-ph/0012393];

G. Gelmini and P. Gondolo, 'WIMP annual modulation with opposite phase in late-infall halo models', *Phys. Rev.* **D64** (2001) 023504 [arXiv:hep-ph/0012315].

[45] R. Bernabei et al., 'On the investigation of possible systematics in WIMP annual modulation search', *Eur. Phys. J.* **C18** (2000) 283.

[46] R. Bernabei et al., 'DAMA results', talk given at Neutrino Telescopes Conference, Venice (2003), astro-ph/0305542.

[47] CDMS Collaboration, D.S. Akerib et al., 'First results from the cryogenic dark matter search in the Soudan underground lab' *Phys. Rev. Lett.* **93** (2004) 211301 [arXiv:hep-ph/0405033].

[48] EDELWEISS Collaboration, A. Benoit et al., 'First results of the EDELWEISS WIMP search using a 320-g heat-and-ionization Ge detector', *Phys. Lett.* **B513** (2001) 15 [astro-ph/0106094]; 'Improved exclusion limits from the EDELWEISS WIMP search', *Phys. Lett.* **B545** (2002) 43 [arXiv:astro-ph/0206271].

[49] G. J. Alner et al. [UK Dark Matter Collaboration], 'First limits on nuclear recoil events from the ZEPLIN I galactic dark matter detector', *Astroparticle. Phys.* **23** (2005) 444.

[50] J. Amare *et al.*, 'Dark matter searches with NaI scintillators in the Canfranc underground laboratory: ANAIS experiment', *J. Phys. Conf. Ser.* **39** (2006) 123;
J. Amare *et al.*, 'UZ Dark Matter Searches at Canfranc'. Proceeding of the International Conference "The Dark Side of the Universe", Madrid, AIP 878 (2006) 99.

[51] See e.g., E. Aprile et al., 'The XENON dark matter search experiment', *Nucl. Phys. Proc. Suppl.* **138** (2005) 156 [arXiv:astro-ph/0407575].

[52] For recent results, see e.g. S. Baek, D.G. Cerdeno, Y.G. Kim, P. Ko, C. Munoz, 'Direct detection of neutralino dark matter in supergravity', *JHEP* **0506** (2005) 017 [hep-ph/0505019].

[53] J.E. Kim and H.P. Nilles, 'The μ problem and the strong CP problem' *Phys. Lett.* **B138** (1984) 150.

[54] G.F. Giudice and A. Masiero, 'A natural solution to the μ problem in supergravity theories', *Phys. Lett.* **B206** (1988) 480;

J.E. Kim and H.P. Nilles, Gaugino condensation and the cosmological implications of the hidden sector', *Phys. Lett.* **B263** (1991) 79;

E.J. Chun, J.E. Kim and H.P. Nilles, 'A natural solution of the μ problem with a composite axion in the hidden sector', *Nucl. Phys.* **B370** (1992) 105;

J.A. Casas and C. Muñoz, 'A natural solution to the μ problem', *Phys. Lett.* **B306** (1993) 288 [arXiv:hep-ph/9302227];

G. Lopes-Cardoso, D. Lüst and T. Mohaupt, 'Moduli spaces and target space duality symmetries in (0,2) Z_n orbifold theories with continuous Wilson lines', *Nucl. Phys.* **B432** (1994) 68 [arXiv:hep-th/9405002];

I. Antoniadis, E. Gava, K.S. Narain and T.R. Taylor, 'Effective μ term in superstring theory', *Nucl. Phys.* **B432** (1994) 187 [arXiv:hep-th/9405024];

A. Brignole, L.E. Ibáñez and C. Muñoz, 'Orbifold-induced μ term and electroweak symmetry breaking', *Phys. Lett.* **B387** (1996) 769 [arXiv:hep-ph/9607405];

K. Choi, J.S. Lee and C. Muñoz, 'Supergravity radiative effects on soft terms and the μ term', *Phys. Rev. Lett.* **80** (1998) 3686 [arXiv:hep-ph/9709250].

[55] P. Fayet, 'Supergauge Invariant Extension of the Higgs Mechanism and a Model for the electron and Its Neutrino', *Nucl. Phys.* **B90** (1975) 104;

H. P. Nilles, M. Srednicki and D. Wyler, 'Weak interaction breakdown induced by supergravity', *Phys. Lett.* **B120** (1983) 346;

J. M. Frere, D. R. T. Jones and S. Raby, 'Fermion masses and induction of the weak scale by supergravity', *Nucl. Phys.* **B222** (1983) 11;

J. P. Derendinger and C. A. Savoy, 'Quantum effects and SU(2) $\times$ U(1) breaking in supergravity gauge theories', *Nucl. Phys.* **B237** (1984) 307;

J. R. Ellis, J. F. Gunion, H. E. Haber, L. Roszkowski and F. Zwirner, *Phys. Rev.* **D39** (1989) 844;

M. Drees, 'Supersymmetric models with extended Higgs sector', *Int. J. Mod. Phys.* **A4** (1989) 3635;

U. Ellwanger, M. Rausch de Traubenberg and C. A. Savoy, 'Particle spectrum in supersymmetric models with a gauge singlet', *Phys. Lett.* **B315** (1993) 331 [arXiv:hep-ph/9307322];

P. N. Pandita, 'One loop radiative corrections to the lightest Higgs scalar mass in nonminimal supersymmetric Standard Model', *Phys. Lett.* **B318** (1993) 338; 'Radiative corrections to the scalar Higgs masses in a nonminimal supersymmetric Standard Model', *Z. Phys.* **C59** (1993) 575;

S. F. King and P. L. White, 'Resolving the constrained minimal and next-to-minimal supersymmetric standard models', *Phys. Rev.* **D52** (1995) 4183 [arXiv:hep-ph/9505326];

U. Ellwanger and C. Hugonie, 'Particle spectrum in supersymmetric models with a gauge singlet', *Eur. Phys. J.* **C13** (2000) 681 [arXiv:hep-ph/9812427].

[56] M. Bastero-Gil, C. Hugonie, S. F. King, D. P. Roy and S. Vempati, 'Does LEP prefer the NMSSM?', *Phys. Lett.* **B489** (2000) 359 [arXiv:hep-ph/0006198].

[57] S. A. Abel, S. Sarkar and P. L. White, 'On the cosmological domain wall problem for the minimally extended supersymmetric standard model', *Nucl. Phys.* **B454** (1995) 663 [arXiv:hep-ph/9506359].

[58] S. A. Abel, 'Destabilising divergences in the NMSSM', *Nucl. Phys.* **B480** (1996) 55 [arXiv:hep-ph/9609323];

C. Panagiotakopoulos and K. Tamvakis, 'Stabilized NMSSM without domain walls', *Phys. Lett.* **B446** (1999) 224 [arXiv:hep-ph/9809475].

[59] H. P. Nilles, M. Srednicki and D. Wyler, 'Constraints on the stability of mass hierarchies in supergravity', *Phys. Lett.* **B124** (1983) 337;

U. Ellwanger, 'Nonrenormalizable interactions from supergravity, quantum corrections and effective low-energy theories', *Phys. Lett.* **B133** (1983) 187;

J. Bagger and E. Poppitz, 'Destabilizing divergences in supergravity coupled supersymmetric theories', *Phys. Rev. Lett.* **71** (1993) 2380 [arXiv:hep-ph/9307317];

J. Bagger, E. Poppitz and L. Randall, 'Destabilizing divergences in supergravity theories at two loops', *Nucl. Phys.* **B455** (1995) 59 [arXiv:hep-ph/9505244].

[60] U. Ellwanger and C. Hugonie, 'Topologies of the (M+1)SSM with a singlino LSP at LEP2', *Eur. Phys. J.* **C13** (2000) 681 [arXiv:hep-ph/9812427].

[61] U. Ellwanger and C. Hugonie, 'Masses and couplings of the lightest Higgs bosons in the (M+1)SSM', *Eur. Phys. J.* **C25** (2002) 297 [arXiv:hep-ph/9909260].

[62] U. Ellwanger, J. F. Gunion and C. Hugonie, 'NMHDECAY: A Fortran code for the Higgs masses, couplings and decay widths in the NMSSM', arXiv:hep-ph/0406215.

[63] U. Ellwanger, J. F. Gunion, C. Hugonie and S. Moretti, 'NMSSM Higgs discovery at the LHC', arXiv:hep-ph/0401228.

[64] R. Flores, K.A. Olive and D. Thomas, 'Light-neutralino interactions in matter in an extended supersymmetric standard model', *Phys. Lett.* **B263** (1991) 425.

[65] V.A. Bednyakov and H.V. Klapdor-Kleingrothaus, 'About direct dark matter detection in next-to-minimal supersymmetric standard model', *Phys. Rev.* **D59** (1999) 023514 [arXiv:hep-ph/9802344].

[66] B.R. Greene and P.J. Miron, 'Supersymmetric cosmology with a gauge singlet', *Phys. Lett.* **B168** (1986) 226;

R. Flores, K.A. Olive and D. Thomas, 'A new dark matter candidate in the minimal extension of the supersymmetric standard model', *Phys. Lett.* **B245** (1990) 509;

K.A. Olive and D. Thomas, 'A light dark matter candidate in an extended supersymmetric model', *Nucl. Phys.* **B355** (1991) 192;

S.A. Abel, S. Sarkar and I.B. Whittingham, 'Neutralino dark matter in a class of unified theories', *Nucl. Phys.* **B392** (1993) 83 [arXiv:hep-ph/9209292];

A. Stephan, 'Dark matter constraints on the parameter space and particle spectra in the nonminimal SUSY standard model', *Phys. Lett.* **B411** (1997) 97 [arXiv:hep-ph/9704232];

'Dark matter constraints in the minimal and nonminimal SUSY standard model', *Phys. Rev.* **D58** (1998) 035011 [arXiv:hep-ph/9709262];

A. Menon, D. E. Morrissey and C. E. M. Wagner, 'Electroweak baryogenesis and dark matter in the nMSSM' [arXiv:hep-ph/0404184].

[67] J. C. Romao, 'Spontaneous CP violation in susy models: a no go theorem', *Phys. Lett.* **B173** (1986) 309.

[68] W. M. Yao et al. [Particle Data Group], 'Review of particle physics', *J. Phys.* **G33** (2006) 1.

[69] DELPHI Collaboration, J. Abdallah et al., 'Searches for supersymmetric particles in e+ e- collisions up to 208-GeV and interpretation of the results within the MSSM', *Eur. Phys. J.* **C31** (2004) 421 [arXiv:hep-ex/0311019];

OPAL Collaboration, G. Abbiendi *et al.*, 'Search for chargino and neutralino production at $\sqrt{s}$ = 192 GeV - 209 GeV at LEP', *Eur. Phys. J.* **C35** (2004) 1 [arXiv:hep-ex/0401026].

[70] LEP SUSY Working Group, LEPSUSYWG Note/02-04.1.

[71] LEP Higgs Working Group for Higgs boson searches Collaboration, 'Search for charged Higgs bosons: Preliminary combined results using LEP data collected at energies up to 209-GeV', arXiv:hep-ex/0107031.

[72] LEP Higgs Working Group for Higgs boson searches Collaboration, R. Barate et al., 'Search for the standard model Higgs boson at LEP', *Phys. Lett.* **B565** (2003) 61 [arXiv:hep-ex/0306033];

OPAL Collaboration, G. Abbiendi et al., 'Flavour independent search for Higgs bosons decaying into hadronic final states in e+ e- collisions at LEP' [arXiv:hep-ex/0312042]; 'Decay-mode independent searches for new scalar bosons with the OPAL detector at LEP', *Eur. Phys. J.* **C27** (2003) 311 [arXiv:hep-ex/0206022];

LEP Higgs Working Group for Higgs boson searches Collaboration, 'Flavor independent search for hadronically decaying neutral Higgs bosons at LEP' [arXiv:hep-ex/0107034]; 'Searches for Higgs Bosons Decaying into Photons: Combined Results from the LEP Experiments' LHWG Note/2002-02; 'Searches for invisible Higgs bosons: Preliminary combined results using LEP data collected at energies up to 209-GeV' [arXiv:hep-ex/0107032];

ALEPH Collaboration, D. Buskulic et al., 'Search for a nonminimal Higgs boson produced in the reaction e+ e- → h Z*', *Phys. Lett.* **B313** (1993) 312;

DELPHI Collaboration, 'Search for Neutral Higgs Bosons in Extended Models' CERN EP 2003-061 (Submitted to EPJ).

[73] For a summary, see also: U. Chattopadhyay, T. Ibrahim and P. Nath, 'Effects of CP violation on event rates in the direct detection of dark matter', *Phys. Rev.* **D60** (1999) 063505 [arXiv:hep-ph/9811362];

T. Falk, A. Ferstl and K. A. Olive, 'Variations of the neutralino elastic cross-section with CP violating phases', *Astroparticle. Phys.* **13** (2000) 301 [arXiv:hep-ph/9908311].

[74] See e.g., D. G. Cerdeño and C. Muñoz, 'Neutralino dark matter in supergravity theories with non-universal scalar and gaugino masses', *JHEP* **0410** (2004) 015 [arXiv:hep-ph/0405057], and references therein.

[75] J. R. Ellis, A. Ferstl and K. A. Olive, 'Re-evaluation of the elastic scattering of supersymmetric dark matter', *Phys. Lett.* **B481** (2000) 304 [arXiv:hep-ph/0001005].

[76] U. Ellwanger and C. Hugonie, 'NMHDECAY 2.0: An updated program for sparticleicle masses, Higgs masses, couplings and decay widths in the NMSSM', *Comput. Phys.* Commun. **175** (2006) 290 (2006) [arXiv:hep-ph/0508022].

[77] G. Belanger, F. Boudjema, A. Pukhov and A. Semenov, 'MicrOMEGAs: A program for calculating the relic density in the MSSM', *Comput. Phys. Commun.* **149** (2002) 103 [arXiv:hep-ph/0112278]; 'MicrOMEGAs: Version 1.3', *Comput. Phys. Commun.* **174** (2006) 577 [arXiv:hep-ph/0405253].

[78] LEPSUSYWG, ALEPH, DELPHI, L3, OPAL experiments, note LEPSUSYWG/4-01.1 and 04-02.1 (http://lepsusy.web.cern.ch/lepsusy/Welcome.html);

LEP Higgs Working Group for Higgs boson searches Collaboration, 'Search for charged Higgs bosons: Preliminary combined results using LEP data collected at energies up to 209-GeV', arXiv:hep-ex/0107031.

[79] T. Affolder et al. [CDF Collaboration], 'Search for gluinos and scalar quarks in $p\bar{p}$ collisions at $\sqrt{s} = 1.8$-TeV using the missing energy plus multijets signature', *Phys. Rev. Lett.* **88** (2002) 041801 [arXiv:hep-ex/0106001];

B. Abbott et al. [D0 Collaboration], 'Search for squarks and gluinos in events containing jets and a large imbalance in transverse energy', *Phys. Rev. Lett.* **83** (1999) 4937 [arXiv:hep-ex/9902013].

[80] G. Hiller, 'b-physics signals of the lightest CP-odd Higgs in the NMSSM at large tan(beta)', *Phys. Rev.* **D70** (2004) 034018 [arXiv:hep-ph/0404220].

[81] K. Adel and Y.P. Yao, 'Exact α_s calculation of $b \to s + \gamma$ $b \to s + g$', *Phys. Rev.* **D49** (1994) 4945 [arXiv:hep-ph/9308349];

A. Ali and C. Greub, 'Photon energy spectrum in B $\to$ X(s) + γ and comparison with data', *Phys. Lett.* **B361**(1995) 146 [arXiv:hep-ph/9506374];

M. Misiak and M. Münz, 'Two loop mixing of dimension five flavor changing operators', *Phys. Lett.* **B344** (1995) 308 [arXiv:hep-ph/9409454];

C. Greub, T. Hurth, and D. Wyler, 'Virtual $O(\alpha_s)$ corrections to the inclusive decay $b \to s\gamma$', *Phys. Rev.* **D54** (1996) 3350 [arXiv:hep-ph/9603404];

C. Greub and T. Hurth, 'Two-loop matching of the dipole operators for $b \to s\gamma$ and $b \to sg$', *Phys. Rev.* **D56** (1997) 2934 [arXiv:hep-ph/9703349];

N. Pott, 'Bremsstrahlung corrections to the decay $b \to s\gamma$', *Phys. Rev.* **D54** (1996) 938 [arXiv:hep-ph/9512252];

K. G. Chetyrkin, M. Misiak and M. Munz, 'Weak radiative B-meson decay beyond leading logarithms', *Phys. Lett.* **B400** (1997) 206 [Erratum-ibid. B **425** (1998) 414] [arXiv:hep-ph/9612313];

A. J. Buras, A. Kwiatkowski and N. Pott, 'Next-to-leading order matching for the magnetic photon penguin operator in the $B \to X_s\gamma$ decay', *Nucl. Phys.* **B517** (1998) 353 [arXiv:hep-ph/9710336];

A. J. Buras, A. Czarnecki, M. Misiak and J. Urban, 'Completing the NLO QCD calculation of $\bar{B} \to X_s\gamma$', *Nucl. Phys.* **B631** (2002) 219 [arXiv:hep-ph/0203135].

[82] P. Gambino and M. Misiak, 'Quark mass effects in $\bar{B} \to X_s\gamma$', *Nucl. Phys.* **B611** (2001) 338 [arXiv:hep-ph/0104034].

[83] A. L. Kagan and M. Neubert, 'QCD anatomy of $B \to X_s\gamma$ decays', *Eur. Phys. J.* **C7**, 5 (1999) [arXiv:hep-ph/9805303].

[84] S. Bertolini, F. Borzumati, A. Masiero and G. Ridolfi, 'Effects of supergravity induced electroweak breaking on rare B decays and mixings', *Nucl. Phys.* **B353** (1991) 591.

[85] M. Ciuchini, G. Degrassi, P. Gambino and G. F. Giudice, 'Next-to-leading QCD corrections to $B \to X_s\gamma$: Standard model and two-Higgs doublet model', *Nucl. Phys.* **B527** (1998) 21 [arXiv:hep-ph/9710335]; 'Next-to-leading QCD corrections to $B \to X_s\gamma$ in supersymmetry', *Nucl. Phys.* **B534** (1998) 3 [arXiv:hep-ph/9806308];

P. Ciafaloni, A. Romanino and A. Strumia, 'Two-loop QCD corrections to charged-Higgs-mediated $b \to s\gamma$ decay', *Nucl. Phys.* **B524** (1998) 361 [arXiv:hep-ph/9710312];

F. Borzumati and C. Greub, '2HDMs predictions for $\bar{B} \to X_s\gamma$ in NLO QCD', *Phys. Rev.* **D58** (1998) 074004 [arXiv:hep-ph/9802391]; 'Two Higgs doublet model predictions for $\bar{B} \to X_s\gamma$ in NLO QCD. (Addendum)', *Phys. Rev.* **D59** (1999) 057501 [arXiv:hep-ph/9809438];

G. Degrassi, P. Gambino and G. F. Giudice, '$B \to X_s\gamma$ in supersymmetry: Large contributions beyond the leading order', *JHEP* **0012** (2000) 009 [arXiv:hep-ph/0009337];

M. Carena, D. Garcia, U. Nierste and C. E. M. Wagner, '$b \to s\gamma$ and supersymmetry with large $\tan\beta$', *Phys. Lett.* **B499** (2001) 141 [arXiv:hep-ph/0010003];

F. Borzumati, C. Greub and Y. Yamada, 'Beyond leading-order corrections to $\bar{B} \to X_s\gamma$ at large $\tan\beta$: The charged-Higgs contribution', *Phys. Rev.* **D69**, 055005 (2004) [arXiv:hep-ph/0311151].

[86] The Heavy Flavour Averaging Group, http://www.slac.stanford.edu/xorg/hfag/;

J. Walsh for the BaBar Collaboration, talk presented at Moriond EW, 2005;

P. Koppenburg et al. [Belle Collaboration], 'An inclusive measurement of the photon energy spectrum in $b \to s\gamma$ decays', *Phys. Rev. Lett.* **93** (2004) 061803 [arXiv:hep-ex/0403004];

S. Chen et al. [CLEO Collaboration], 'Branching fraction and photon energy spectrum for $b \to s\gamma$', *Phys. Rev. Lett.* **87** (2001) 251807 [arXiv:hep-ex/0108032].

[87] P. Gambino, 'Semileptonic and radiative B decays circa 2005', *Nucl. Phys. Proc. Suppl.* **156** (2006) 169 [arXiv:hep-ph/0510085] (Talk given at 10th Int. Conference on B Physics at Hadron Machines (BEAUTY 2005), Assisi, Perugia, Italy, 20-24 Jun 2005).

[88] J. L. Lopez, D. V. Nanopoulos and X. Wang, 'Large $(g-2)_\mu$ in SU(5)×U(1) supergravity models', Phys. Rev. D **49** (1994) 366 [arXiv:hep-ph/9308336];

U. Chattopadhyay and P. Nath, 'Probing supergravity grand unification in the Brookhaven $g-2$ experiment', *Phys. Rev.* **D53** (1996) 1648 [arXiv:hep-ph/9507386];

T. Moroi, 'The Muon Anomalous Magnetic Dipole Moment in the Minimal Supersymmetric Standard Model', *Phys. Rev.* **D53** (1996) 6565 [Erratum-ibid. D **56** (1997) 4424] [arXiv:hep-ph/9512396];

M. Carena, G. F. Giudice and C. E. M. Wagner, 'Constraints on supersymmetric models from the muon anomalous magnetic moment', *Phys. Lett.* **B390** (1997) 234 [arXiv:hep-ph/9610233].

[89] T. Kinoshita and W.J. Marciano, in *Quantum Electrodynamics*, ed. T. Kinoshita (World Scientific, Singapore, 1990), p. 419;

T. Kinoshita, 'New value of the α^3 electron anomalous magnetic moment', *Phys. Rev. Lett.* **75** (1995) 4728;

A. Czarnecki, B. Krause and W. J. Marciano, 'Electroweak corrections to the muon anomalous magnetic moment', *Phys. Rev. Lett.* **76** (1996) 3267 [arXiv:hep-ph/9512369];

S. Eidelman and F. Jegerlehner, 'Hadronic contributions to $g-2$ of the leptons and to the effective fine structure constant $\alpha(M_Z^2)$', *Z. Phys.* **C67** (1995) 585 [arXiv:hep-ph/9502298];

K. Adel and F. J. Yndurain, 'Improved evaluation of the hadronic vacuum polarization contributions to muon $g-2$ and $\bar{\alpha}_{\rm QED}(M_Z)$ using high order QCD calculations', arXiv:hep-ph/9509378;

T. Kinoshita, B. Nizic and Y. Okamoto, 'Hadronic Contributions To The Anomalous Magnetic Moment Of The Muon', *Phys. Rev.* **D31** (1985) 2108;

J. Bijnens, E. Pallante and J. Prades, 'Hadronic light by light contributions to the muon $g-2$ in the large N(c) limit', *Phys. Rev. Lett.* **75** (1995) 1447 [Erratum-ibid. **75** (1995) 3781] [arXiv:hep-ph/9505251].

[90] M. Davier, S. Eidelman, A. Hocker and Z. Zhang, 'Updated estimate of the muon magnetic moment using revised results from e^+e^- annihilation', *Eur. Phys. J.* **C31** (2003) 503 [arXiv:hep-ph/0308213];

K. Hagiwara, A. D. Martin, D. Nomura and T. Teubner, 'Predictions for $g-2$ of the muon and $\alpha_{QED}(M_Z^2)$', Phys. Rev. D **69** (2004) 093003 [arXiv:hep-ph/0312250];

J. F. de Troconiz and F. J. Yndurain, 'The hadronic contributions to the anomalous magnetic moment of the muon', *Phys. Rev.* **D71** (2005) 073008 [arXiv:hep-ph/0402285].

[91] T. Kinoshita and M. Nio, 'The tenth-order QED contribution to the lepton $g-2$: Evaluation of dominant α^5 terms of muon $g-2$', *Phys. Rev.* **D73** (2006) 053007 [arXiv:hep-ph/0512330];

K. Hagiwara, A. D. Martin, D. Nomura and T. Teubner, 'Improved predictions for $g-2$ of the muon and $\alpha_{QED}(M_Z^2)$', [arXiv:hep-ph/0611102].

[92] G. W. Bennett et al. [Muon g-2 Collaboration], 'Measurement of the negative muon anomalous magnetic moment to 0.7-ppm', *Phys. Rev. Lett.* **92** (2004) 161802 [arXiv:hep-ex/0401008].

[93] J. F. Gunion, D. Hooper and B. McElrath, 'Light neutralino dark matter in the NMSSM', *Phys. Rev.* **D73** (2006) 015011 [arXiv:hep-ph/0509024].

[94] G. Belanger, F. Boudjema, C. Hugonie, A. Pukhov and A. Semenov, 'Relic density of dark matter in the NMSSM', *JCAP* **0509** (2005) 001 [arXiv:hep-ph/0505142].

[95] Super-Kamiokande collaboration, Y. Fukuda et al., 'Evidence for oscillation of atmosferic neutrinos', *Phys. Rev. Lett.* **81** (1998) 1562 [arXiv:hep-ex/9807003];

SNO collaboration, Q.R. Ahmad et al., 'Direct evidence for neutrino flavor transformation from neutral-current interactions in the Sudbury Neutrino Observatory', *Phys. Rev. Lett.* **89** (2002) 011301 [arXiv:nucl-ex/0204008];

KamLAND collaboration, K. Eguchi et al., 'First results from KamLAND: evidence for reactor anti-neutrino disappearance', *Phys. Rev. Lett.* **90** (2003) 021802 [arXiv:hep-ex/0212021].

[96] A. Strumia and F. Vissani, 'Neutrino masses and mixings and...', arXiv:hep-ph/0606054;

J. F. W. Valle, 'Neutrino physics overview', arXiv:hep-ph/0608101.

[97] R. Barbier et al., 'R-Parity Violating Supersymmetry' *Phys. Rept.* **420** (2005) 1 [arXiv:hep-ph/0406039].

[98] See e.g., M. Hirsch and J.W.F. Valle, 'Supersymmetric origin of neutrino mass', *New J. Phys.* **6** (2004) 76 [arXiv:hep-ph/0405015], and references therein.

[99] For analyses of gravitino dark matter without R-parity, see: F. Takayama and M. Yamaguchi, 'Gravitino Dark Matter without R-parity' *Phys. Lett.* **B485** (2000) 388 [arXiv:hep-ph/0005214];

M. Hirsch, W. Porod and D. Restrepo, 'Collider signals of gravitino dark matter in bilinearly broken R-parity', *J. High Energy Phys.* **03** (2005) 062 [arXiv:hep-ph/0503059];

W. Buchmuller, L. Covi, K. Hamaguchi, A. Ibarra, T. Yanagida, 'Gravitino Dark Matter in R-Parity Breaking Vacua', arXiv:hep-ph/0702184.

[100] J. R. Ellis, K. Enqvist, D. V. Nanopoulos, K. A. Olive, M. Quiros and F. Zwirner, 'Problems For (2,0) Compactifications', *Phys. Lett.* **B176** (1986) 403;

B. Ray and G. Senjanovic, 'Gravity and Domain Wall Problem', *Phys. Rev.* **D49** (1994) 2729 [arXiv:hep-ph/9301240].

[101] A. Masiero and J.W.F. Valle, 'A model for spontaneous R parity breaking', *Phys. Lett.* **B251** (1990) 273.

[102] R. Kitano and K.Y. Oda, 'Neutrino Masses in the Supersymmetric Standard Model with Right-Handed Neutrinos and Spontaneous R-Parity Violation' *Phys. Rev.* **D61** (2000) 113001 [arXiv:hep-ph/9911327].

[103] S.A. Abel and C. Muñoz, 'Quark and lepton masses and mixing angles from superstring constructions', *J. High Energy Phys.* **02** (2003) 010 [arXiv:hep-ph/0212258].

[104] Y. Grossman and H.E. Haber, 'Sneutrino Mixing Phenomena' *Phys. Rev. Lett.* **78** (1997) 3438 [arXiv:hep-ph/9702421]; '(S)neutrino properties in R-parity violating supersymmetry: I. CP-conserving Phenomena', *Phys. Rev.* **D59** (1999) 093008 [arXiv:hep-ph/9810536]; 'Neutrino masses and sneutrino mixing in R-parity violating supersymmetry' [arXiv:hep-ph/9906310].

[105] N. Escudero, D. E. López-Fogliani, C. Muñoz and R. Ruiz de Austri, 'Phenomenology of the $\mu\nu$SSM', in preparation.